

BWR Zircaloy Corrosion and Water Chemistry Tests: Joint EPRI/Japan Joint Utility Group/Tokyo Electric Power Company Funded Studies

Joint EPRI/Japan Joint Utility Group/Tokyo Electric Power Company Funded Studies



WARNING:
Please read the Export Control
and License Agreement on the
back cover before removing the
Wrapping Material.

Technical Report

Effective December 6, 2006, this report has been made publicly available in accordance with Section 734.3(b)(3) and published in accordance with Section 734.7 of the U.S. Export Administration Regulations. As a result of this publication, this report is subject to only copyright protection and does not require any license agreement from EPRI. This notice supersedes the export control restrictions and any proprietary licensed material notices embedded in the document prior to publication.

BWR Zircaloy Corrosion and Water Chemistry Tests

**Joint EPRI/Japan Joint Utility Group/Tokyo
Electric Power Company Funded Studies**

TR-106830
3247-01

Final Report, December 1996

Prepared by
General Electric Company
Vallecitos Nuclear Center
Pleasanton, California 94566

Principal Investigators
D.R. Lutz
C.C. Lin

With inputs from
T. Kogai, Nippon Nuclear Fuel Development Co., Ltd.
E. Ibe, Hitachi, Ltd.
N. Ichkawa, Toshiba Corporation

Prepared for
Electric Power Research Institute
3412 Hillview Avenue
Palo Alto, California 94304

EPRI Project Manager
B. Cheng
Nuclear Power Group

Tokyo Electric Power Company
Nuclear Power R&D Center
44-1 Egasaki-Cho, Tsurumi-Ku,
Yokohama, Japan

Senior Researcher
Y. Shirai

DISCLAIMER OF WARRANTIES AND LIMITATION OF LIABILITIES

THIS REPORT WAS PREPARED BY THE ORGANIZATION(S) NAMED BELOW AS AN ACCOUNT OF WORK SPONSORED OR COSPONSORED BY THE ELECTRIC POWER RESEARCH INSTITUTE, INC. (EPRI). NEITHER EPRI, ANY MEMBER OF EPRI, ANY COSPONSOR, THE ORGANIZATION(S) NAMED BELOW, NOR ANY PERSON ACTING ON BEHALF OF ANY OF THEM:

(A) MAKES ANY WARRANTY OR REPRESENTATION WHATSOEVER, EXPRESS OR IMPLIED, (I) WITH RESPECT TO THE USE OF ANY INFORMATION, APPARATUS, METHOD, PROCESS, OR SIMILAR ITEM DISCLOSED IN THIS REPORT, INCLUDING MERCHANTABILITY AND FITNESS FOR A PARTICULAR PURPOSE, OR (II) THAT SUCH USE DOES NOT INFRINGE ON OR INTERFERE WITH PRIVATELY OWNED RIGHTS, INCLUDING ANY PARTY'S INTELLECTUAL PROPERTY, OR (III) THAT THIS REPORT IS SUITABLE TO ANY PARTICULAR USER'S CIRCUMSTANCE; OR

(B) ASSUMES RESPONSIBILITY FOR ANY DAMAGES OR OTHER LIABILITY WHATSOEVER (INCLUDING ANY CONSEQUENTIAL DAMAGES, EVEN IF EPRI OR ANY EPRI REPRESENTATIVE HAS BEEN ADVISED OF THE POSSIBILITY OF SUCH DAMAGES) RESULTING FROM YOUR SELECTION OR USE OF THIS REPORT OR ANY INFORMATION, APPARATUS, METHOD, PROCESS, OR SIMILAR ITEM DISCLOSED IN THIS REPORT.

ORGANIZATION THAT PREPARED THIS REPORT:

GENERAL ELECTRIC COMPANY

TR-106830

Interest Category

Fuel assembly reliability and performance

Key Words

Zircaloy corrosion

Primary coolant chemistry

Fuel reliability

ORDERING INFORMATION

Requests for copies of this report should be directed to EPRI Distribution Center, 207 Coggins Drive, P.O. Box 23205, Pleasant Hill, CA 94523, (510) 934-4212.

Electric Power Research Institute and EPRI are registered service marks of Electric Power Research Institute, Inc. POWERING PROGRESS is a service mark of Electric Power Research Institute, Inc.
Copyright © 1996 Electric Power Research Institute, Inc., Tokyo Electric Power Company, Japan Joint Utility Group, General Electric Company, Hitachi Ltd., and Toshiba Corporation. All rights reserved.

REPORT SUMMARY

Zircaloy-2 cladding was historically susceptible to nodular corrosion, with several cases of corrosion-related fuel failures documented in the 1970s and 1980s. This report summarizes the results of in-core Zircaloy corrosion tests performed in the Halden reactor from 1990 through 1995. Both fuel rod and coupon test results confirmed the effectiveness of cladding processing control on the resistance of Zircaloy-2 to in-reactor nodular corrosion under BWR conditions. Among the various water chemistry impurities tested, only a few species actually influenced in-reactor corrosion of Zircaloy-2.

Background

Changes in thermo-mechanical processing of cladding and alloy chemistry resulted in corrosion improvement of Zircaloy-2. Despite these changes, however, the role of water chemistry impurities on corrosion was not well known. A program to investigate these areas was conducted under the sponsorship of EPRI, Japan Joint Utility Group (JJUG), Tokyo Electric Power Company (TEPCO), GE, Hitachi, and Toshiba.

Objectives

- To identify the chemistry impurities that are deleterious to in-reactor corrosion of Zircaloy-2 cladding.
- To demonstrate that the improved Zircaloy-2 is resistant to in-reactor nodular corrosion under severe chemistry conditions.
- To evaluate the effects of hydrogen and zinc additions to the reactor water on corrosion and hydriding of Zircaloy-2.

Approach

Investigators designed two test rigs for irradiation in the Halden reactor, one for fuel rods and the other for coupon specimens placed in mini-autoclaves. Zircaloy-2 cladding of the traditional type with nodular corrosion susceptibility and the current improved cladding material were included in the test program. In addition, investigators tested four types of new Zr-alloy cladding material developed by JJUG, TEPCO, Hitachi, Toshiba, and GE. The loop water chemistry, temperature, and neutronic conditions simulated conditions in high-power-density BWRs. However, the loop water for fuel rod tests or feedwater tanks for mini-autoclave tests contained additives or impurities

at concentrations that were ~10 to 100 times higher than normally found in BWR water. Irradiated specimens were inspected at the reactor site, then sent to hot cell laboratories for detailed analyses.

Results

Oxygen is the only species confirmed to increase nodular corrosion susceptibility of Zircaloy-2. Nitrogen also increased nodular corrosion, but the role of nitrogen is not evident, as oxygen was also present in the test. Chromate increased the uniform corrosion, as did sodium carbonate at pH=10.8. Zinc had a small effect on nodular corrosion. No deleterious effects on Zircaloy-2 corrosion were found from the following species: copper (as sulfate or nitrate), silica (at 200 ppm), sulfate, and hydrogen. The cladding specimens fabricated in the late 1970s were susceptible to nodular corrosion, while the tubeshell or in-process heat-treated cladding (current product) specimens were more resistant to nodular corrosion. Research showed, however, that the processing changes had no significant effect on the uniform corrosion rate in chromate or carbonate environments. Tests with hydrogen addition of ~400 ppb in loop water (~4 ppm in BWR feedwater) largely increased crud deposition on fuel surfaces, but no effect on cladding corrosion or hydriding was found. Finally, zinc addition promoted the formation of a thin tenacious deposit on fuel rod surfaces.

EPRI Perspective

This test program identified the common water impurities which can accelerate cladding corrosion and/or cause cladding damages. The program also demonstrated that the tubeshell or in-process heat treatments implemented by all cladding vendors are effective in mitigating cladding nodular corrosion. These results—which confirm that the current water chemistry measures are effective in preventing impurity-induced fuel failures—have been incorporated into the 1996 version of EPRI's *BWR Water Chemistry Guidelines*.

Results on the common impurities proven to be benign to cladding corrosion are valuable to utilities in managing chemistry transients during plant operation. The test results with high hydrogen addition have provided a basis for utilities considering the addition of hydrogen at concentrations exceeding the plant experience base of 1.6-1.8 ppm for mitigation of stress corrosion cracking of in-core components. The zinc test results provide an important reference for understanding how zinc injection may affect fuel performance. Finally, the excellent corrosion resistance of some of the new Zr-alloys indicate that further improvement in cladding corrosion will be possible should a need be identified.

ABSTRACT

An evaluation of the water chemistry impurities that cause accelerated corrosion of Zircaloy-2 and alternate Zr alloys was conducted using the BWR corrosion loop of the Halden test reactor. The BWR corrosion loop simulates the nuclear and thermo-hydraulic characteristics of commercial boiling water reactors. Single fuel rods under boiling conditions and coupons placed in mini-autoclave containers under non-boiling conditions were tested.

Significant amounts of nodular and uniform oxide growth were observed in the 100-140 day duration of the fuel rod and mini-autoclave tests. The effect of a particular impurity on corrosion was determined by comparison to a reference water chemistry environment.

Oxygen accelerated the corrosion of Zircaloy-2 but its effect was reduced by the presence of other impurities in the water. Water radiolysis modeling showed a correlation between dissolved oxygen content and the production of copious amounts of hydrogen peroxide and lesser amounts of other species. These radiolytic species are thought to have caused the accelerated corrosion. Hydrogen water chemistry was shown to promote a reducing environment (by suppressing water radiolysis) in which Zircaloy-2 corrosion was minimized. The oxide thickness in hydrogen water chemistry and ZnO was approximately 1 micron thicker than in hydrogen water chemistry alone.

Zinc nitrate and nitrogen accelerated the nodular corrosion of Zircaloy-2. NaHCrO_4 substantially accelerated the uniform corrosion of Zircaloy-2.

The corrosion of Zircaloy-2 was either reduced or was not accelerated in CuSO_4 , ZnSO_4 , Na_2SO_4 , Na_2SiO_3 , SiO_2 , Resin, and EHC oil.

The deleterious effects of oxidizing water chemistry conditions were reduced by using Zircaloy-2 cladding with high corrosion resistance or some alternate Zr alloys. The alternate Zr alloys E, F, and G had slightly better nodular corrosion resistance than the highest corrosion-resistant Zircaloy-2 material used in this study; alloy H had low hydrogen pickup but its corrosion resistance was not as good as Zircaloy-2; alloy I had exceptionally high hydrogen pickup; alloy J had neither superior corrosion resistance nor hydrogen pickup characteristics compared to Zircaloy-2.

The fuel rod crud deposition behavior was dependent on the water chemistry environment. There was very little crud deposition in oxygenated water. Hydrogen water chemistry promoted the release of oxide films from the loop construction materials and, consequently, a thick but non-adherent crud deposit composed of ferrimagnetic NiFe_2O_4 was found on the fuel surface. For the combination of hydrogen water chemistry and ZnO , a thin but tenacious crud was deposited in addition to the loose crud that occurred in hydrogen water chemistry alone. The tenacious crud caused the eddy current liftoff measurements to be overpredicted.

ACKNOWLEDGMENTS

This experimental program was conducted with the cooperative efforts of many individuals from the participating organizations of GE Nuclear Energy, Electric Power Research Institute (EPRI), Nippon Nuclear Fuel Development (NFD), Hitachi, Ltd., Toshiba Corporation, and the Halden Test Reactor operated by the Institute of Energiteknikk (IFE). This work was sponsored in part by the Japan Joint Utility Group whose members include the Tokyo Electric Power Company, the Tohoku Electric Power Company, the Chubu Electric Power Company, the Hokuriku Electric Power Company, the Chugoku Electric Power Company, and the Japan Atomic Power Company. Active participants in the comprehensive evaluation were M. Aomi of NFD, S. Shimada of NFD, R. Adamson of GE, and B. Cheng of EPRI. Many other individuals too numerous to list in the participating organizations contributed to the successful completion of this program.

CONTENTS

Section	Page
1 HALDEN BWR CORROSION LOOP EXPERIMENTAL PROGRAM	1-1
2 SUMMARY OF CORROSION TESTS AND RESULTS	2-1
Mini-Autoclave Tests	2-1
Fuel Rod Tests	2-12
3 COMPREHENSIVE EVALUATION	3-1
Zircaloy-2 Corrosion	3-1
Mini-Autoclave Tests	3-1
Fuel Rod Tests	3-23
Effect of Water Chemistry Environment on Hydrogen Pickup of Zircaloy-2	3-43
Mini-autoclave Tests	3-43
Fuel Rod Tests	3-45
Performance of Alternate Alloys in Mini-autoclave and Fuel Rod Tests	3-46
Alloy E	3-46
Alloy F	3-46
Alloy G	3-52
Alloy H	3-52
Alloy I	3-53
Alloy J	3-54
Crud Deposition Behavior	3-54
Normal Water Chemistry (NWC)	3-54
Hydrogen Water Chemistry (HWC)	3-54

Section	Page
Hydrogen Water Chemistry + ZnO (HWC + ZnO)	3-56
NaHCrO ₄ + 1000 ppb O ₂	3-56
Corrosion of Mini-Autoclave Containers.....	3-56
4 CONCLUSIONS.....	4-1
5 REFERENCES.....	5-1
APPENDIX A FUNDAMENTALS OF WATER RADIOLYSIS.....	A-1

TABLES

Table	Page
1 Specifications for BWR Corrosion Loop	1-2
2 Mini-Autoclave Irradiation Test Water Chemistry Conditions (Inlet)	2-2
3 Summary of Water Chemistries in the Mini-Autoclave Irradiation Tests.....	2-3
4 Summary of Water Chemistry Data in the Mini-Autoclave Radiation Water Chemistry Experiment	2-4
5 Alloy Materials Used for the Mini-Autoclave Irradiation Tests	2-5
6 Summary of the Mini-Autoclave Specimen Outer Surface Oxide Thicknesses	2-6
7 Summary of the Mini-Autoclave Specimen Hydrogen Contents (Metallographic Estimates)	2-13
8 Fuel Rod Irradiation Test Water Chemistry Conditions	2-14
9 Summary of Fuel Rod Irradiation Test Operational Data.....	2-15
10 Alloy Materials Used for the Fuel Rod Irradiation Tests	2-16
11 Summary of Fuel Rod Irradiation Test Specimen Oxide Thicknesses	2-19
12 Summary of Fuel Rod Irradiation Test Specimen Hydrogen Contents	2-20
13 Corrosion Resistance Ranking Criteria for Mini-Autoclave Irradiation Tests	3-2
14 Ranking of Corrosion Resistance of Zircaloy-2 Alloys A, B, and C in the Mini-Autoclave Irradiation Tests	3-3
15 Nitrogen Compounds and Assumed Transient Species in Water Under Irradiation	3-12

Table	Page
16 Comparison of Hitachi Radiolysis Model Calculation with Experimental Data for Mini-Autoclave Test 2-A.....	3-21
17 Comparison of Hitachi's Radiolysis Model Calculations with Experimental Data for the Fuel Rod Irradiation Tests	3-25
18 Comparison of Corrosion Resistance of Alternate Zr Alloys and Zircaloy-2 (Alloy A) in Mini-Autoclave Irradiation Tests	3-48
A1 Analysis Cases for the Mini-Autoclave Irradiation Tests.....	A-6
A2 Analysis Cases for the Fuel Rod Irradiation Tests.....	A-6
A3 Comparison of GE's, Hitachi's, and Toshiba's Radiolysis Model Calculations for the Mini-Autoclave Irradiation Tests	A-7
A4 Comparison of Toshiba's Radiolysis Model Calculation with Experimental Data for Mini-Autoclave Irradiation Test 2-C (Nitrogen Injection)	A-8

ILLUSTRATIONS

Figure	Page
1 Schematic of BWR Corrosion Loop	1-3
2 In-Core Rig Configuration	1-4
3 Schematic of Mini-Autoclave Rig Containing Four Mini-Autoclaves.	1-5
4 Outer Surface Oxide Thickness of the Mini-Autoclave Specimens in the First Test	2-7
5 Outer Surface Oxide Thickness of the Mini-Autoclave Specimens in the Second Test	2-8
6 Outer Surface Oxide Thickness of the Mini-Autoclave Specimens in the Third Test	2-9
7 Outer Surface Oxide Thickness of the Mini-Autoclave Specimens in the Fourth Test	2-10
8 Outer Surface Oxide Thickness of the Mini-Autoclave Specimens in the Fifth Test	2-11
9 Schematic of Fuel Rod Design for Tests 4, 5, 6a and 6b	2-17
10 Schematic of Pellet Loading Design for the Second and Third Fuel Rod Tests	2-18
11 Toshiba's Mini-Autoclave Analysis Case 5 (Corrosion Test 1 – A).....	3-5
12 Toshiba's Mini-Autoclave Analysis Case 3 (Corrosion Test 1 – C).....	3-6
13 Toshiba's Mini-Autoclave Analysis Case 4 (Corrosion Test 3 – C).....	3-7
14 Effects of Dissolved Oxygen Content on the Concentration of Radiation Decomposition Products in the Mini-Autoclave Irradiation Tests (RWCE A-1, 1-A, 1-C, 3-C).....	3-8

Figure	Page
15 Toshiba's Mini-Autoclave Analysis Case 6 (Corrosion Test 4 – C).....	3-10
16 Mini-Autoclave Analysis Case 7 (Corrosion Test 2 – C).....	3-13
17 Effects of Nitrogen Addition on the Concentration of Radiation Decomposition Products in the Mini-Autoclave Irradiation Tests (RWCE A-1, 1-A, 1-C, 3-C, 2-C).....	3-15
18 Reaction Scheme of Chromium Chemical Species Under Irradiation Assumed in Model Calculation [15]	3-17
19 Hitachi's Mini-Autoclave Analysis Case 8 (Corrosion Test 2 – A).....	3-18
20 Hitachi's Mini-Autoclave Analysis Case 8 (Corrosion Test 2 – A).....	3-19
21 Effects of Chromium Addition on the Concentration of Radiation Dissociation Products in the Mini-Autoclave Irradiation Tests (RWCE A-1, 1-A, 1-C, 3-C, 2-A)	3-20
22 Hitachi's Water Chemistry Analysis of Fuel Rod Irradiation Test 1.....	3-26
23 Hitachi's Water Chemistry Analysis of Fuel Rod Irradiation Test 2.....	3-27
24 Hitachi's Water Chemistry Analysis of Fuel Rod Irradiation Test 3.....	3-28
25 Hitachi's Water Chemistry Analysis of Fuel Rod Irradiation Test 4.....	3-29
26 Outer Surface Oxide Thickness of Zircaloy-2 Alloy C Fuel Cladding in the First Fuel Rod Test with 250 ppb Dissolved Oxygen.....	3-30
27 Outer Surface Oxide Thickness of Zircaloy-2 Alloy C Fuel Cladding in the Second Fuel Rod Test with 350 ppb Dissolved Oxygen	3-31
28 Outer Surface Oxide Thickness of Zircaloy-2 Alloy C Fuel Cladding in the Third Fuel Rod Test with 500 ppb Dissolved Oxygen.....	3-32
29 Outer Surface Oxide Thickness of Zircaloy-2 Alloy B Fuel Cladding in the Fourth Fuel Rod Test with 1000 ppb Dissolved Oxygen	3-34
30 Outer Surface Oxide Thickness of Zircaloy-2 Alloy B Fuel Cladding in the Fifth Fuel Rod Test with 350 ppb Dissolved Hydrogen.....	3-35
31 Hitachi's Water Chemistry Analysis of Fuel Rod Irradiation Test 5.....	3-36
32 Outer Surface Oxide Thickness of Zircaloy-2 Alloy B Fuel Cladding in the Sixth Fuel Rod Test with 400 ppb Dissolved Hydrogen + ZnO	3-38

Figure	Page
33 Outer Surface Oxide Thickness of Zircaloy-2 Alloy B Fuel Cladding in the Sixth Fuel Rod Test with NaHCrO_4 + 1000 ppb Dissolved Oxygen	3-39
34 Water Chemistry Analysis of Fuel Rod Irradiation Test 6b	3-40
35 Water Chemistry Analysis of Fuel Rod Irradiation Test 6b	3-41
36 Hydrogen Content of Zircaloy-2 Alloy B in the Mini-Autoclave Tests	3-44
37 Hydrogen Content of Zircaloy-2 and the Alternate Alloys in the Mini-Autoclave 810 ppb O_2 Normal Water Chemistry Condition	3-49
38 Comparison of the Oxide Thickness of Zircaloy-2 Alloy B and the Alternate Alloys in the Fuel Rod Irradiation Tests	3-50
39 Comparison of the Hydrogen Content of Zircaloy-2 Alloy B and the Alternate Alloys in the Fuel Rod Irradiation Tests	3-51
40 Crud Deposition Characteristics in the Fuel rod Irradiation Tests	3-55
41 Axial Oxide Thickness Profile (Eddy Current) of the Fuel Rod in the Hydrogen Water Chemistry + Zinc Injection Fuel Rod Irradiation Test	3-57
42 Axial Oxide Thickness Profile (Eddy Current) of the Fuel Rod in the NaHCrO_4 + 1000 ppb O_2 Fuel Rod Irradiation Test	3-58
43 Comparison of the Mini-Autoclave Container Inner and Outer Surface Oxide Thickness for Mini-Autoclave Tests 4-D and 5-D	3-60
A1 Mini-Autoclave Analysis Case 1 (RWCE A-1)	A-9
A2 Mini-Autoclave Analysis Case 1 (RWCE B-1)	A-10

1

HALDEN BWR CORROSION LOOP EXPERIMENTAL PROGRAM

The Halden BWR corrosion (HBWRC) loop operated by the Institute of Energiteknikk (IFE) in Halden, Norway was used to study the effects of reactor water chemistry on the corrosion properties of Zircaloy-2 and new Zr-alloys. The objectives of the corrosion test program are (1) to identify the chemical impurities which accelerate Zircaloy-2 corrosion and (2) to identify new Zr-alloys which have good corrosion resistance suitable for high burnup applications.

The HBWRC loop consists of two in-core rigs connected in series with an 80 cm axial test zone surrounded by PWR type power booster rods; the basic loop design and in-core configuration are shown in Figures 1 and 2. The HBWRC loop simulates the thermo-hydraulic and nuclear conditions typical of high power density BWRs as specified in Table 1.

The program consists of six tests, each lasting from 100-140 effective full power days (EFPD). The first test was started in 1990, while the last test, including post-irradiation examination (PIE), was completed in 1995. In Tests 1 through 5, one of the rigs was used for testing fuel rods (in which boiling conditions develop) and the other was used for testing coupon specimens placed inside four mini-autoclaves (MACs), as shown in Figure 3. In the sixth test, both rigs were used for testing fuel rods.

The loop design allows separate water chemistry conditions to be run for each fuel rod and each mini-autoclave. Chemical impurities were pre-mixed into the feedwater, and gaseous additives, such as oxygen and hydrogen, were added by saturating the feedwater with a gas mixture of He containing known amounts of oxygen or hydrogen.

The nuclear and thermo-hydraulic parameters and water chemistry impurities are monitored and recorded using on-line sensors and a process computer. The electrical conductivity and pH are also monitored.

Table 1
Specifications for BWR Corrosion Loop

Temperature	288°C
Pressure	70 bars
Neutron Flux (E > 1 MeV)	$5\text{-}8 \times 10^{13} \text{ n/cm}^2/\text{s}$
Flow Velocity	1-2 m/s
Water Purity	
Conductivity	0.1-0.3 $\mu\text{S/cm}$
pH (Room Temperature)	6.5-7.5
Silicates	< 100 ppb
Chlorides	< 20 ppb
Total Organics (As Carbon)	< 100 ppb
Dissolved Oxygen	Test Dependent
Dissolved Hydrogen	Test Dependent

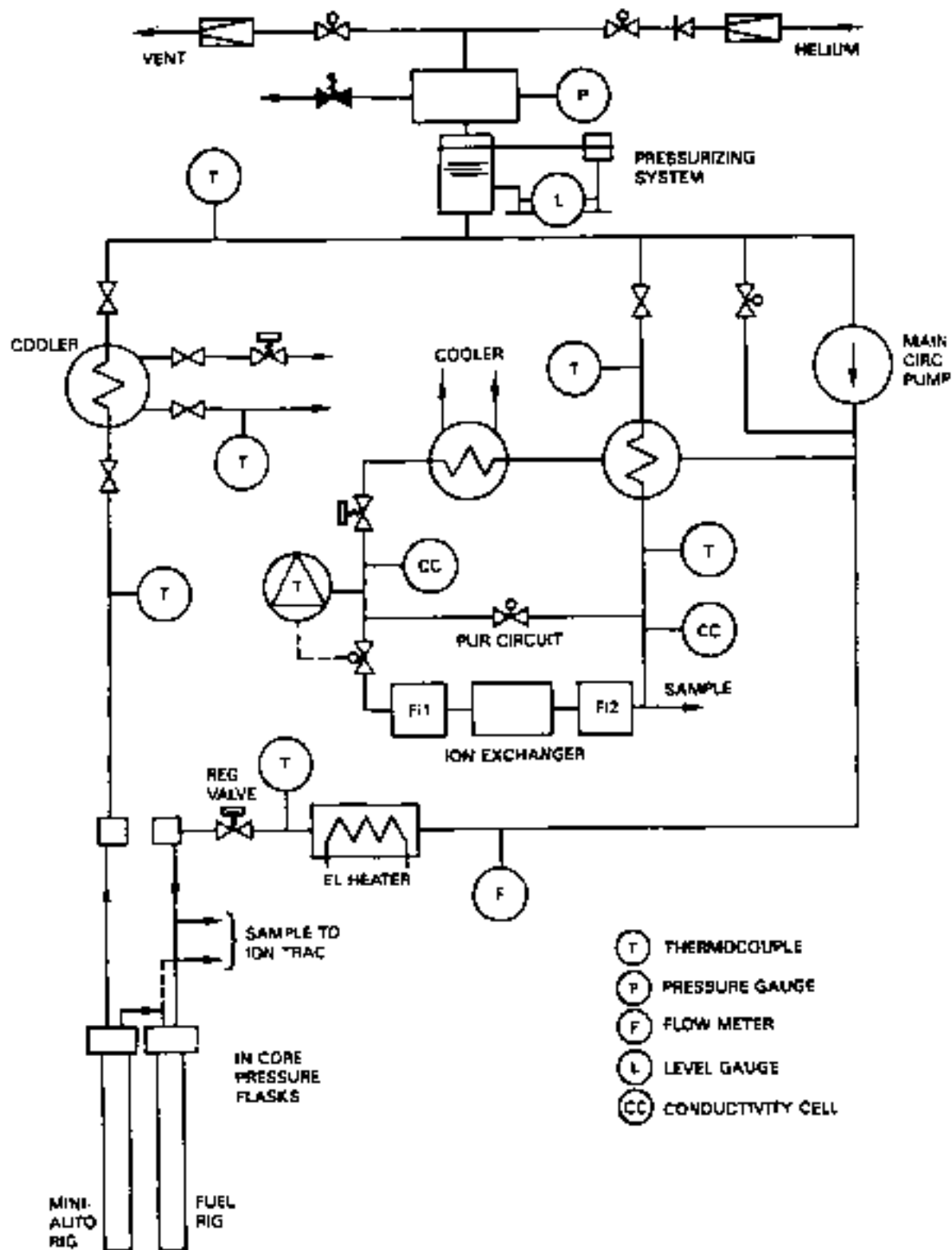


Figure 1 Schematic of BWR Corrosion Loop

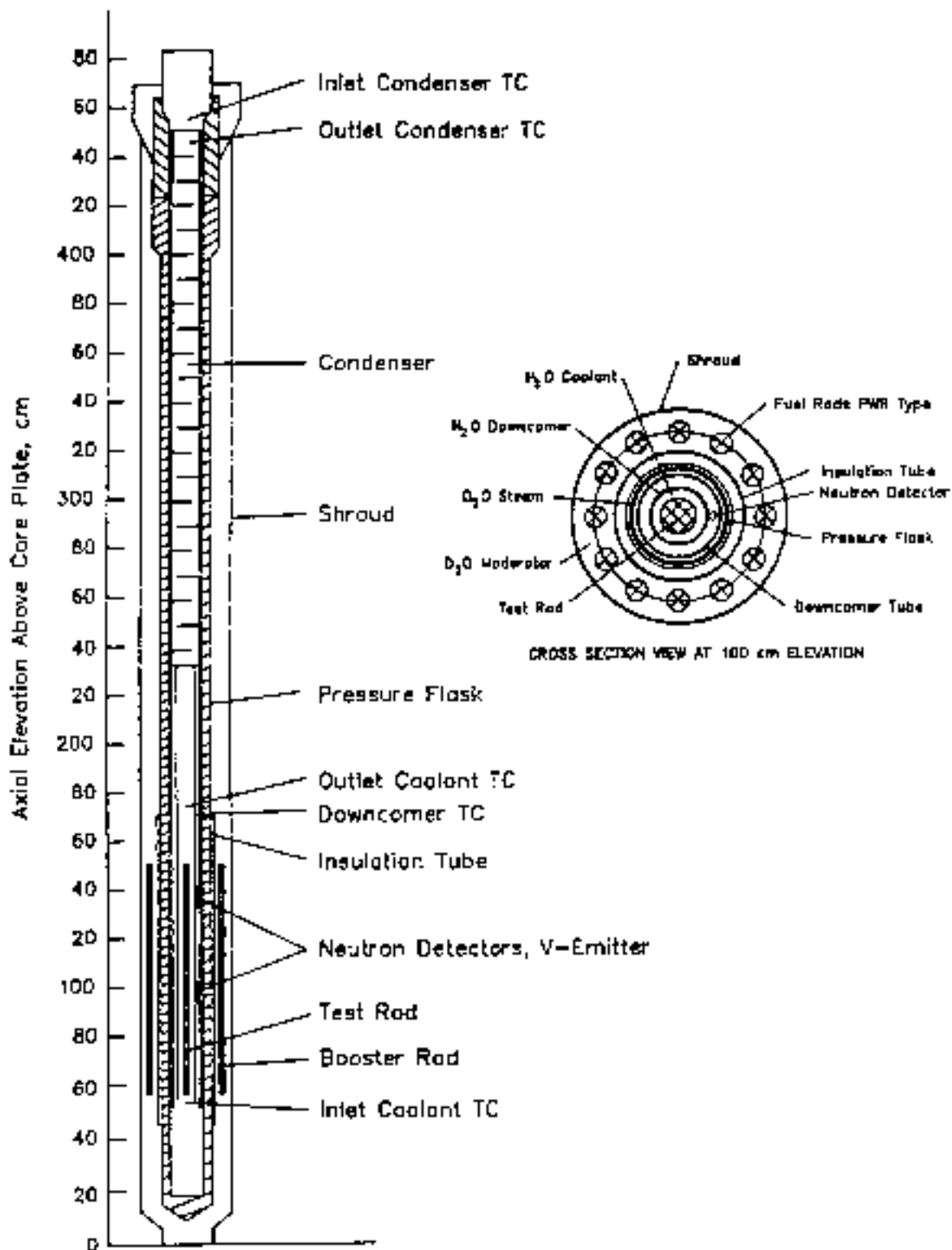


Figure 2 In-Core Rig Configuration

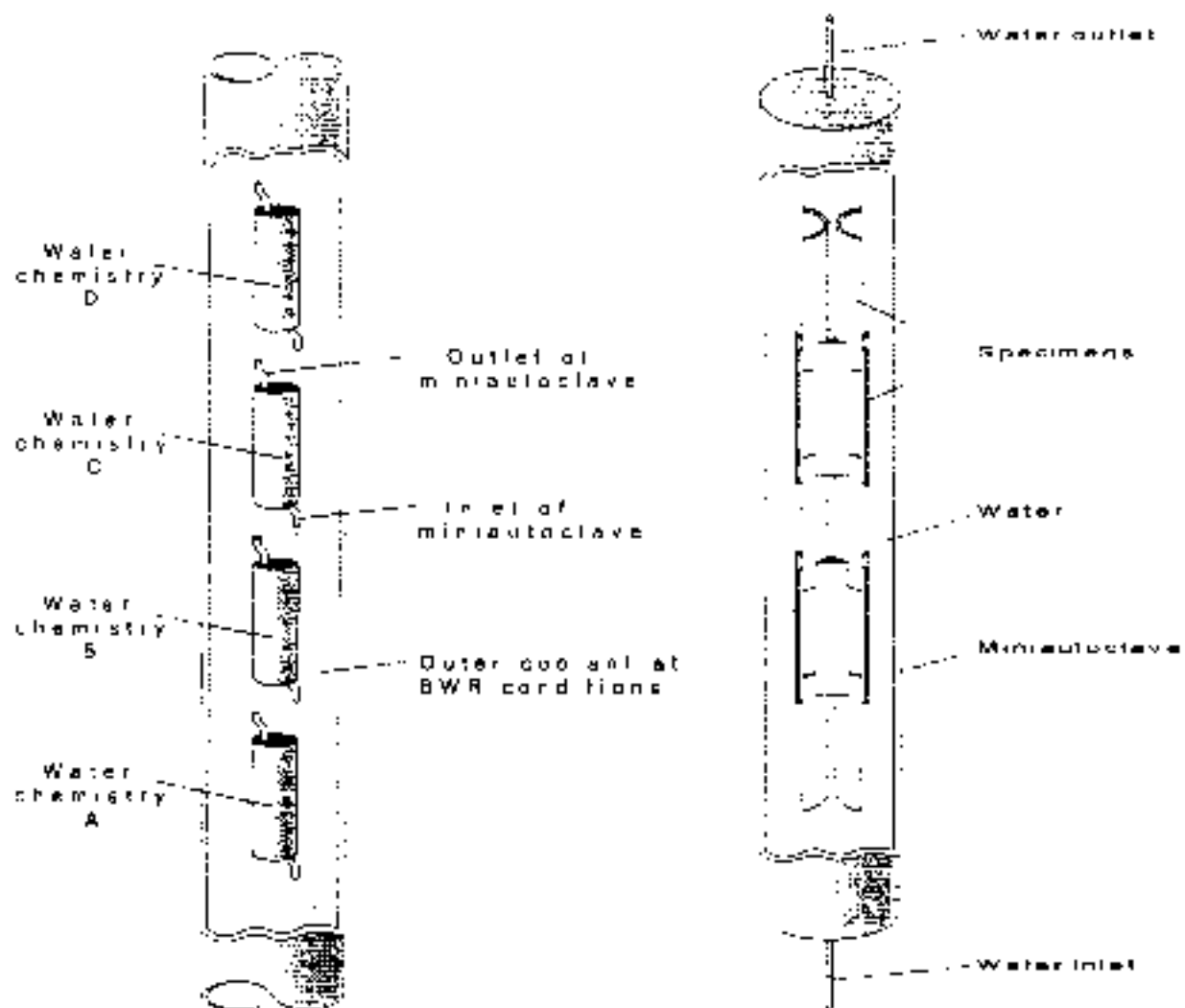


Figure 3 Schematic of Mini-Autoclave Rig Containing Four Mini-Autoclaves (left). On the right is a detailed view of an individual mini-autoclave and the specimen loading scheme.

After each test, the fuel rods, mini-autoclave containers, and mini-autoclave specimens were examined extensively at the IFE laboratory in Kjeller, Norway, at the NFD laboratory in Oarai, Japan, and at the GE Vallecitos Nuclear Center in Pleasanton, California. The examinations included visuals, macro-photography, fuel rod eddy current liftoff measurements, x-ray diffraction and electron probe micro-analysis (EPMA) of crud deposits, optical microscopy, and hydrogen content measurements.

This final report contains (1) a summary of the program results that have been presented in interim reports [1-10] and (2) a comprehensive evaluation of the program results.

2

SUMMARY OF CORROSION TESTS AND RESULTS

Mini-Autoclave Tests

The nominal loop inlet water chemistry conditions for the five mini-autoclave tests are summarized in Table 2. Table 3 lists the measured values of dissolved oxygen, dissolved hydrogen and major impurity elements at both the loop inlet and outlet. The radiation water chemistry experiment (RWCE, 5-C) was used to acquire data for verification of the water radiolysis codes and includes seventeen short-term tests; Table 4 summarizes the water chemistry data for that test.

The fifteen alloy materials used in the mini-autoclave irradiation tests are summarized in Table 5. Ten specimens were loaded in the mini-autoclave containers in Tests 1-4, whereas eleven specimens were loaded in the fifth test. Alloys A, A2, A3, B, and C are heat treated Zircaloy-2 materials, whereas Alloy D is not. Alloys A, A2, and A3 have controlled chemistry (e.g., 1.3% Sn, 0.18 Fe, 0.10 Cr, 0.07 Ni), whereas B, C, and D are from normal chemistry ingots (e.g., 1.5% Sn, 0.16 Fe, 0.10 Cr, 0.05 Ni). The Zircaloy materials were ranked in ex-reactor nodular corrosion steam tests (410°C/4 hours + 520°C/16 hours at 1750 psig) in the following order: A (including A, A2, A3), B, C and D, with A having the highest corrosion resistance and D having the lowest corrosion resistance. Alloys E, F, G, H, I, and J are all alternate (non-Zircaloy) Zr alloys. The cumulative annealing parameter, ΣA^1 , for the materials is also given in Table 5.

The oxide thicknesses of the mini-autoclave specimens are summarized in Table 6. The average uniform oxide thickness and nodular oxide thickness are tabulated separately. The nodular oxide thickness values include the maximum nodule thickness as well as the nodular coverage or the number of nodules. Figures 4 through 8 graphically display the mini-autoclave specimen corrosion results based on the data in Table 6. The oxide thicknesses are quite varied due to the broad nature of the test environments.

¹ $\Sigma A = \Sigma t_i \exp(Q/RT_i)$, where t_i and T_i are the time and temperature, respectively, of the i_{th} heat treatment after the last precipitate solution anneal and quench; $Q/R = 40,000$ K.

Table 2
Mini-Autoclave Irradiation Test Water Chemistry Conditions (Inlet)

MAC#		Test 1	Test 2	Test 3	Test 4	Test 5
A	Added Ingredients	Na ₂ S	350 ppb Cr as Na ₂ Cr ₂ O ₇	LHC oil	valerizing FW (CNSWC)	200 ppm SrO ₂
	O ₂	275	821	759	0742	703
	H ₂	26	0	0	0253	0
B	Added Ingredients	300 ppb Cu as Cu ₂ SO ₄	400 ppb Cu as CuSO ₄	200 ppm Na ₂ SO ₃ + 1 ppm for initial 5 days	Res. p. Induron	500 ppm Na ₂ CO ₃
	O ₂	277	790	513	729	723
	H ₂	27	0	0	0	0
C	Added Ingredients	none	300 ppb Na ₂ S	none	none	(Radiation Water Chemistry Experiment)
	O ₂	810	765	1221	0	var. pp. b
	H ₂	0	0	0	500	var. pp. b
D	Added Ingredients	100 ppb Zn as Zn(NO ₃) ₂	300 ppb Cu as Cu ₂ SO ₄ 100 ppb Zn as ZnSO ₄ 400 ppb Cr as Na ₂ Cr ₂ O ₄	500 ppm Na ₂ SO ₃	1 ppm Zn as ZnSO ₄	1 ppm Zn as ZnSO ₄
	O ₂	287	756	796	747	0
	H ₂	27	0	0	0	385

O₂ and H₂ concentrations in ppb

Table 3
Summary of Water Chemistries in the Mini-Autoclave Irradiation Tests

MAC	Test 1		Test 2		Test 3		Test 4		Test 5	
	inlet	outlet	inlet	outlet	inlet	outlet	inlet	outlet	inlet	outlet
A	O ₂	275	7				O ₂	0792		
	H ₂	35	0	410	759	277	H ₂	48300	0	445
	pH	6.9	6.1	6.2	5.2	6.5	pH	5.2	5.8	5.5
	Fe ²⁺	2	0	N.A.	N.A.	200	Fe ²⁺	1	0	0
	Ni ²⁺	2	4	200	N.A.	20	Ni ²⁺	1	1	0
					N.A.	20			171,000	147,000
B	O ₂	231	450	526	815	2,407	O ₂	729	0	8,462
	H ₂	27	105	16	0	0	H ₂	0	0	925
	pH	6.6	5.5	5.7	5.8	9.5	pH	2.5	3.3	10.8
	Cu ²⁺	900	80	70	20,380	40,000	Fe ²⁺	13	237,000	299,000
	NO ₃ ⁻	600	275	400	65,386	65,000	SO ₄ ²⁻	890	0	0
	NO ₂ ⁻	0	130				NO ₂ ⁻	0	400	0
C	O ₂	850	391	348	1,221	219	O ₂	0	0	0
	H ₂	0	4	0	0	0	H ₂	501	451	0
	pH	7.0	5.9	6.1	4.5	6.0	pH	5.5	6.1	5.2
	Ni ²⁺	0	1	N.A.			Fe ²⁺	0	80	0
	Ni ³⁺	0	1	10			Ni ³⁺	0	5	0
D	O ₂	357	10	346	786	295	O ₂	347	466	226
	H ₂	27	26	7	0	0	H ₂	0	0	397
	pH	6.1	6.6	4.5	6.2	6.0	pH	5.8	5.0	5.2
	Zn ²⁺	200	100	100	160,000	160,000	Fe ²⁺	0	0	700
	NO ₃ ⁻	200	15	90	160,380	150,000	Zn ²⁺	901	600	1,400
	NO ₂ ⁻	0	10	1,000	160,380	150,000	SO ₄ ²⁻	1,400	1,400	1,400

Test Spec:	1A: 250ppmCu ²⁺ as CuCl ₂	2A: 300ppmCu ²⁺ as NaHCO ₃	3A: 300ppmCu ²⁺ as CuSO ₄	4A: 400ppmCu ²⁺ as CuSO ₄	5A: 200ppmCu ²⁺ as Na ₂ CO ₃
	1B: 400ppmCu ²⁺ as CuCl ₂	2B: 500ppmCu ²⁺ as CuSO ₄	3B: 200ppmNa ₂ SO ₄	4B: 400ppmNa ₂ SO ₄	5B: 600ppmNa ₂ SO ₄
	1C: 800ppmCu ²⁺	2C: 100ppmFe ²⁺	3C: 120ppmFe ²⁺	4C: 500ppmFe ²⁺ as FeCl ₃	5C: 400ppmZn ²⁺ as ZnSO ₄
	1D: 200ppmZn ²⁺ as ZnSO ₄	2D: Mixed (Cu ²⁺ :2.5 * 10 ³ ppm)	3D: 500ppmNa ₂ SO ₄	4D: 100ppmZn ²⁺ as ZnSO ₄	5D: 100ppmZn ²⁺ as ZnSO ₄

Table 4
Summary of Water Chemistry Data in the Mini-Autoclave Radiation Water Chemistry Experiment

Sequence	A1		A2		A3		A4		B1		B2		B3		B4		B5	
	inlet	outlet	inlet	outlet	inlet	outlet	inlet	outlet	inlet	outlet	inlet	outlet	inlet	outlet	inlet	outlet	inlet	outlet
O ₂ (ppb)	0	0	0	0	0	0	0	0	544	16	760	490	753	156	770	13	768	27
H ₂ (ppb)	0	0	0	0	0	0	0	0	0	0	0	0	0	0	0	0	0	0
pH	5.7	7	5.3	5.8	5.85	6	6.3	5.95	5.6	5.7	5.6	5.7	5.2	5.2	5.6	5.6	6.4	5.5
Ca ²⁺ (ppm)	6.15	0.4	1.05	0.63	0.09	0.34	0.75	0.46	0.12	0.37	0.12	0.34	1.84	1.84	0.11	0.11	0.47	1.03
NaH ₂ PO ₄	-	-	14.6	16.5	0	0	54.5	6.2	-	-	-	-	0.85	1.47	3	1.7	35.5	4.1
Na ₂ HPO ₄	-	-	0	7.2	0	0	0	0	-	-	-	-	0	0	0	0.2	0	2.9
Na ₂ CO ₃ (ppb)	-	-	37.0	152	0.95	0.83	1.1	0.1	-	-	-	-	3.25	32.3	3	30.7	2.3	16.4
NaHPO ₄	-	-	-	-	-	10	-	40	-	-	-	-	-	-	11.7	108	11	11
Sequence	B6		B7		B8		B9		B10		C1		C2		D1			
	inlet	outlet	inlet	outlet	inlet	outlet	inlet	outlet	inlet	outlet	inlet	outlet	inlet	outlet	inlet	outlet		
O ₂ (ppb)	765	465	773	524	452	560	819	505	813	565	0	0	0	0	792	400		
H ₂ (ppb)	0	0	0	0	0	0	0	0	0	0	0	0	0	0	-	-		
pH	5.9	5.6	5.9	5.7	5.7	5.9	6	6.1	6	5.7	6.1	6.2	6.2	6.2	6	5.7		
Ca ²⁺ (ppm)	0.51	1	0.49	0.82	0.93	0.42	0.53	0.34	0.63	0.6	1.6	0.53	0.1	0.34	0.77	0.8		
NaH ₂ PO ₄	4.2	5.5	-	-	-	-	-	-	-	-	2	12.2	0.4	3.8	1.1	2.2		
Na ₂ HPO ₄	0	4	-	-	-	-	-	-	-	-	6.7	52.7	0	0	0	1.4		
Na ₂ CO ₃ (ppb)	179	183	-	-	-	-	-	-	-	-	28.1	18.4	0	0	17.1	157		
NaHPO ₄	-	-	-	-	-	-	-	-	-	-	34	38	-	10	-	-		
C ¹⁴ (ppb)	-	-	-	-	-	-	-	-	-	-	-	-	-	-	-	-		
Cu ²⁺ (ppb)	90	5.3	90	25.0	-	-	-	-	-	-	-	-	-	-	-	-		
SO ₄ ²⁻ (ppm)	-	-	16.5	16.7	-	-	-	-	-	-	-	-	-	-	90	30		
Na ⁺ (ppm)	-	-	-	-	-	-	34	30.1	-	173	-	-	-	-	-	-		
Zn ²⁺ (ppb)	-	-	-	-	-	-	-	-	-	5.5	-	-	-	-	-	-		
CrO ₄ ²⁻	-	-	-	-	24.7	133	238	131	-	-	-	-	-	-	-	-		
Cu ²⁺ (ppm)	-	-	-	-	1.13	60	9.5	51.2	-	-	-	-	-	-	-	-		
Na ⁺ (ppm)	-	-	-	-	-	-	55	40	-	-	-	-	-	-	-	-		

Test spec:

- A1: High purity water only
 A2: High purity water + 400ppb HNO₃
 A3: High purity water + 100ppb N₂
 A4: High purity water + 100ppb NH₄OH
 B1: High purity water + 300ppb O₂
 B2: High purity water + 800ppb O₂
 B3: High purity water + 800ppb O₂ + 300ppb HNO₃
 B4: High purity water + 800ppb O₂ + 300ppb H₂O₂
 B5: High purity water + 800ppb O₂ + 300ppb H₂O₂
 B6: High purity water + 800ppb O₂ + 300ppb H₂O₂
 B7: High purity water + 800ppb O₂ + 300ppb H₂O₂
 B8: High purity water + 800ppb O₂ + 300ppb H₂O₂
 B9: High purity water + 800ppb O₂ + 300ppb H₂O₂
 B10: High purity water + 800ppb O₂ + 300ppb H₂O₂
 C1: High purity water + 25ppb H₂ + 300ppb HNO₃
 C2: High purity water + 25ppb H₂ + 300ppb N₂
 D1: High purity water + 25ppb H₂ + 300ppb O₂ + 300ppb H₂O₂

Table 5
Alloy Materials Used for the Mini-Autoclave Irradiation Tests

Alloy ID	Alloy Description	ΣA	1	2	3	4	5
A	Zircaloy-2 IPHT* (High Corrosion Resistance)	1.5 E-20	•	•			
A2	Zircaloy-2 IPHT (High Corrosion Resistance)	1.5 E-20			•		
A3	Zircaloy-2 IPHT (High Corrosion resistance)	1.5 E-20				•	•
B	Zircaloy-2 TSHT** (NFD, MAC Container)	1.5 E-19	•	•	•	•	•
C	Zircaloy-2 TSHT (Intermediate Corrosion Resistance)	1.6 E-19	•	•	•	•	•
D	Non-Heat Treated Zircaloy-2 (Low Corrosion Resistance)	1.2 E-18	•	•	•		
D2	Zircaloy-2 TSHT (High Corrosion Resistance)	1.2 E-18				•	•
E	High Fe Zircaloy-2 (Zr-1.5Sn-0.25Fe-0.10Cr-0.05Ni)	4.2 E-20	•	•	•	•	•
F	High Fe/Ni Zircaloy-2 (Zr-1.5Sn-0.25Fe-0.10Cr-0.10Ni)	4.2 E-20	•	•	•	•	•
G	Zircaloy-2 + 0.5Nb	1.4 E-19	•	•	•	•	•
H	Zr + 0.3Nb + 0.3Mo	4.2 E-19	•	•	•	•	•
I	Zr + 1.2Bi + 0.5Nb	2.1 E-19	•	•	•	•	•
J	Zr + 0.7Bi + 0.5Nb	1.0 E-19	•	•	•	•	
J2	Zircaloy-2 MAC Container (alloy B)	1.5 E-19					•
J3	Alloy D (pre-oxidized in 520°C steam)	1.2 E-18					•

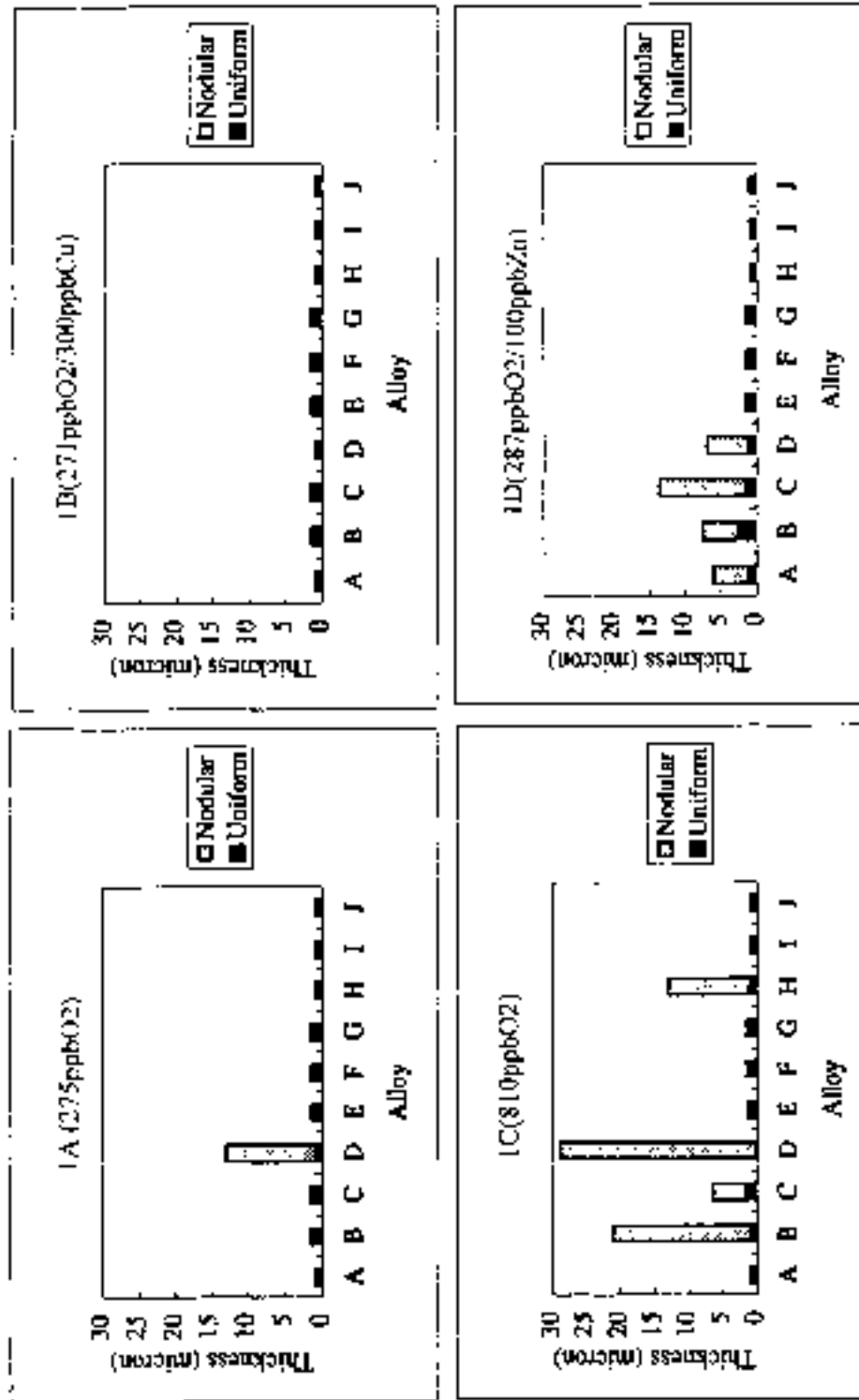
* In process heat treatment

** Tubeshell heat treatment

Summary of Corrosion Tests and Results

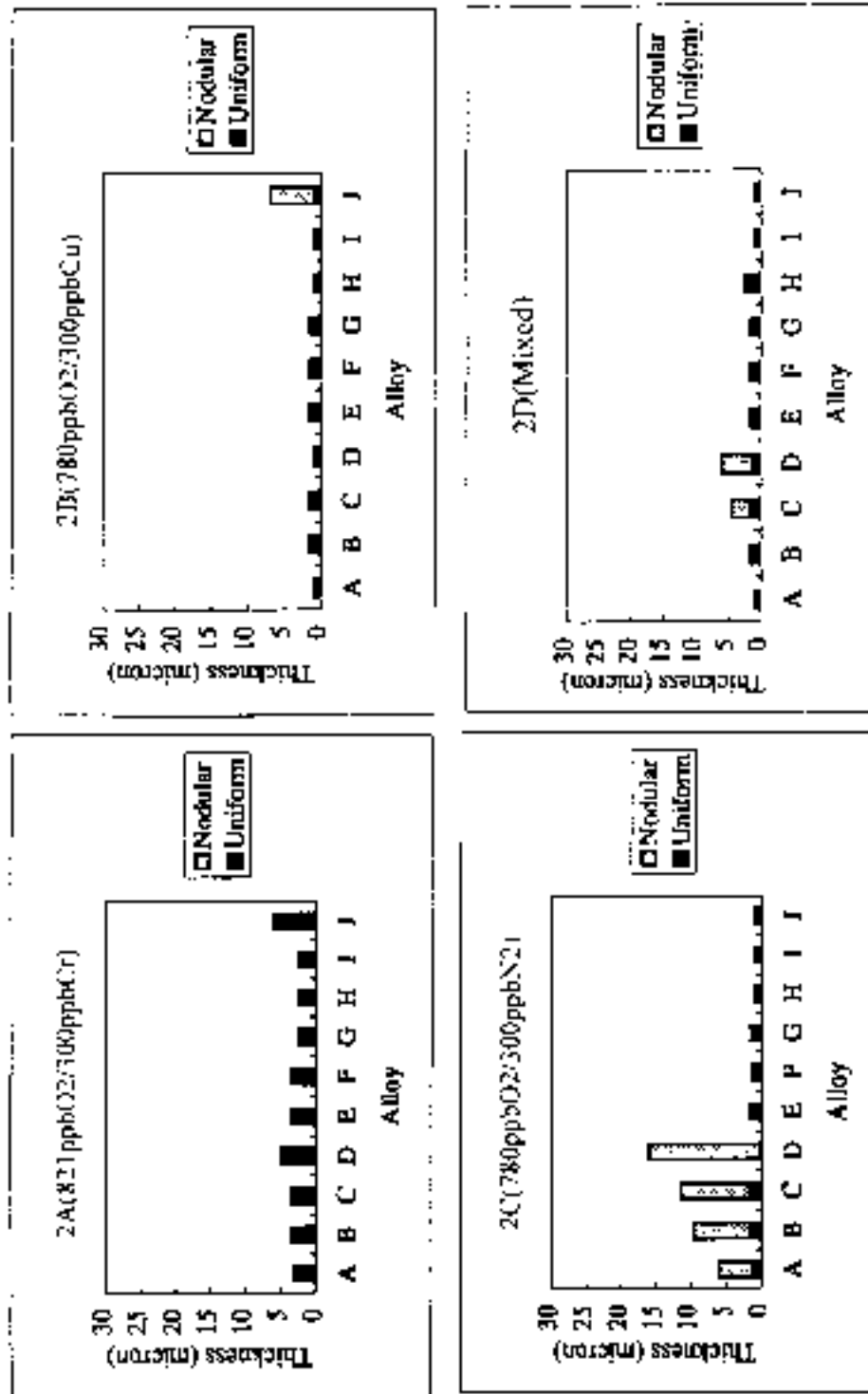
Table 6
Summary of the Mini-Autoclave Specimen Outer Surface Oxide Thicknesses

Material	Alloy	Test 1		Test 2		Test 3		Test 4		Test 5		Thickness (microns)
		Uniform	Spicular	Uniform	Spicular	Uniform	Spicular	Uniform	Spicular	Uniform	Spicular	
A	A	-1	-	-3	-	1-2(A3)	-	1-2(A3)	-	1-2(A3)	-	-
	B	1-2	-	1-4	-	1-2	-	1-2	-	1-2	-	
	C	1-2	-	1-4	-	1-2	-	1-2	-	1-2	-	
	D	-1	-12(A3)	-5(A3)	-	1-2	-	1-2(12)	3(1)	1-2(12)	-	
	E	1-2	-	3-4	-	1-2	-	1-2	-	1-2	-	
	F	1-2	-	3-4	-	1-2	-	1-2	-	1-2	-	
	G	1-2	-	3-4	-	1-2	-	1-2	-	1-2	-	
	H	-1	-	2-5	-	1-2	-	1-2	-	1-2	-	
	I	-3	-	2-5	-	1-2	-	1-2	-	1-2	-	
	J	-1	-	-6	-	1-2	-	1-2	-	1-2(20)(A3)	-	
B	A	-1	-	-1	-	1-2(A3)	-	1-2(A3)	-	1-2(A3)	-	-
	B	1-2	-	-1	-	1-2	-	1-2	-	1-2	-	
	C	1-2	-	-1	-	1-2	-	1-2	-	1-2	-	
	D	-1	-	-1	-	1-2	-	1-2(12)	3(1)	2-2(12)	-	
	E	1-2	-	1-2	-	1-2	-	1-2	-	1-2	-	
	F	1-2	-	1-2	-	1-2	-	1-2	-	1-2	-	
	G	1-2	-	1-2	-	1-2	-	1-2	-	1-2	-	
	H	-1	-	-1	-	1-2	-	1-2	-	1-2	-	
	I	-1	-	-1	-	1-2	-	1-2	-	1-2	-	
	J	-1	-	-1	-	1-2	-	1-2	-	1-2	-	
C	A	-1	-	-1	-	1-2(A3)	-	1-2(A3)	-	1-2(A3)	-	-
	B	-1	-2(A3)	-1	-8(A3)	1-2	-	1-2	-	1-2	-	
	C	-1	-6(A3)	-1	-10(A3)	1-2	-	1-2	-	1-2	-	
	D	-1	-2(A3)	-1	-10(A3)	1-2	-	1-2(12)	-	1-2(12)	-	
	E	1-2	-	1-2	-	1-2	-	1-2	-	1-2	-	
	F	1-2	-	1-2	-	1-2	-	1-2	-	1-2	-	
	G	1-2	-	1-2	-	1-2	-	1-2	-	1-2	-	
	H	-1	-12(A3)	-1	-	1-2	-	1-2	-	1-2	-	
	I	-1	-	-1	-	1-2	-	1-2	-	1-2	-	
	J	-1	-	-1	-	1-2	-	1-2	-	1-2	-	
D	A	-1	-5(A3)	-1	-	1-2(A3)	-	1-2(A3)	-	1-2(A3)	-	-
	B	1-2	-5(A3)	1-2	-	1-2	-	1-2	-	1-2	-	
	C	1-2	-5(A3)	1-2	-	1-2	-	1-2	-	1-2	-	
	D	-1	-6(A3)	-1	-	1-2	-	1-2(12)	-	1-2(12)	-	
	E	1-2	-	1-2	-	1-2	-	1-2	-	1-2	-	
	F	1-2	-	1-2	-	1-2	-	1-2	-	1-2	-	
	G	1-2	-	1-2	-	1-2	-	1-2	-	1-2	-	
	H	-1	-	-1	-	1-2	-	1-2	-	1-2	-	
	I	-1	-	-1	-	1-2	-	1-2	-	1-2	-	
	J	-1	-	-1	-	1-2	-	1-2	-	1-2	-	
E	A	-1	-	-1	-	1-2	-	1-2	-	1-2	-	-
	B	1-2	-	1-2	-	1-2	-	1-2	-	1-2	-	
	C	1-2	-	1-2	-	1-2	-	1-2	-	1-2	-	
	D	-1	-	-1	-	1-2	-	1-2(12)	-	1-2(12)	-	
	E	1-2	-	1-2	-	1-2	-	1-2	-	1-2	-	
	F	1-2	-	1-2	-	1-2	-	1-2	-	1-2	-	
	G	1-2	-	1-2	-	1-2	-	1-2	-	1-2	-	
	H	-1	-	-1	-	1-2	-	1-2	-	1-2	-	
	I	-1	-	-1	-	1-2	-	1-2	-	1-2	-	
	J	-1	-	-1	-	1-2	-	1-2	-	1-2	-	
F	A	-1	-	-1	-	1-2	-	1-2	-	1-2	-	-
	B	1-2	-	1-2	-	1-2	-	1-2	-	1-2	-	
	C	1-2	-	1-2	-	1-2	-	1-2	-	1-2	-	
	D	-1	-	-1	-	1-2	-	1-2(12)	-	1-2(12)	-	
	E	1-2	-	1-2	-	1-2	-	1-2	-	1-2	-	
	F	1-2	-	1-2	-	1-2	-	1-2	-	1-2	-	
	G	1-2	-	1-2	-	1-2	-	1-2	-	1-2	-	
	H	-1	-	-1	-	1-2	-	1-2	-	1-2	-	
	I	-1	-	-1	-	1-2	-	1-2	-	1-2	-	
	J	-1	-	-1	-	1-2	-	1-2	-	1-2	-	
G	A	-1	-	-1	-	1-2	-	1-2	-	1-2	-	-
	B	1-2	-	1-2	-	1-2	-	1-2	-	1-2	-	
	C	1-2	-	1-2	-	1-2	-	1-2	-	1-2	-	
	D	-1	-	-1	-	1-2	-	1-2(12)	-	1-2(12)	-	
	E	1-2	-	1-2	-	1-2	-	1-2	-	1-2	-	
	F	1-2	-	1-2	-	1-2	-	1-2	-	1-2	-	
	G	1-2	-	1-2	-	1-2	-	1-2	-	1-2	-	
	H	-1	-	-1	-	1-2	-	1-2	-	1-2	-	
	I	-1	-	-1	-	1-2	-	1-2	-	1-2	-	
	J	-1	-	-1	-	1-2	-	1-2	-	1-2	-	
H	A	-1	-	-1	-	1-2	-	1-2	-	1-2	-	-
	B	1-2	-	1-2	-	1-2	-	1-2	-	1-2	-	
	C	1-2	-	1-2	-	1-2	-	1-2	-	1-2	-	
	D	-1	-	-1	-	1-2	-	1-2(12)	-	1-2(12)	-	
	E	1-2	-	1-2	-	1-2	-	1-2	-	1-2	-	
	F	1-2	-	1-2	-	1-2	-	1-2	-	1-2	-	
	G	1-2	-	1-2	-	1-2	-	1-2	-	1-2	-	
	H	-1	-	-1	-	1-2	-	1-2	-	1-2	-	
	I	-1	-	-1	-	1-2	-	1-2	-	1-2	-	
	J	-1	-	-1	-	1-2	-	1-2	-	1-2	-	
I	A	-1	-	-1	-	1-2	-	1-2	-	1-2	-	-
	B	1-2	-	1-2	-	1-2	-	1-2	-	1-2	-	
	C	1-2	-	1-2	-	1-2	-	1-2	-	1-2	-	
	D	-1	-	-1	-	1-2	-	1-2(12)	-	1-2(12)	-	
	E	1-2	-	1-2	-	1-2	-	1-2	-	1-2	-	
	F	1-2	-	1-2	-	1-2	-	1-2	-	1-2	-	
	G	1-2	-	1-2	-	1-2	-	1-2	-	1-2	-	
	H	-1	-	-1	-	1-2	-	1-2	-	1-2	-	
	I	-1	-	-1	-	1-2	-	1-2	-	1-2	-	
	J	-1	-	-1	-	1-2	-	1-2	-	1-2	-	
J	A	-1	-	-1	-	1-2	-	1-2	-	1-2	-	-
	B	1-2	-	1-2	-	1-2	-	1-2	-	1-2	-	
	C	1-2	-	1-2	-	1-2	-	1-2	-	1-2	-	
	D	-1	-	-1	-	1-2	-	1-2(12)	-	1-2(12)	-	
	E	1-2	-	1-2	-	1-2	-	1-2	-	1-2	-	
	F	1-2	-	1-2	-	1-2	-	1-2	-	1-2	-	
	G	1-2	-	1-2	-	1-2	-	1-2	-	1-2	-	
	H	-1	-	-1	-	1-2	-	1-2	-	1-2	-	
	I	-1	-	-1	-	1-2	-	1-2	-	1-2	-	
	J	-1	-	-1	-	1-2	-	1-2	-	1-2	-	
Footnote	1-2(12)ppb(12) to 600(12)	2-4	400ppb(16) to 500(16)	1-4	100... 1000ppb(12)	4-10	100ppb(12) to 400(12)	4-10	100ppb(12) to 400(12)	4-10	100ppb(12) to 400(12)	90(12)
	1-2(12)ppb(12) to 600(12)	2-4	400ppb(16) to 500(16)	1-4	100... 1000ppb(12)	4-10	100ppb(12) to 400(12)	4-10	100ppb(12) to 400(12)	4-10	100ppb(12) to 400(12)	90(12)
	1-2(12)ppb(12) to 600(12)	2-4	400ppb(16) to 500(16)	1-4	100... 1000ppb(12)	4-10	100ppb(12) to 400(12)	4-10	100ppb(12) to 400(12)	4-10	100ppb(12) to 400(12)	90(12)
	1-2(12)ppb(12) to 600(12)	2-4	400ppb(16) to 500(16)	1-4	100... 1000ppb(12)	4-10	100ppb(12) to 400(12)	4-10	100ppb(12) to 400(12)	4-10	100ppb(12) to 400(12)	90(12)
	1-2(12)ppb(12) to 600(12)	2-4	400ppb(16) to 500(16)	1-4	100... 1000ppb(12)	4-10	100ppb(12) to 400(12)	4-10	100ppb(12) to 400(12)	4-10	100ppb(12) to 400(12)	90(12)
	1-2(12)ppb(12) to 600(12)	2-4	400ppb(16) to 500(16)	1-4	100... 1000ppb(12)	4-10	100ppb(12) to 400(12)	4-10	100ppb(12) to 400(12)	4-10	100ppb(12) to 400(12)	90(12)
	1-2(12)ppb(12) to 600(12)	2-4	400ppb(16) to 500(16)	1-4	100... 1000ppb(12)	4-10	100ppb(12) to 400(12)	4-10	100ppb(12) to 400(12)	4-10	100ppb(12) to 400(12)	90(12)
	1-2(12)ppb(12) to 600(12)	2-4	400ppb(16) to 500(16)	1-4	100... 1000ppb(12)	4-10	100ppb(12) to 400(12)	4-10	100ppb(12) to 400(12)	4-10	100ppb(12) to 400(12)	90(12)
	1-2(12)ppb(12) to 600(12)	2-4	400ppb(16) to 500(16)	1-4	100... 1000ppb(12)	4-10	100ppb(12) to 400(12)	4-10	100ppb(12) to 400(12)	4-10	100ppb(12) to 400(12)	90(12)
1-2(12)ppb(12) to 600(12)	2-4	400ppb(16) to 500(16)	1-4	100... 1000ppb(12)	4-10	100ppb(12) to 400(12)	4-10	100ppb(12) to 400(12)	4-10	100ppb(12) to 400(12)	90(12)	



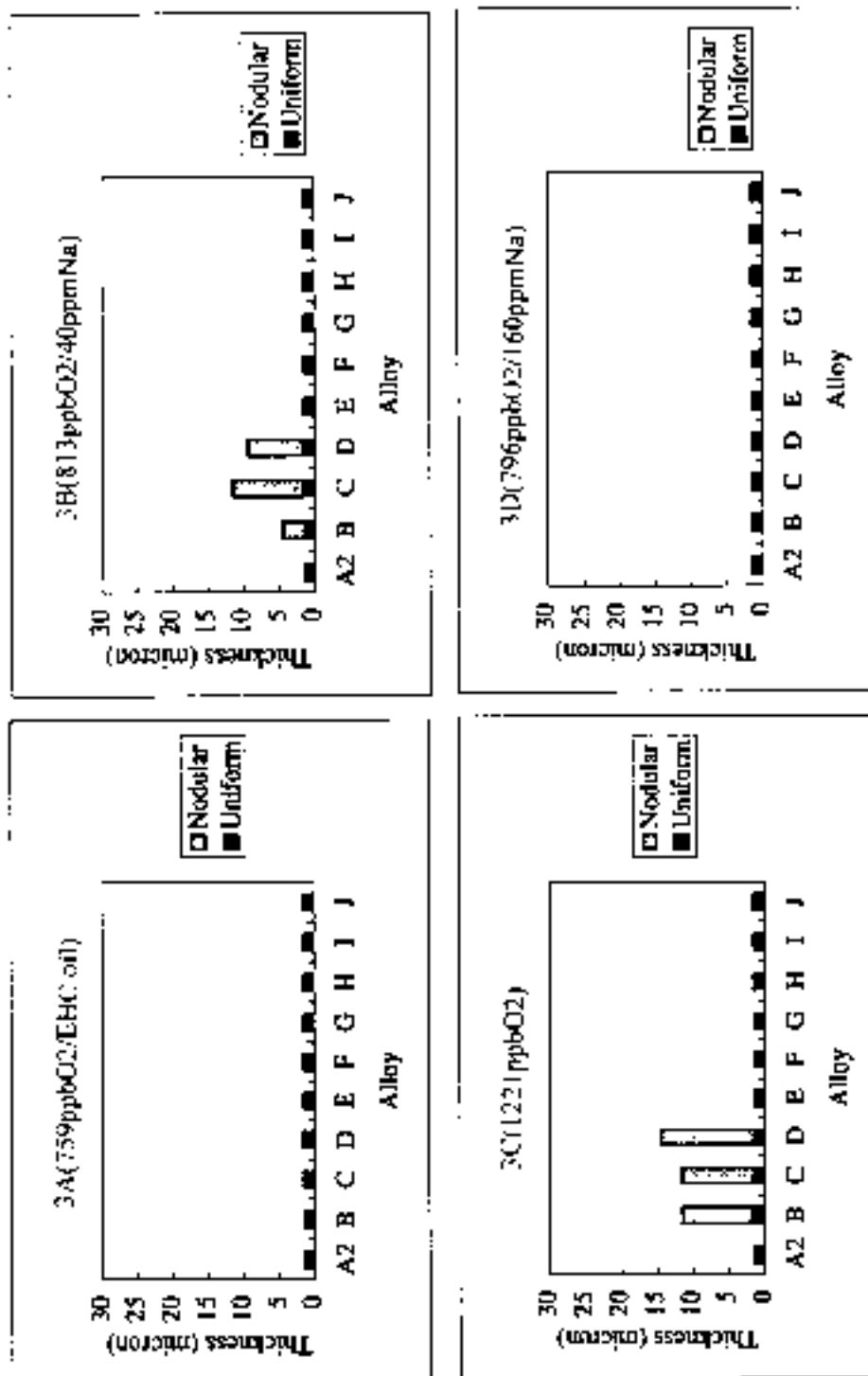
Alloy A: IPHT/Zry-2; B: TSH/Zry-2; C: Zry-2; D: Zry-2; Alloy E, Alloy F, Alloy G, Alloy H, Alloy I, Alloy J

Figure 4 Outer Surface Oxide Thickness of the Mini-Autoclave Specimens in the First Test



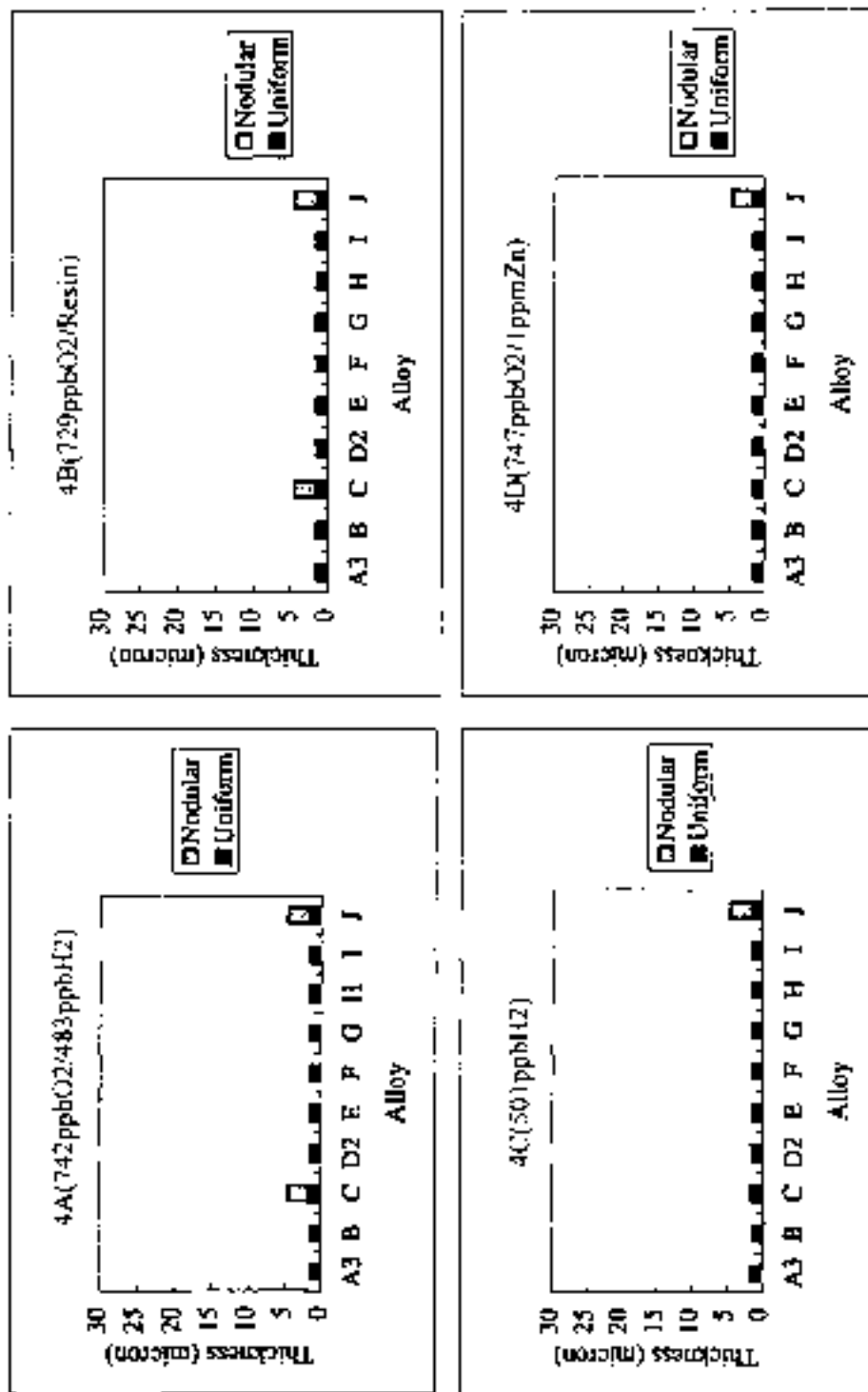
Alloy A: IPH1/Zry-2, B: TSH1/Zry-2, C: Zry-2, D: Zry-2, Alloy E: Alloy F, Alloy G, Alloy H, Alloy I, Alloy J

Figure 5 Outer Surface Oxide Thickness of the Mini-Autoclave Specimens in the Second Test



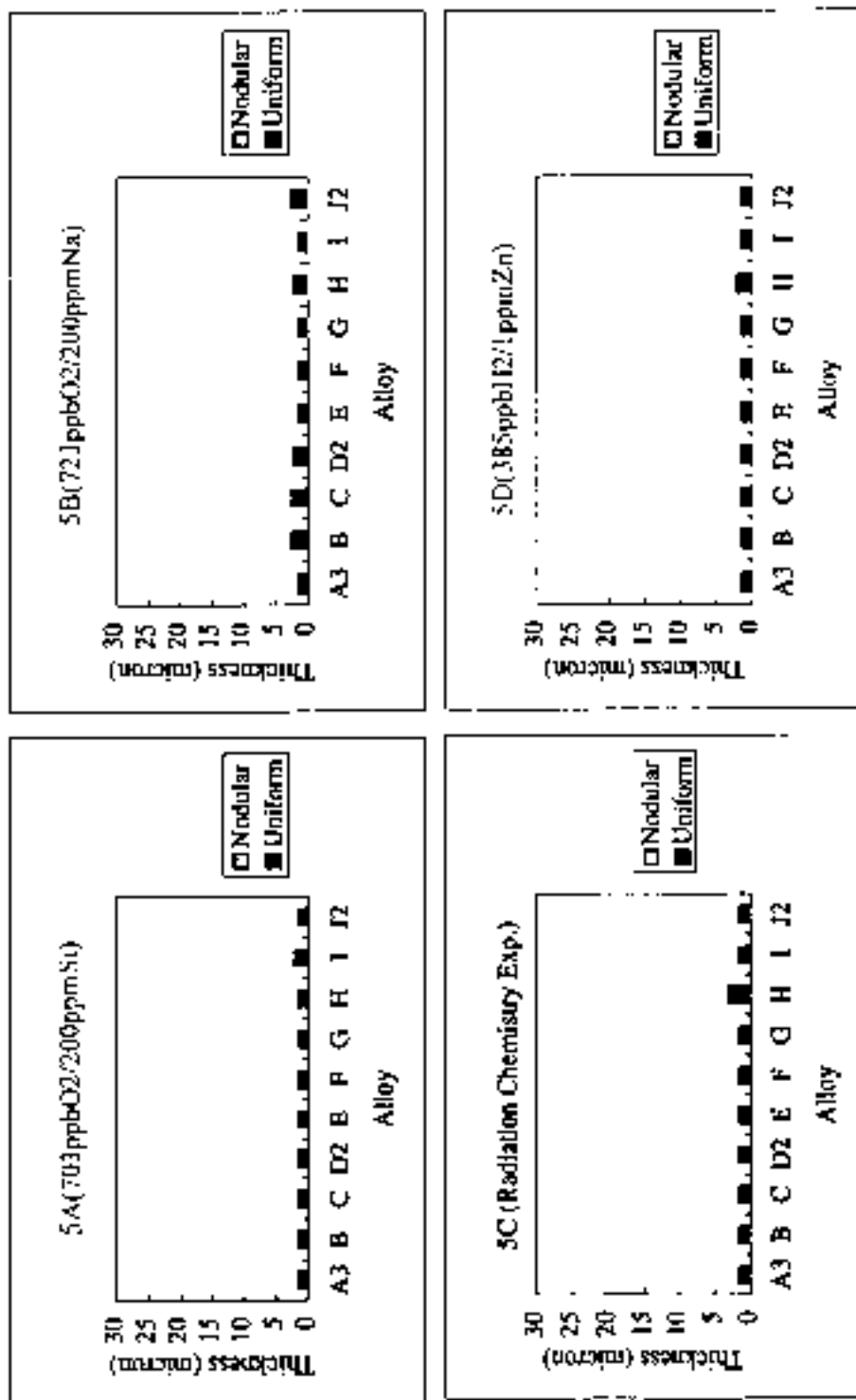
Alloy A: IPHT/Zry-2, B: TSHT/Zry-2, C: Zry-2, D: Zry-2,
Alloy E, Alloy F, Alloy G, Alloy H, Alloy I, Alloy J

Figure 6 Outer Surface Oxide Thickness of the Mini-Autoclave Specimens in the Third Test



Alloy A3: IPHT/Zry-2, B: TSHT/Zry-2, C: Zry-2, D: Zry-2,
Alloy E, Alloy F, Alloy G, Alloy H, Alloy I, Alloy J

Figure 7 Outer Surface Oxide Thickness of the Mini-Autoclave Specimens in the Fourth Test



Alloy A3: IPHT/Zry-2, B: TSHT/Zry-2, C: Zry-2, D: Zry-2,
Alloy E, Alloy F, Alloy G, Alloy H, Alloy I, Alloy J

Figure 8 Outer Surface Oxide Thickness of the Mini-Autoclave Specimens in the Fifth Test

Significant levels of nodular and uniform oxide growth occurred in some instances, even though the tests were short (100-140 days) compared to a typical BWR cycle (~500 days).

The hydrogen contents of the mini-autoclave specimens are summarized in Table 7. All of the mini-autoclave specimen hydrogen contents were estimated using metallographic standards. It should be noted that Alloys A and C in mini-autoclave Tests 1 and 2 had remnants of Zr liner on the inner surface; oxidation of the Zr caused anomalous hydrogen absorption in these instances.

Fuel Rod Tests

The nominal loop water chemistry conditions that were used in the six fuel rod tests are summarized in Table 8. Table 9 summarizes the measured water chemistry data, the neutronics data and the thermo-hydraulic conditions for the individual tests. The values listed in Table 9 are typical or average values representative of the test periods. For the most part, the test conditions met those specified in Table 1.

The alloy materials used in the fuel rod irradiation tests are summarized in Table 10. The five alloys are a subset of those used in the mini-autoclave tests. Zircaloy-2 Alloy C was used for the fuel cladding in Tests 1, 2 and 3. Tests 4, 5, 6a, and 6b used "zebra" cladding. The zebra cladding was fabricated by welding together segments of Alloys B, F, G and I, as shown in Figure 9.

UO₂ pellets were used in Tests 1, 4, 5, 6a, and 6b, while some alumina and UO₂ + 4% Gd₂O₃ pellets were loaded in Tests 2 and 3 to determine the effect of heat flux on cladding corrosion. The location of the alumina and gadolinia pellets in the Test 2 and 3 fuel rods is shown in Figure 10.

The outer surface oxide thicknesses of the fuel cladding specimens are summarized in Table 11. The data includes the maximum nodular thickness as well as the nodular coverage or the number of nodules. As with the mini-autoclave tests, the oxide thicknesses are quite varied due to the broad nature of the test environments, and significant levels of nodular and uniform oxide growth occurred in some instances.

The fuel rod cladding hydrogen contents are summarized in Table 12. The hydrogen contents were estimated using metallographic standards or were measured using inert gas fusion.

Table 8
Fuel Rod Irradiation Test Water Chemistry Conditions

Test No.	Test Description
1	UO ₂ 250 ppb O ₂ (inlet)
2	Gd zoned 350 ppb O ₂ (inlet)
3	Gd zoned 500 ppb O ₂ (inlet)
4	UO ₂ /Zebra cladding 1000 ppb O ₂ (outlet)
5	UO ₂ /Zebra cladding 350 ppb H ₂ (outlet)
6	UO ₂ /Zebra cladding (a) 25 ppb Zn + 400 ppb H ₂ (outlet) (b) 300 ppb Cr + 1000 ppb O ₂ (outlet)

Table 9
Summary of Fuel Rod Irradiation Test Operational Data

Cladding Type/ Fuel Type	Test 1 Zry-2 UO ₂	Test 2 Zry-2 UO ₂ -(U,Gd)O ₂	Test 3 Zry-2 UO ₂ -(U,Gd)O ₂	Test 4 Zebra UO ₂	Test 5 Zebra UO ₂	Test 6a Zebra UO ₂	Test 6b Zebra UO ₂
Water Chemistry							
Oxygen							
inlet (ppb)	250	350	500	1000			-
outlet (ppb)	-	600	1000	1000	-	-	1000
Hydrogen							
inlet (ppb)	-	30	30	30	350	-	-
outlet (ppb)	-	40	40	70	400	-	-
Injected Species							
	-	-	-	-	-	26ppbZn	300ppbCr ⁶⁺
Cations							
(ppb)	10	5	5	5	20	40	150 (Na ⁺)
Anions							
(ppb)	40	30	55	30	20	10	700 (CrO ₄ ²⁻)
Conductivity							
(μS/cm)	0.3	0.2	0.2	0.2	0.2	0.3	0.6
pH							
(-)	-	6.5	-	-	-	6.1	5.9
Coolant Condition							
Temperature							
(°C)	288	288	288	288	288	288	288
Pressure							
(bar)	74	74	74	73	73	73	73
Velocity							
(m/s)	2	2	2	2	2	2	2
Boiling Condition							
Onset of Boiling							
(cm)	30	35	40	35	35	40	35
Void Fraction							
(%)	45	35	40	50	45	45	45
Quality							
(-)	0.05	0.03	0.03	0.04	0.04	0.03	0.04
γ intensity							
(W/g)	1.3	1.3	1.2	1.2	0.9	1	-
φ (>1 MeV)							
(n/cm ² s)	6x10 ¹¹	4x10 ¹¹	5x10 ¹⁰	5x10 ¹¹	5x10 ¹¹	4x10 ¹²	5x10 ¹²
LEIR							
(W/cm)	200	140	150	240	200	230	250
BFPI							
(days)	120	140	120	140	110	100	100

Zebra cladding: Patchwork cladding of Zircaloy 2 (alloy B), alloy F, alloy G, and alloy I

Table 10
Alloy Materials Used for the Fuel Rod Irradiation Tests

Alloy ID	Alloy Description	ΣA
B	Zircaloy-2 TSHT*	1.5 E-19
C	Zircaloy-2 TSHT	1.6 E-19
F	High Fe/Ni Zircaloy-2 (Zr-1.5Sn-0.25Fe-0.10Cr-0.10Ni)	4.2 E-20
G	Zircaloy-2 + 0.5Nb	1.4 E-19
I	Zr + 1.2Bi + 0.5Nb	2.1 E-19

*Tubeshell heat treatment

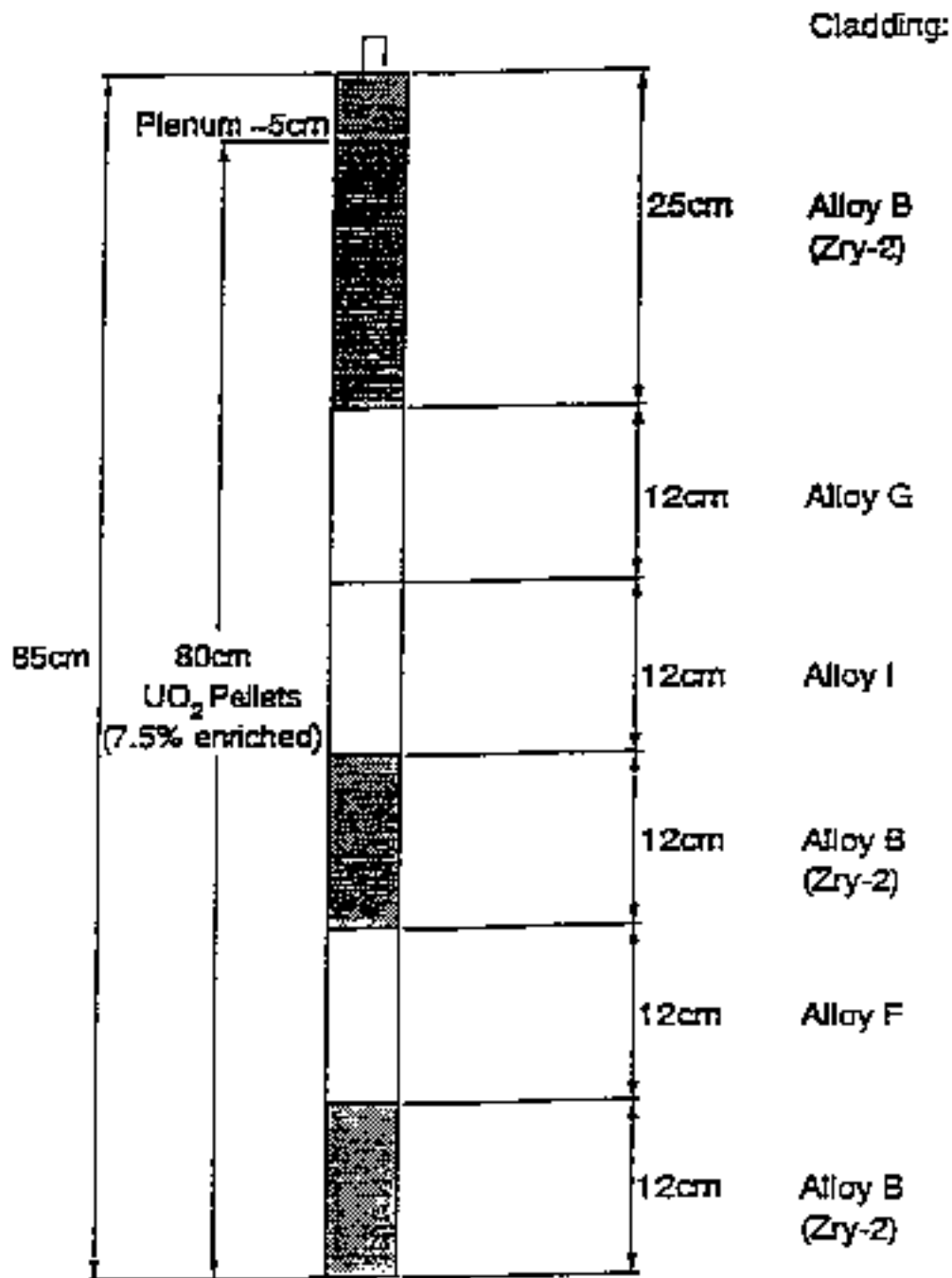


Figure 9 Schematic of Fuel Rod Design for Test 4, 5, 6a and 6b (The individual materials are welded together and for "zebra" cladding)

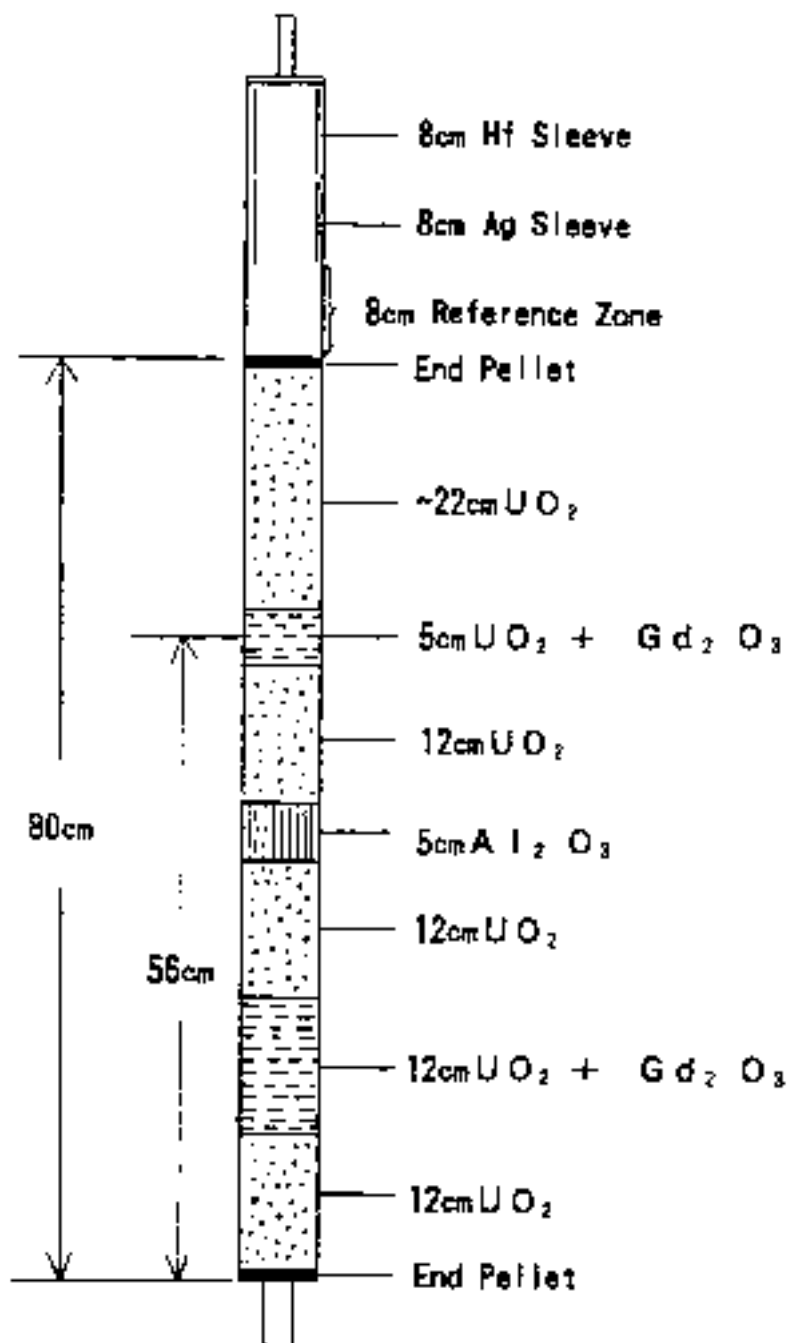


Figure 10 Schematic of Pellet Loading Design for the Second and Third Fuel Rod Tests

Table 11
Summary of Fuel Rod Irradiation Test Specimen Oxide Thicknesses

Distance from the fuel bottom	Test 1 Alloy C	Name: Tests 2 & 3 plenum (H ₂) plenum (Ar) plenum UO ₂ UO ₂ UO ₂ UO ₂ UO ₂ UO ₂ UO ₂ (U,Gd)O ₂ (U,Gd)O ₂ (U,Gd)O ₂ UO ₂ UO ₂ UO ₂ UO ₂ Al ₂ O ₃ Al ₂ O ₃ Al ₂ O ₃ UO ₂ UO ₂ UO ₂ UO ₂ (U,Gd)O ₂ (U,Gd)O ₂ (U,Gd)O ₂ (U,Gd)O ₂ UO ₂ UO ₂ UO ₂ UO ₂	Test 2 ppm	Test 3 ppm	Name: Tests 4, 6 Alloy B Alloy B Alloy B Alloy B Alloy B Alloy B Alloy B Weld Alloy G Alloy G Alloy G Alloy G Alloy I Alloy I Alloy I Alloy I Alloy I Alloy B Alloy B Alloy B Weld Alloy J Alloy F Alloy F Alloy J Weld Alloy B Alloy B Alloy B	Test 4 ppm	Test 5 ppm	Test 6a ppm	Test 6b ppm
92	10(a few)		4(80%)	4(90%)					
85			4(80%)	4(80%)					
84			3.9	5.5(49%)				2	9.7
73			5	5(50%)					
72									
71									
66			6(80%)	6(70%)				1.1	13.8
65									
61									
58			2.8	7(50%)					
57			4					1.3	7.9
55									
51	6(a few)		1.4	10(60%)					
48									
47									
46			4(80%)	5(80%)					
41	12(40%)		3.5	5(70%)				0.8	1.8
39									
37									
34									
32			6(60%)	8(60%)				2.1	15.7
30			3.1	8(50%)					
25									
22	12(40%)								
18			1.8	4.1(50%)				1.9	10.3
16			5(80%)	5(50%)					
13	12(75%)								
12									
9			6(60%)	6(30%)					
4									
1	250 ppb O ₂		350 ppb O ₂	500 ppb O ₂				1.3	14

...
 X/G, nodular corrosion maximum thickness (x nodular coverage)
 Y: average or typical oxide thickness

Summary of Corrosion Tests and Results

Table 12
Summary of Fuel Rod Irradiation Test Specimen Hydrogen Contents

Distance from the fuel bottom	Test 1 Alloy C	Name Tests 2 & 3	Test 2 (ppm)		Name Tests 4 & 5	Test 4 (ppm)		Test 5 (ppm)	Test 6a (ppm)		Test 6b (ppm)
62		plenum (Hf)			Alloy B						
65		plenum (Ag)			Alloy B						
64		plenum	-50		Alloy B	-15		19	19		17
73		UO ₂	-10		Alloy B	-15		-15			
72		UO ₂			Alloy B	-15					
71		UO ₂			Alloy B	-15					
66		UO ₂			Alloy B			8.9	34		-20
65		UO ₂			Alloy B						
61		UO ₂			Alloy B	-15		8			
58		(U,Gd)O ₂	-80		Alloy G						
57		(U,Gd)O ₂			Alloy G	-10		-10	23		16
55		(U,Gd)O ₂			Alloy G						
51		UO ₂			Alloy G						
48		UO ₂	-50		Alloy F						
47		UO ₂			Alloy F						
46		UO ₂			Alloy F						
41	-25	Al ₂ O ₃			Alloy F	-25		-25	35		-45
39		Al ₂ O ₃			Alloy F						
37		Al ₂ O ₃			Alloy F	-25		-17	23		17
31		UO ₂			Alloy B	-10					
32		UO ₂			Alloy B						
30		UO ₂	-25		Alloy B						
25		UO ₂			Weld						
22		(U,Gd)O ₂			Alloy F						
18		(U,Gd)O ₂			Alloy F	-10		-10	23		15
16		(U,Gd)O ₂	-80		Alloy F						
13	-25	(U,Gd)O ₂			Alloy F						
12		UO ₂			Weld	-15		13			
9		UO ₂			Alloy B			5.13			
4		UO ₂			Alloy B						
1	250 ppb U ₂	UO ₂	350 ppb O ₂	500 ppb O ₂	Alloy B	-10	1000 ppb O ₂	350 ppb H ₂	100 ppb H ₂ + ZnO	1000 ppb O ₂ - NaHCO ₃	~15

3

COMPREHENSIVE EVALUATION

This section identifies the water chemistry conditions that are detrimental to Zircaloy-2 nodular and uniform corrosion resistances. In addition to chemical additives, water radiolysis plays an important role in material corrosion in high temperature water under irradiation and is therefore used to interpret the corrosion results in some cases. In order to help understand the radiolysis process, simplified fundamentals of water radiolysis and a brief description of the radiolysis modeling are presented in the Appendix. The hydrogen pickup characteristics, performance of the alternate alloys, fuel rod crud deposition characteristics, and mini-autoclave container corrosion are also discussed.

Zircaloy-2 Corrosion

Mini-Autoclave Tests

Effect of Water Chemistry on Zircaloy-2 Corrosion

Ranking of Water Chemistry Environments. The relative effect of the various mini-autoclave water chemistry environments on Zircaloy-2 corrosion was determined by assigning a ranking from 1 to 4 for Zircaloy-2 Alloys A, B, and C based on the corrosion data summarized in Table 6. The ranking criteria used is outlined in Table 13. In this ranking, the least aggressive environment, or for that matter the most corrosion-resistant material, has zero nodules and thin uniform oxide; the most aggressive environment has more than 70% nodular coverage or greater than 4 microns of uniform oxide.

The water chemistry conditions are arranged in Table 14 to reflect the aggressiveness of each individual environment. Table 14 provides a convenient manner in which the three Zircaloy-2 alloys can be compared in all of the mini-autoclave tests. A determination of the relative effect of a given impurity is made by comparing the ranking of the three Zircaloy-2 materials to a reference condition. In most of the tests, the reference condition is mini-autoclave Test 1-C with 810 ppb O₂. But the reference

condition for the $\text{Cu}(\text{NO}_3)_2$ and $\text{Zn}(\text{NO}_3)_2$ tests is mini-autoclave Test 1-A with 275 ppb O_2 .

It is seen in Table 14 that many of the mini-autoclave environments are less aggressive than the reference condition of 810 ppb O_2 . In these non-aggressive environments, the three grades of Zircaloy-2 are all resistant to nodular corrosion and have very thin uniform oxides (<2 microns). As the mini-autoclave environments become more aggressive, there is a distinction in corrosion resistance between the three grades of Zircaloy-2 in a given environment. Alloy A performs consistently better than Alloy B, which performs better than Alloy C. The most aggressive environments are high oxygen environment (1221 ppb O_2), the zinc nitrate environment, the nitrogen environment, and the sodium hydrogen chromate environment. The individual mini-autoclave environments are discussed below in terms of their effect on Zircaloy-2 corrosion. The discussion is augmented in some instances by radiolysis modeling.

Table 13
Corrosion Resistance Ranking Criteria for Mini-Autoclave Irradiation Tests

Rank	Corrosion Characteristics
1	No nodules and uniform oxide thickness of <2 μm (highest corrosion resistance)
2	Nodular coverage of less than 5% or uniform oxide thickness of 2~3 μm
3	Nodular coverage of less than 5-70% or uniform oxide thickness of 3~4 μm
4	Nodular coverage of more than 70% or uniform oxide thickness of more than 4 μm (lowest corrosion resistance)

Table 14
Ranking of Corrosion Resistance of Zircaloy-2 Alloys A, B, and C in the Mini-Autoclave Irradiation Tests

	High ← Corrosion Resistance → Low			
	Rank			
Test Water Chemistry	1	2	3	4
5C: RWCE	A,B,C			
4C: HWC simulation (501 ppb H ₂)	A,B,C			
5D: 1 ppm Zn[ZnSO ₄] + 385 ppb H ₂	A,B,C			
1B: 300 ppb Cu[Cu(NO ₃) ₂] (271 ppb O ₂)	A,B,C			
1A: 275 ppb O ₂	A,B,C			
5A: 200 ppm SiO ₂ (703 ppb O ₂)	A,B,C			
4D: 1 ppm Zn [ZnSO ₄] (747 ppb O ₂)	A,B,C			
3A: EHC oil (759 ppb O ₂)	A,B,C			
2B: 300 ppb Cu[CuSO ₄] (780 ppb O ₂)	A,B,C			
3D: 500 ppm Na ₂ SO ₄ (796 ppb O ₂)	A,B,C			
4A: HWC/NWC alternate (483 ppb H ₂ /742 ppb O ₂)	A,B	C		
4B: Resin (729 ppb O ₂)	A,B	C		
2D: CILC (Cu,Zn,Na) (796 ppb O ₂)	A,B	C		
5B: 162 ppm Na[Na ₂ CO ₃] (723 ppb O ₂)	A	B,C		
3B: 200 ppm Na ₂ SiO ₃ (813 ppb O ₂)	A	B	C	
1C: 810 ppb O ₂	A	B	C	
3C: 1221 ppb O ₂	A		B	C
1D: 100 ppb Zn[Zn(NO ₃) ₂] (287 ppb O ₂)		A	B,C	
2C: 300 ppb N ₂ (765 ppb O ₂)		A	B,C	
2A: 300 ppb Cr[NaHCrO ₄] (821 ppb O ₂)			A,B,C	

Assessment of the Water Chemistry Impurities that Affect Zircaloy-2 Corrosion

Dissolved Oxygen. A parametric study of the mini-autoclave dissolved oxygen concentration was conducted. Mini-autoclave tests were run with average inlet oxygen concentrations of 275, 810, and 1221 ppb oxygen with no additional additives. The nodular corrosion increased as the oxygen content increased. For example, Zircaloy-2 Alloy B does not have nodular oxide in 275 ppb O_2 , has a few thick nodules (20 microns) in 810 ppb O_2 , and has 60% nodular coverage in 1221 ppb O_2 . This trend is evident in the Table 14 ranking.

The three mini-autoclave tests were analyzed using Toshiba's, Hitachi's, and GE's radiolysis codes¹ [11-14]. Toshiba's modeling results showing specific chemical species along the mini-autoclave loop are shown in Figures 11, 12, and 13 for the 275, 810, and 1221 ppb oxygen tests, respectively (see Table A3 in the Appendix for tabulated results). Water radiolysis occurs in the vicinity of the mini-autoclave, as can be seen by the decrease of oxygen and the production of hydrogen peroxide, hydrogen and species such as O_2^- , HO_2^- , and OH .

The relationship between the concentration of chemical species inside the mini-autoclave and the inlet dissolved oxygen content is summarized in Figure 14; each concentration in the mini-autoclave is the average of Toshiba's, Hitachi's and GE's results. Hydrogen peroxide, hydrogen, O_2^- , HO_2^- , and HO_2 all increase as the dissolved oxygen concentration increases. The increase in these species occurs because water radiolysis is promoted by an excess of oxygen. The concentration of OH decreases as the oxygen concentration increases because it is consumed or recombined much more rapidly than the other decomposition products.

² The radiation water chemistry experiment (RWCE) mini-autoclave test was used to benchmark these radiolysis codes. The results of the RWCE analysis are contained in the Appendix along with other modeling data that is not contained in the body of the report.

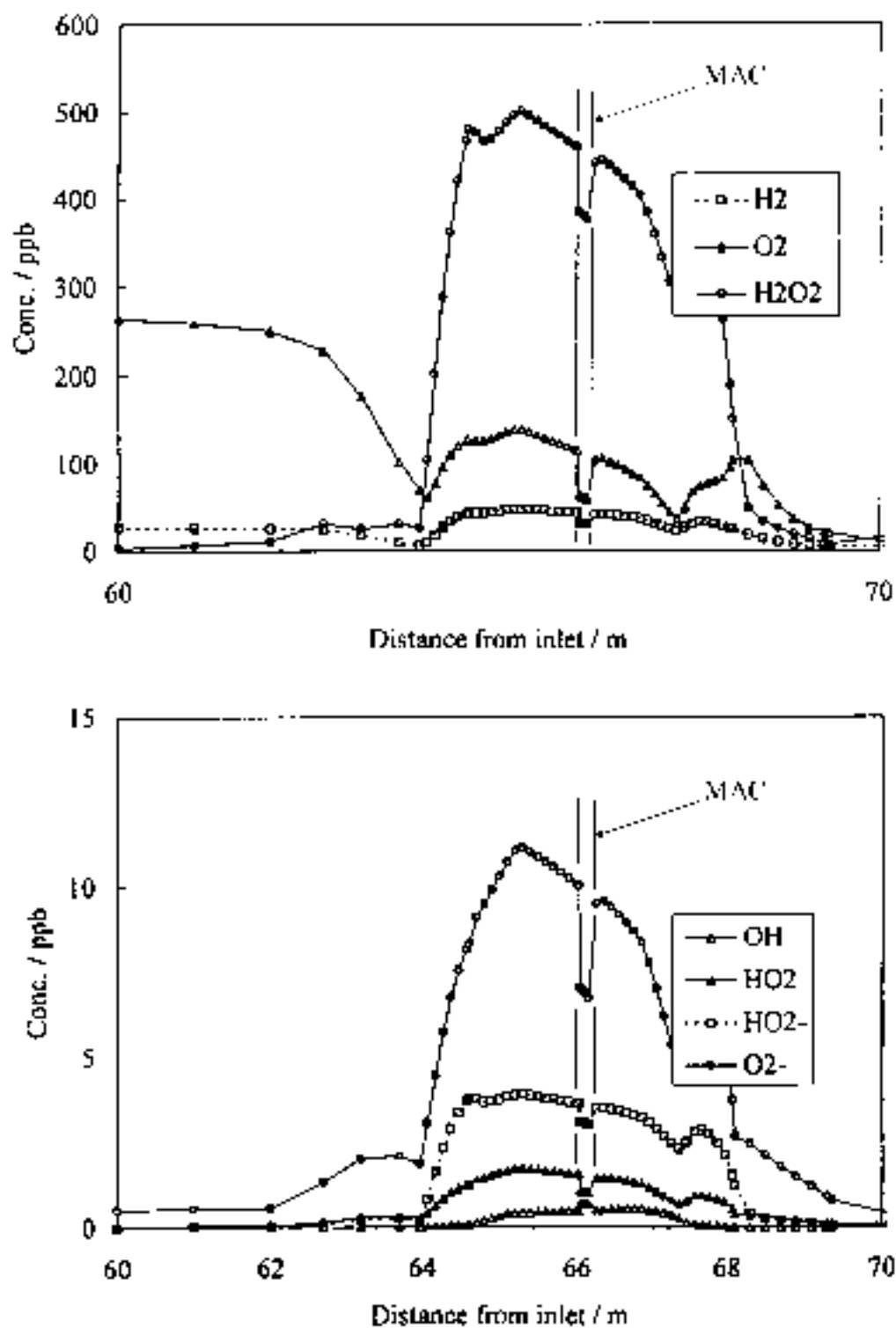


Figure 11 Toshiba's Mini-Autoclave Analysis Case 5 (Corrosion Test 1-A)
($O_2=275$ ppb, $H_2=26$ ppb)

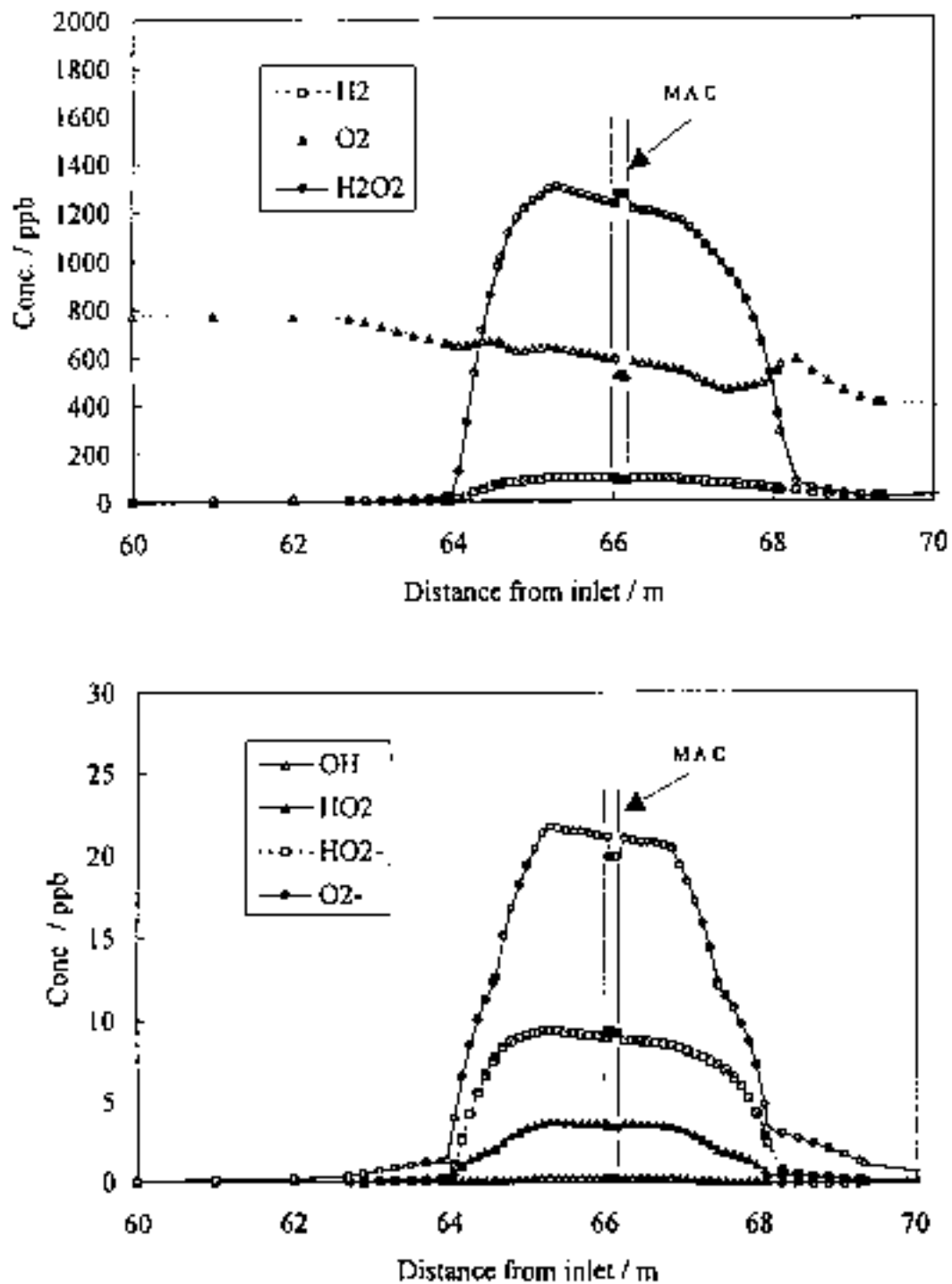


Figure 12 Toshiba's Mini-Autoclave Analysis Case 3 (Corrosion Test 1-C)
($\text{O}_2=810$ ppb)

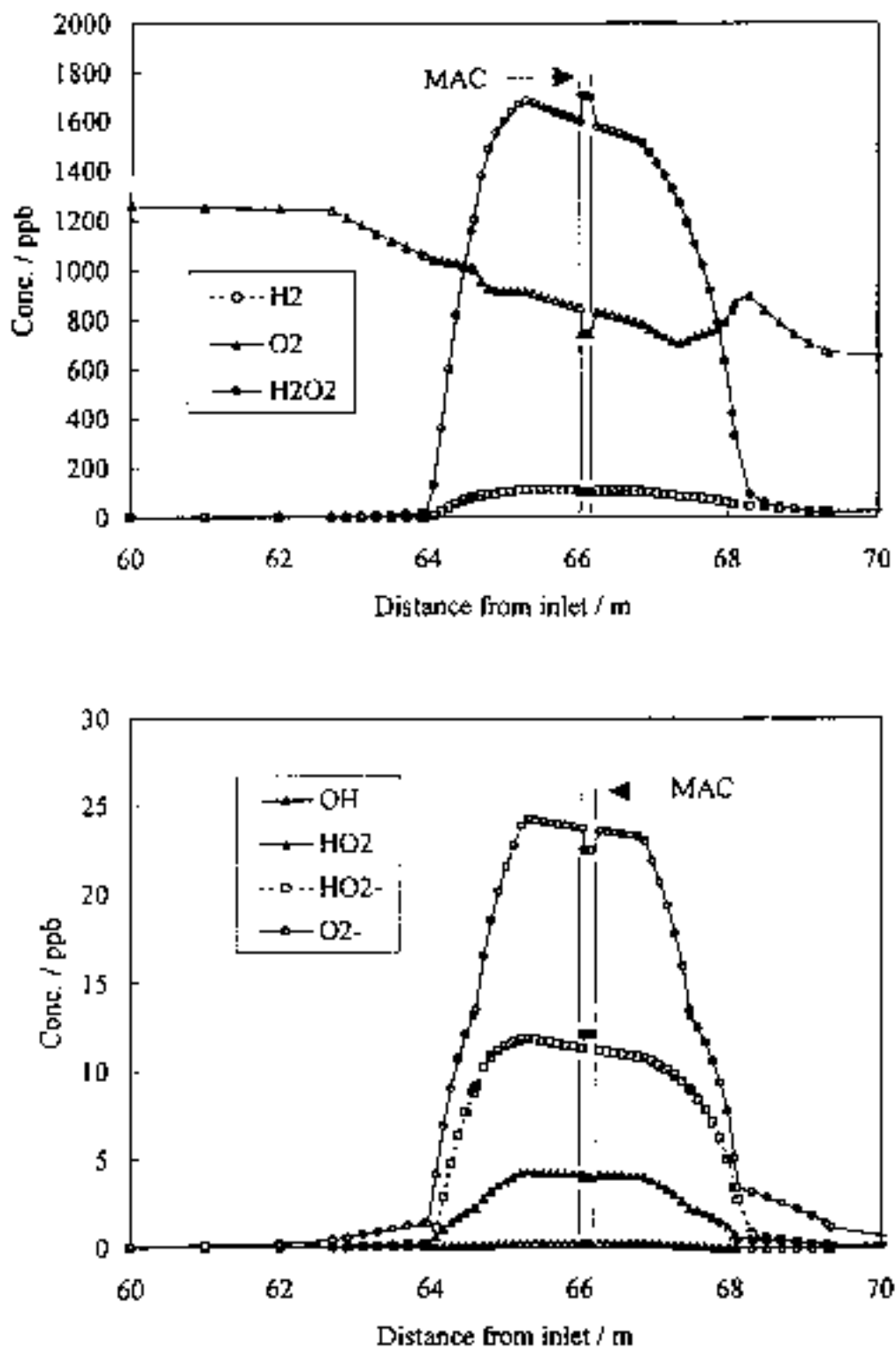


Figure 13 Toshiba's Mini-Autoclave Analysis Case 4 (Corrosion Test 3 – C)
($O_2 = 1221$ ppb)

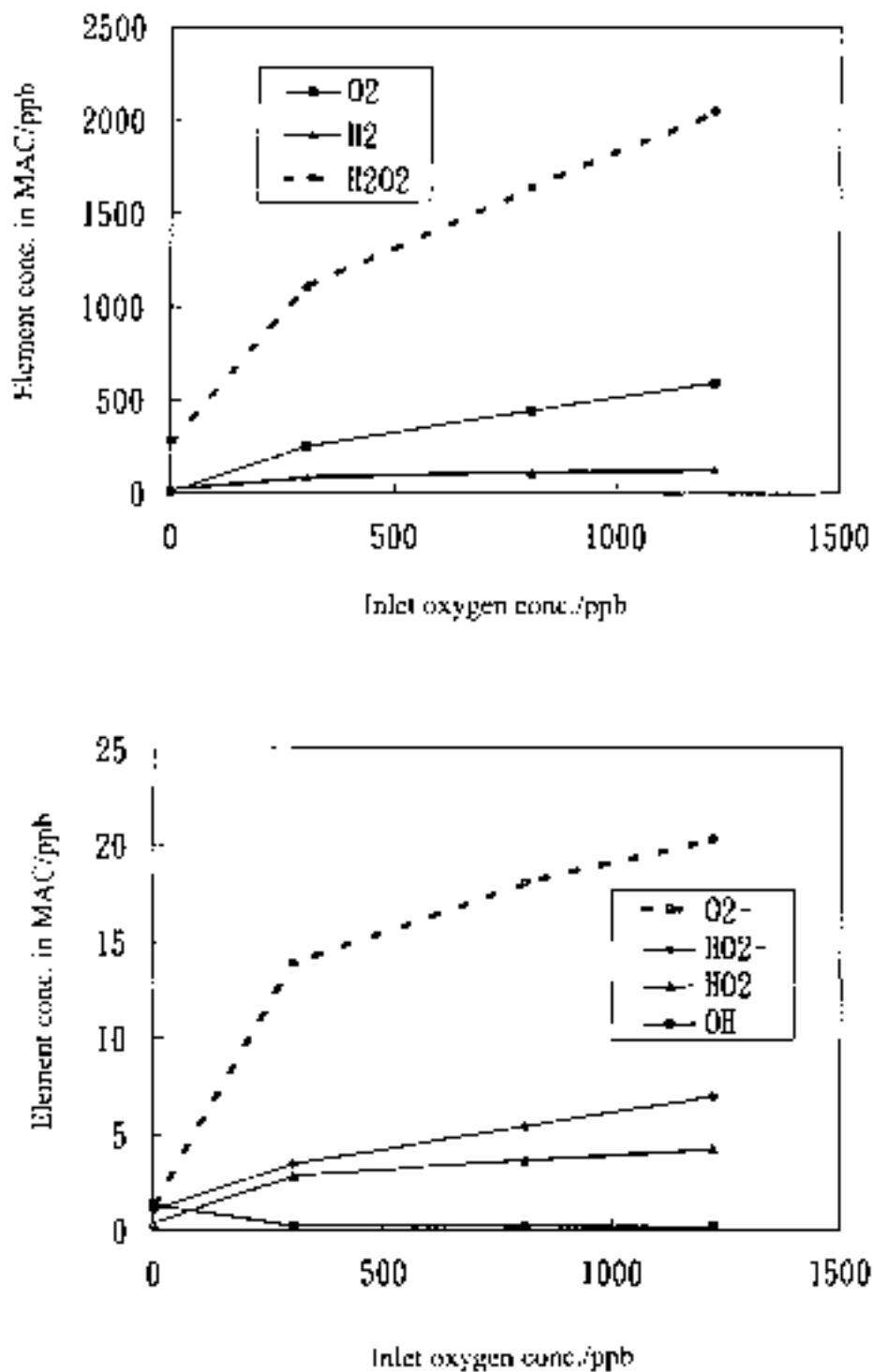


Figure 14 Effect of Dissolved Oxygen Content on the Concentration of Radiation Decomposition Products in the Mini-Autoclave Irradiation Tests (RWCE A-1, 1-A, 1-C, 3-C). [The data is an average of the Hitachi and Toshiba analyses.]

The experimental observation is that the corrosion of Zircaloy-2 increases as the oxygen content is increased. Attributing this increase unequivocally to a particular species is not possible because the reaction mechanisms and kinetics are largely unknown. Hydrogen peroxide seems to be the most likely candidate because it dominates the radiolytic spectrum with ~ 2200 ppb for an inlet concentration of 1221 ppb O₂. The concentrations of other radiolytic species such as O₂⁻ and HO₂ also increase with increased oxygen content, but they are less than 25 ppb even for 1221 ppb O₂. In comparison to hydrogen peroxide, these other species, which could have very high oxidizing potentials as free radicals, do not seem to be present in sufficient quantity to account for the observed increases in corrosion. In any case, the production of radiolytic species is dependent on the oxygen concentration and, thus, oxygen seems to indirectly increase corrosion by producing highly oxidizing species through water radiolysis.

The methodology used to determine if a given impurity has an effect on Zircaloy-2 corrosion is to compare the corrosion results from a given mini-autoclave environment to the corrosion results from a reference test. Because the corrosion of Zircaloy-2 is sensitive to the oxygen content of the test water, the oxygen content must be considered when evaluating the mini-autoclave test corrosion results. In most cases, the reference test is the 810 ppb O₂ test. In that test, the outlet O₂ and H₂ contents of 391 and 4 ppb, respectively, were comparable to the values measured in the recirculation lines in BWRs (i.e., 200-300 ppb O₂ and 25-35 ppb H₂).

Hydrogen Water Chemistry Simulation. The hydrogen water chemistry (HWC) environment was simulated by testing in 501 ppb H₂ measured at the inlet and no oxygen injection. The corrosion of Zircaloy-2 was reduced compared to the reference test of 810 ppb O₂. Nodular corrosion was suppressed and the amount of uniform corrosion was relatively small.

The simulated HWC mini-autoclave test was analyzed using radiolysis model codes [11-14]. The calculated concentrations of oxygen, hydrogen, hydrogen peroxide, O₂⁻, HO₂ and other species inside the mini-autoclave are shown in Figure 15 for the Toshiba analysis (see Table A3 in the Appendix for additional results). The radiolytic production of the oxidizing species is very small in this case and there is only a slight decrease in the hydrogen content. The most significantly produced radiolytic species is ~50 ppb of hydrogen peroxide. The concentration of O₂⁻ is less than 0.1 ppb.

The low production of radiolytic species occurs because an excess of hydrogen promotes the recombination reactions and suppresses the decomposition of water. The radiolytic production of oxygen is low because it is only produced by a secondary reaction with water's decomposition products.

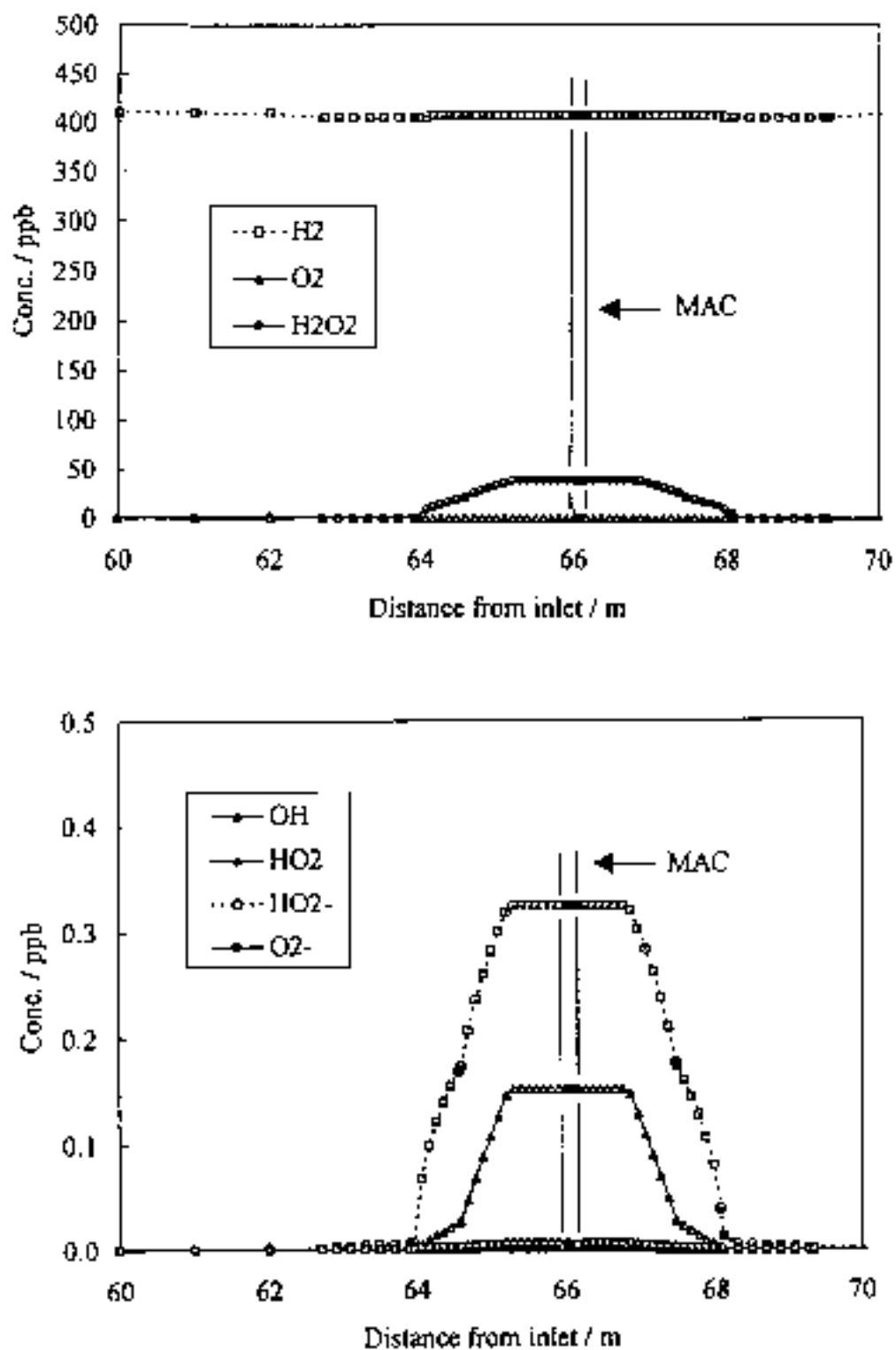


Figure 15 Toshiba's Mini-Autoclave Analysis Case 6 (Corrosion Test 4 – C)
($H_2 = 501$ ppb)

The small amount of corrosion in the simulated HWC environment is not surprising because oxygen, which seems to accelerate Zircaloy-2 corrosion indirectly through a radiolytic process, was not added. The HWC simulation test demonstrated that a reducing environment was maintained with an excess of hydrogen and that Zircaloy-2 corrosion is minimized in a reducing environment in which radiolysis is suppressed. Not adding oxygen to the simulation simply assured that the least oxidizing test environment was attained.

Alternating Normal Water Chemistry/Hydrogen Water Chemistry. The effect of alternating NWC/HWC is important from a practical point of view because BWRs do not operate under HWC conditions 100% of the time. The corrosion of Zircaloy-2 in the alternating NWC/HWC environment was less than the corrosion in the NWC environment but greater than the corrosion in the HWC environment. This is not surprising if one considers that most of the corrosion occurs during the periods of NWC when radiolytically produced species such as hydrogen peroxide and O_2^- exist.

Dissolved Nitrogen. The nodular corrosion of Zircaloy-2 was accelerated in the 300 ppb nitrogen injection + 765 ppb O_2 mini-autoclave test. For example, Zircaloy-2 Alloy B has a few 20 micron nodules in the 810 ppb O_2 reference test and 8 micron nodules with 30% coverage in nitrogen.

The nitrogen injection test was analyzed using the Toshiba radiolysis model code [13]. Nitrogen can exist in various valence states (+5 to -3) and thus it is necessary to construct an *assumed* reaction scheme taking into account the radiolysis of nitrogen in all of its valence states. Table 15 shows the most common chemical species associated with each valence of nitrogen; NO_3^- , NO_2^- , NO, N_2O , N_2 , NH_3 and NH_4^+ and the other species are possible transient products assumed to exist in water under irradiation.

The calculated concentrations of nitrogen, oxygen, hydrogen, hydrogen peroxide and other species inside the mini-autoclave are shown in Figure 16. The oxygen and nitrogen concentrations decrease, whereas hydrogen, hydrogen peroxide and other species are produced radiolytically. The radiolytic spectrum is similar to that of the reference case of 810 ppb O_2 shown in Figure 12 but with the additional species associated with nitrogen.

The production of hydrogen peroxide dominates the radiolytic spectrum, with a maximum concentration of ~1200 ppb, whereas the concentration of O_2^- is less than 20 ppb. The most significant species related to nitrogen is 120 ppb NO_3^- . The NO_2^- , which has a lower valence than that of NO_3^- , is also observed at ~15 ppb. On the other hand, the concentration of the reduced form, NH_4^+ , is low at 3 ppb as expected in the oxidizing environment.

Table 15
Nitrogen Compounds and Assumed Transient Species in Water Under Irradiation [13]

Oxidation Status	Principal Compounds	Important Transients
+ 5	NO_3^- , HNO_3	HOONO , OONO^-
+ 4	NO_2	NO_3^{2-}
+ 3	NO_2^- , HNO_2	
+ 2	NO	NO_2^{2-} , HNO_2^-
+1	N_2O	
0	N , N_2	HNOH , NH_2OH^+
- 1	NH_2OH , HN_3OH^+	NH
- 2		NH_2 , NH_3^+
- 3	NH_4^+ , NH_3	

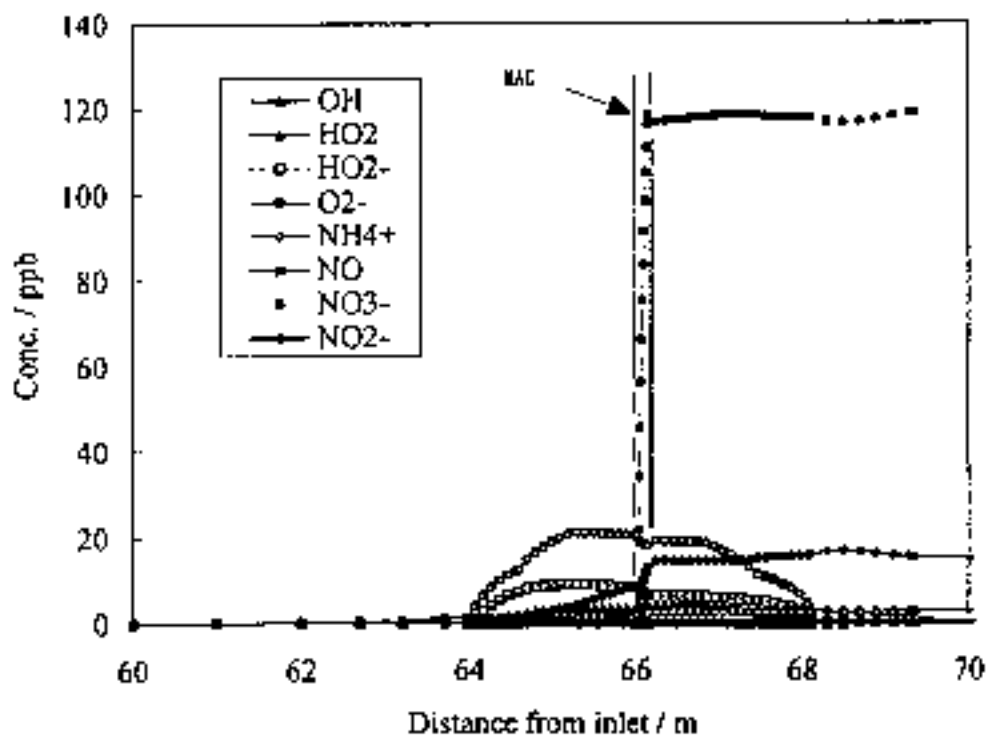
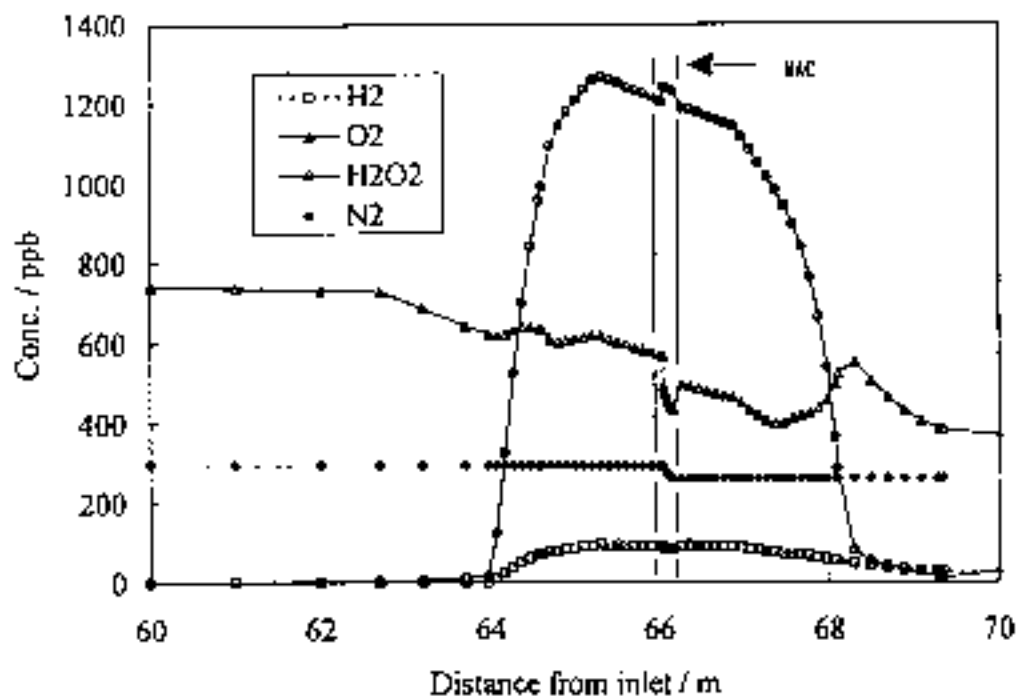


Figure 16 Mini-Autoclave Analysis Case 7 (Corrosion Test 2 – C)
(O₂ = 765 ppb, H₂ = 501 ppb)

Figure 17 compares the concentrations of the chemical species in the nitrogen injection mini-autoclave test with those in the pure oxygen tests for the Toshiba analysis. The concentrations of oxygen, hydrogen and hydrogen peroxide are essentially unchanged when nitrogen is added. The concentrations of the lesser species do not change drastically either, although small differences exist. This comparison demonstrates that the nitrogen injection accelerated the corrosion above and beyond the corrosion caused by the 765 ppb O_2 . Unfortunately, the true mechanism involving N_2 has not been established in this experiment.

$Zn(NO_3)_2$. The corrosion of Zircaloy-2 was accelerated in the $Zn(NO_3)_2$ environment. In this mini-autoclave test, the inlet oxygen concentration was only 287 ppb and so the appropriate reference test for comparison is mini-autoclave Test 1-A, which had an inlet oxygen concentration of 275 ppb O_2 . In 275 ppb O_2 Zircaloy-2 Alloy B did not develop nodular corrosion but it did develop 5 micron nodules with 30% coverage in $Zn(NO_3)_2$.

The oxygen consumptions in the reference test and the $Zn(NO_3)_2$ test were about the same. The NO_3^- ion concentration decreased from 200 ppb to 15 ppb, whereas 10 ppb NO_2^- was detected at the outlet. Apparently, the NO_3^- ion was reduced either radiolytically or by reducing species in the system; no other reduced forms of nitrogen species were measured in the outlet water. The Zn^{2+} concentration remained constant during the test.

$Cu(NO_3)_2$. The corrosion of Zircaloy-2 was essentially unchanged in the $Cu(NO_3)_2$ + 271 ppb O_2 environment. In this mini-autoclave test, the inlet oxygen concentration was only 271 ppb and so the appropriate reference test for comparison is mini-autoclave Test 1-A, which had an inlet oxygen concentration of 275 ppb O_2 . Zircaloy-2 Alloys A, B, and C did not have nodular corrosion in the reference test with 275 ppb O_2 or in $Cu(NO_3)_2$ + 271 ppb O_2 .

The radiolytic processes were apparently very different in the $Cu(NO_3)_2$ test and the reference test. In $Cu(NO_3)_2$, the outlet oxygen concentration increased to 450 ppb from 271 at the inlet compared to almost complete oxygen consumption in the reference test; a substantial amount of hydrogen (105 ppb) was also detected in the outlet. These increases did not occur in the $Zn(NO_3)_2$ test, which suggests that the copper ion can influence radiolysis perhaps through Cu^{2+}/Cu^+ effects on $(H_2 + O_2)$ recombination reactions. It is also of interest to note that much more NO_3^- was reduced to NO_2^- in the $Cu(NO_3)_2$ test compared to the $Zn(NO_3)_2$ test (150 ppb vs. 10 ppb).

The difference in corrosion in the $Cu(NO_3)_2$ and $Zn(NO_3)_2$ environments may be attributed to the Cu^{2+} and Cu^+ ions which scavenge free radicals and retard the O_2 and H_2 recombination reaction. In addition, the Cu^{2+} and Cu^+ ions are known to catalytically decompose hydrogen peroxide in high temperature water [16].

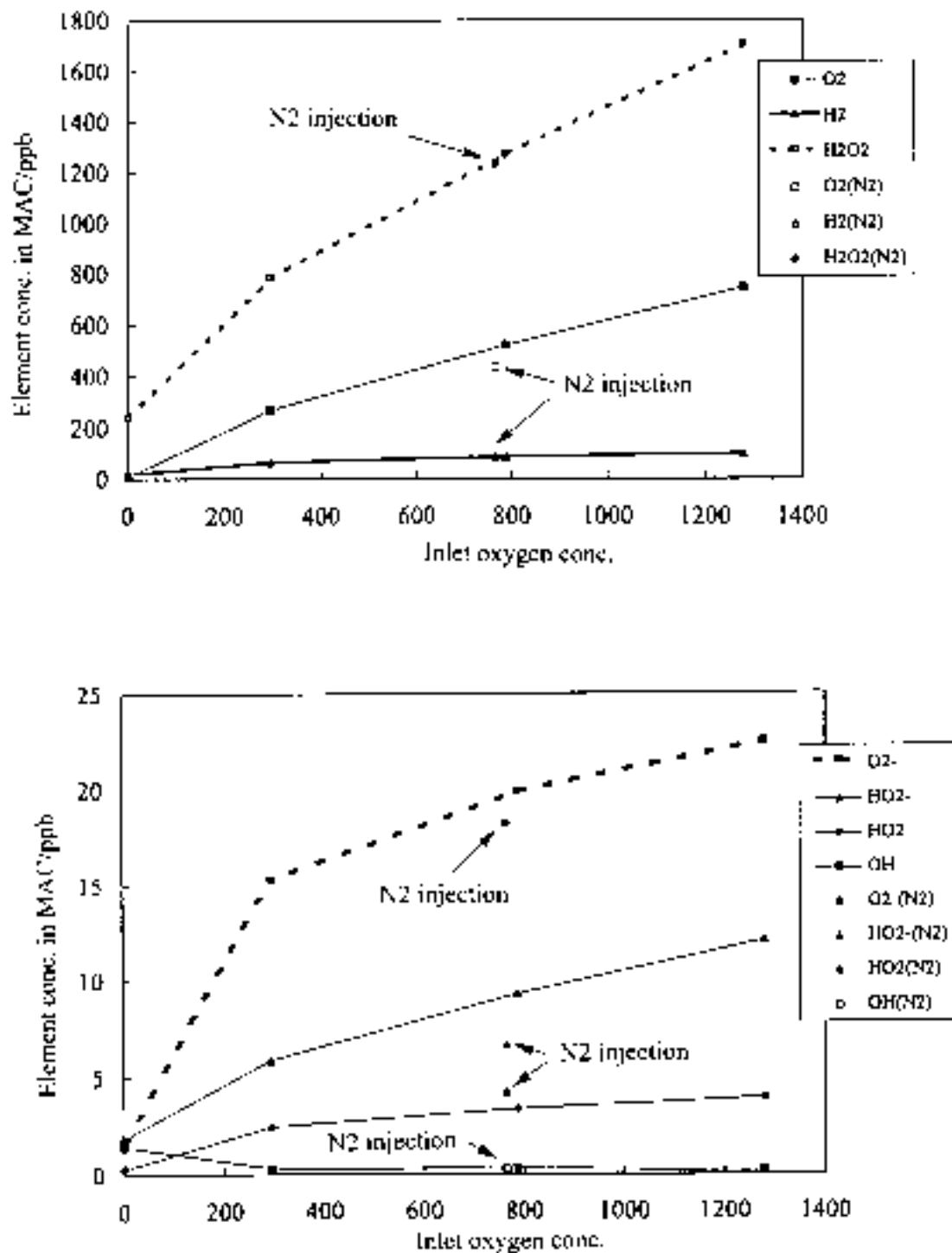


Figure 17 Effects of Nitrogen Addition on the Concentration of Radiation Decomposition Products in the Mini-Autoclave Irradiation Tests (RWCE A-1, 1-A, 1-C, 3-C, 2-C). [The data is from the Toshiba analyses.]

NaHCrO₄. The uniform corrosion of Zircaloy-2 was accelerated in the NaHCrO₄ + 821 ppb O₂ mini-autoclave test, whereas nodular corrosion was suppressed. For example, Zircaloy-2 Alloy B has a 3-4 micron uniform oxide in NaHCrO₄ but has 1-2 micron uniform oxide and a few 20 micron nodules in the reference test of 810 ppb O₂. The inlet oxygen contents (821 and 810 ppb), as well as the oxygen consumption rates, were approximately the same for the two tests.

The increase in corrosion in the NaHCrO₄ test is not surprising because the HCrO₄⁻ and CrO₄²⁻ ions in water are known to be very strong oxidizing agents. Their electrochemical potentials are high enough to oxidize most metals.

The NaHCrO₄ mini-autoclave test was analyzed using Hitachi's radiolysis model code. The effect of the HCrO₄⁻ ion on the radiolytic decomposition of water is largely unknown and thus it was necessary to *assume* the reaction scheme shown in Figure 18. The primary purpose of this analysis was to show that the oxidizing species associated with the radiolytic decomposition of water were not the cause of the accelerated corrosion (i.e., to show that there was not an increase, albeit a calculated one, in hydrogen peroxide and other species in the presence of NaHCrO₄).

The calculated concentrations of the chromium chemical species, oxygen, hydrogen, hydrogen peroxide and other species inside the mini-autoclave are shown in Figures 19 and 20. The oxygen and HCrO₄⁻ concentrations decrease, whereas hydrogen, hydrogen peroxide and other species are produced radiolytically. The radiolytic spectrum is similar to that of the reference case of 810 ppb O₂ shown in Figure 12 but with the additional species associated with chromium (also see Table 16). Again, the production of hydrogen peroxide dominates the radiolytic spectrum.

Figure 21 compares the concentrations of the chemical species in the NaHCrO₄ mini-autoclave with those in the pure oxygen tests. The addition of chromate may have suppressed the decomposition of water and the production of species such as hydrogen peroxide. Hydrogen peroxide was calculated to be ~2000 ppb in 810 ppb O₂ and was calculated to be ~1100 ppb in NaHCrO₄ for the same nominal inlet oxygen concentration. This comparison shows that the uniform corrosion of Zircaloy-2 is most likely accelerated by HCrO₄⁻ or CrO₄²⁻.

Na₂SiO₃. The corrosion of Zircaloy-2 was essentially unchanged in Na₂SiO₃ + 813 ppm O₂ compared to the reference condition of 810 ppb O₂. However, the oxygen concentration in the outlet *increased* to 1400 ppb due to the decomposition of SiO₃²⁻. The net result, however, is that Na₂SiO₃ was essentially inert with respect to Zircaloy-2 corrosion. This result demonstrates that the oxygen content is not the controlling factor in all of the mini-autoclave tests.

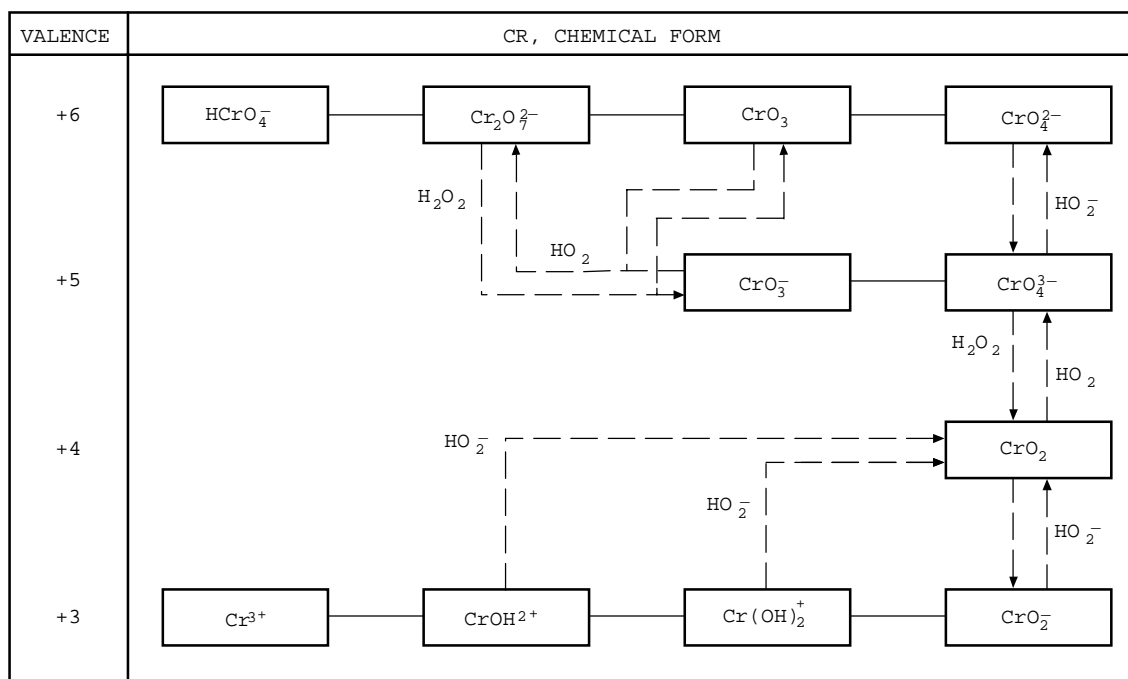


Figure 18 Reaction Scheme of Chromium Chemical Species Under Irradiation Assumed in Model Calculation [15]

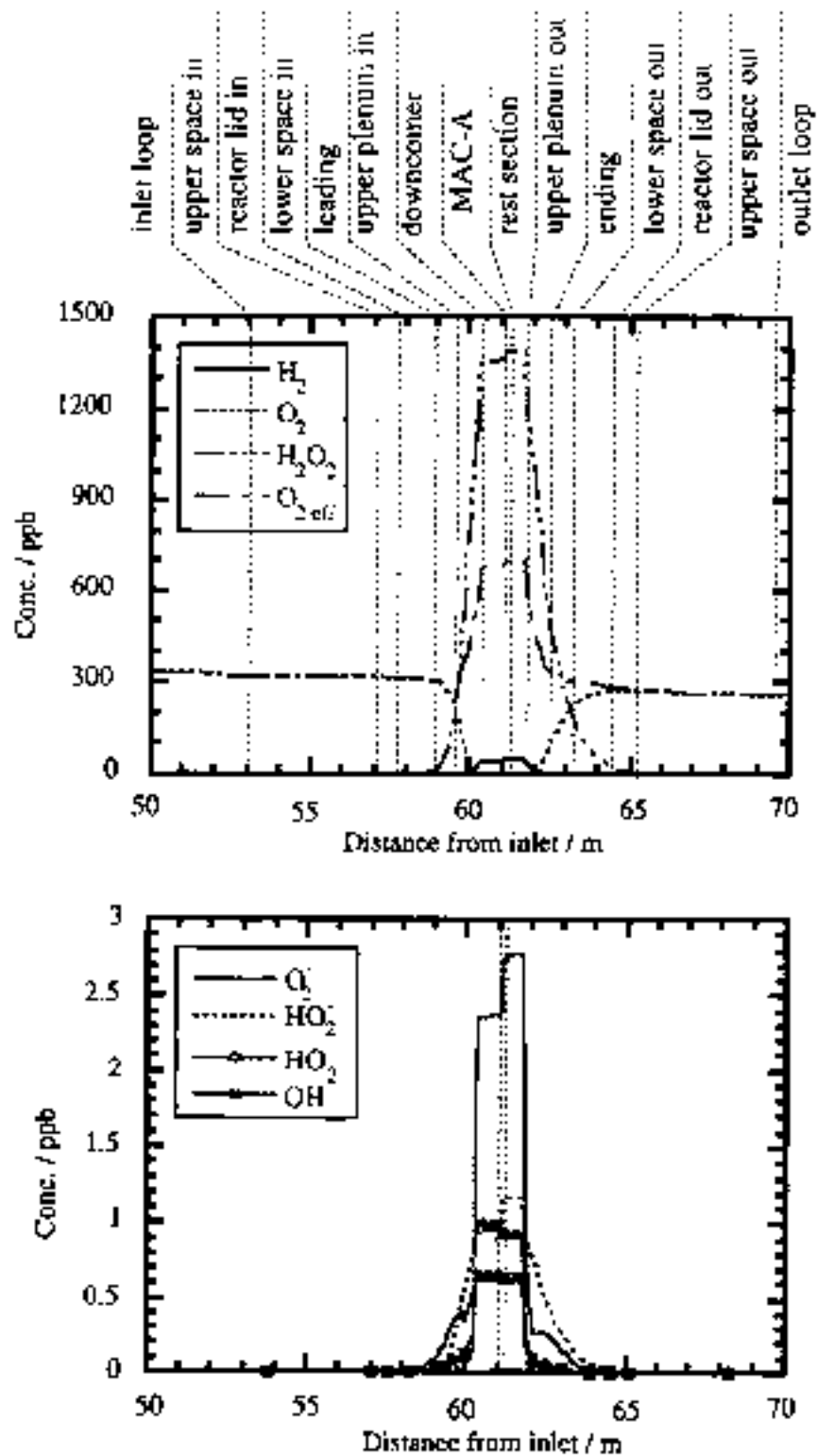


Figure 19 Hitachi's Mini-Autoclave Analysis Case 8 (Corrosion Test 2 – A)
 ($O_2 = 850$ ppb, $H_2 = 0$ ppb, $Cr = 291$ ppb)

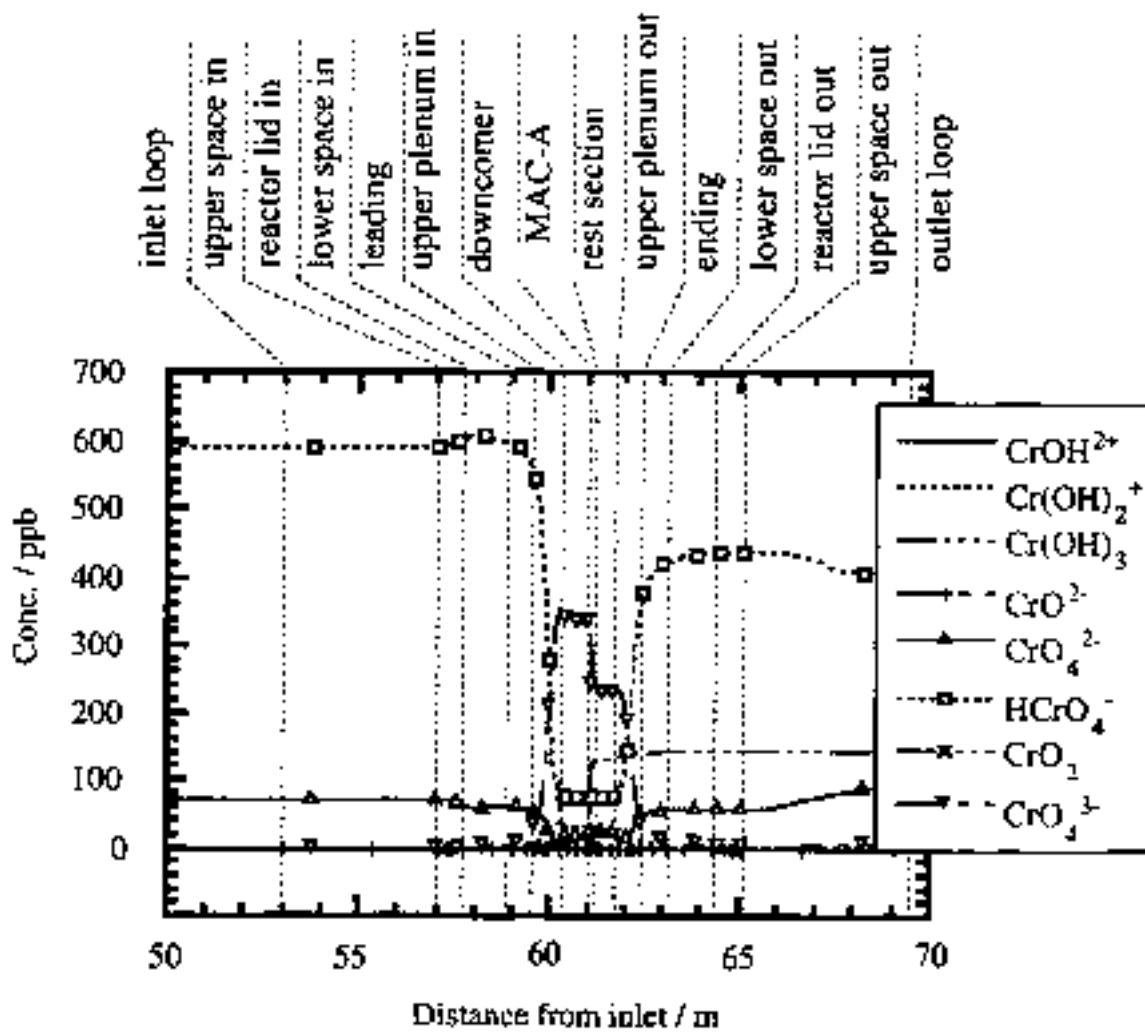


Figure 20 Hitachi's Mini-Autoclave Analysis Case 8 (Corrosion Test 2 – A)
(Chromium chemical species)

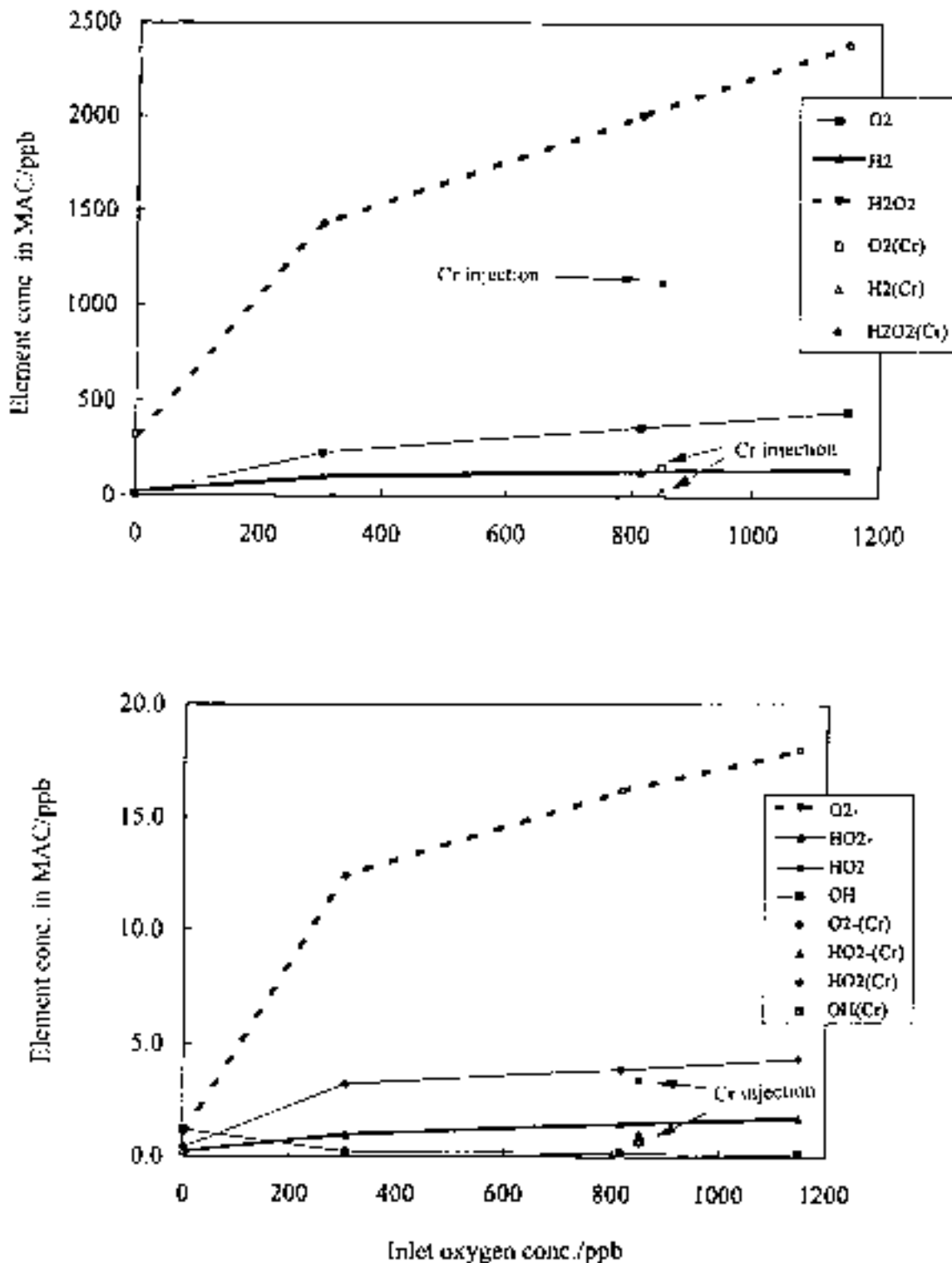


Figure 21 Effects of Chromium Addition on the Concentration of Radiation Dissociation Products in the Mini-Autoclave Irradiation Tests (RWCE A-1, 1-A, 1-C, 3-C, 2-A). [The data is from the Hitachi analyses.]

Table 16
Comparison of Hitachi Radiolysis Model Calculation with Experimental Data for Mini-Autoclave Test 2-A
(NaHCrO₄ + 821 ppb O₂)

Test #	Experimental				Model Calculation				Model Calculation				Concentration in ppb
	Inlet		Outlet		Inlet		Outlet		MAC Chemistry				
	O ₂	H ₂	CrO ₄ 2-	O ₂	H ₂	CrO ₄ 2-	O ₂	H ₂	CrO ₄ 2-	O ₂	H ₂	CrO ₄ 2-	
2-A	850	0	291*	100	0	291	99.5	0.7	2201*	30.8	1118.11	3.4	
										HO ₂	OH	Cr(OH) ₂ +	
										1.1	0.65	0.69	22.3
										Cr(OH) ₃	CrO ₂	CrO ₄ 2-	
										191	0.3	77	31.9
3-C ¹⁰										HCrO ₄ -			
										117			

Na₂CO₃. The nodular corrosion of Zircaloy-2 was reduced and the uniform corrosion increased in Na₂CO₃ compared to the reference condition of 810 ppb O₂. For example, Zircaloy-2 Alloy B has no nodules and 2-3 micron uniform oxide in Na₂CO₃ + 723 ppb O₂, but has only 1 micron uniform oxide and a few 20 micron nodules in 810 ppb O₂.

The oxygen concentration in the outlet water increased to 8400 ppb; similarly, the hydrogen content of the outlet increased to 925 ppb. The production of oxygen is expected to be accompanied with an increase in the production of hydrogen peroxide (and other species) and accelerate the nodular corrosion. But this effect could have been offset by the high hydrogen production rate which suppresses the formation of hydrogen peroxide and other species that may accelerate Zircaloy-2 corrosion.

CuSO₄, ZnSO₄ and Na₂SO₄. CuSO₄, ZnSO₄, and Na₂SO₄ were tested in individual mini-autoclave tests. The corrosion of Zircaloy-2 was reduced in the presence of these impurities relative to the reference condition of 810 ppb O₂. The inlet oxygen content of these three tests is between 747 and 796 ppb, which is not significantly different than the reference oxygen level of 810 ppb.

The reduction in corrosion in these three environments can be attributed to the sulfate ion, which hinders the production of hydrogen peroxide. The sulfate ion, which is not affected significantly by radiation, reacts with high temperature water to produce HSO₄⁻ and OH⁻ according to eq. 1. Under irradiation, HSO₄⁻ can react with the OH radical, and consume OH (eq. 2). OH is the precursor of H₂O₂, which could be an accelerating factor for Zircaloy-2 corrosion.



Mixed (CuSO₄ + ZnSO₄ + NaHCrO₄). Copper (as CuSO₄), zinc (as ZnSO₄) and chromium (as NaHCrO₄) were mixed with 796 ppb O₂ in an attempt to create a severe chemistry environment that would accelerate corrosion. However, this environment caused a reduction in the corrosion of Zircaloy-2 compared to the reference condition of 810 ppb O₂. For example, Zircaloy-2 Alloy B has no nodules and 1-2 micron uniform oxide in this environment, but has 1 micron uniform oxide and a few 20 micron nodules in 810 ppb O₂. The copper, zinc, and chromium ions certainly did not cause accelerated corrosion.

In this environment, the sulfate ion is expected to decrease the corrosion of Zircaloy-2. This is consistent with the experimental observations. On the other hand, the HCrO₄⁻ ion is expected to increase the uniform corrosion, which is contrary to the corrosion results. Perhaps the effects of the two ions offset each other.

ZnSO₄ + Hydrogen Water Chemistry. The corrosion of Zircaloy-2 was reduced in this test condition compared to the reference condition of 810 ppb O₂. As discussed above, the lack of oxygen, an excess of hydrogen and the sulfate ion are all expected to reduce the corrosion of Zircaloy-2 by suppressing the formation of hydrogen peroxide, O₂⁻, etc., which are thought to accelerate corrosion.

Resin. The corrosion of Zircaloy-2 was reduced in the resin intrusion + 729 ppb O₂ test compared to the reference test of 810 ppb O₂. For example, Zircaloy-2 Alloy B has 1-2 micron uniform oxide and no nodules in the resin environment but has a few 20 micron nodules in 810 ppb O₂. The conductivity of the resin intrusion water was high at 10 μS/cm, which is attributed to the resin decomposition products. Significant quantities of SO₄²⁻ (800 ppb) and NH₄⁺ (400 ppb) were detected in the outlet water. The resins were decomposed radiolytically and some organic species were then oxidized by O₂. As a result, O₂ was consumed and 500 ppb H₂ was produced. The sulfate ion, the production of hydrogen, and the consumption of oxygen by resin oxidation may have all contributed to some extent in suppressing the formation of hydrogen peroxide and other radiolytic species which may accelerate Zircaloy-2 corrosion.

SiO₂. The corrosion of Zircaloy-2 was reduced in the SiO₂ + 703 ppb O₂ test compared to the reference test of 810 ppb O₂. For example, Zircaloy-2 Alloy B has 1-2 micron uniform oxide and no nodules in SiO₂, but has 1 micron uniform oxide and a few 20 micron nodules in 810 ppb O₂. The inlet oxygen concentration is a little low at 703 ppb compared to the 810 ppb reference test.

EHC Oil. It was anticipated that the corrosion of Zircaloy-2 would be accelerated in EHC oil (Trixylenyl phosphate or Tri(dimethylphenyl) phosphite) + 759 ppb O₂ but, in fact, the corrosion was reduced compared to the reference test of 810 ppb O₂. For example, Zircaloy-2 Alloy B has 1-2 micron uniform oxide in EHC oil, but has 1 micron uniform oxide and a few 20 micron nodules in 810 ppb O₂.

The inlet oxygen concentrations of the EHC mini-autoclave test and the reference test are comparable, but the oxygen consumption was somewhat greater in EHC oil. SO₄²⁻ (20 ppb) and PO₄³⁻ (20 ppb) were detected in the outlet water. EHC oil is a phosphate based compound and so the presence of the phosphate ion in the outlet water shows that the oil, or its decomposition products, came into contact with the specimens. No further explanation of the effect of the EHC oil is offered at this time.

Fuel Rod Tests

Effect of Water Chemistry on Zircaloy-2 Corrosion

The fuel rod tests were conducted in two different phases. In the first phase, a parametric study of the effect of dissolved oxygen content on corrosion was conducted using the nodular corrosion susceptible Zircaloy-2 Alloy C material (Tests 1-3) and the

corrosion-resistant Zircaloy-2 Alloy B material (Test 4). In the second phase, the effect of HWC, HWC + ZnO, and NaHCrO₄ + 1000 ppb O₂ on corrosion was determined using the nodular corrosion-resistant Zircaloy-2 Alloy B and three of the six alternate alloys (F, G, and I).

Effect of Dissolved Oxygen. The dissolved oxygen content was varied in Tests 1, 2, 3, and 4 from nominal levels of 250 ppb (inlet controlled), 350 ppb (inlet controlled), 500 ppb (inlet controlled), and 1000 ppb (outlet controlled). In Tests 1-3, the susceptible Zircaloy-2 material Alloy C was used, whereas the corrosion-resistant Alloy B was used in Test 4.

Tests 1-4 were analyzed using Hitachi's radiolysis model code [11-12]; the analysis results are summarized in Table 17. The distribution of radiation decomposition products along the fuel rod axial direction is shown in Figures 22-25 for Tests 1-4, respectively. The eddy current liftoff profile, steam quality, steam void fraction, and fluid velocity are also shown for each case.

As shown in Figures 22-25, the concentrations of most of the decomposition products of water are quite low. The concentrations of O₂⁻, HO₂⁻, HO₂⁻, and OH are all less than 20 ppb for Tests 1-4. The oxygen concentration is reduced relative to the inlet, whereas some hydrogen is produced. The most prevalent radiolytic species is hydrogen peroxide. The amount of hydrogen peroxide produced increases as the inlet oxygen content is increased. For 250 ppb O₂ there is ~1100 ppb of H₂O₂ (peak), whereas there is ~2300 ppb H₂O₂ (peak) for 1000 ppb O₂. The concentration of hydrogen peroxide peaks near the center of the fuel rod and has a lower concentration at the top of the fuel rod than at the bottom. O₂⁻ peaks at the bottom of the fuel rod and then decreases towards the top of the fuel rod.

The corrosion of Zircaloy-2 Alloy C increased as the oxygen content increased from 250-500 ppb. In Tests 1 and 2 (250 and 350 ppb O₂, respectively), the hydrogen peroxide distributions are very similar with peak concentrations of approximately 1100 ppb, but Test 1 has a slightly lower peroxide concentration near the top of the fuel rod; the O₂⁻ profile is essentially the same for Tests 1 and 2. In the first test, the maximum nodular oxide thickness near the bottom of the rod is 12 microns with 40-75% coverage and at the top it is 6-10 microns, but there are only a few nodules present (Figure 26). In the second test, the maximum nodular oxide thickness is 6 microns with 60% coverage near the bottom of the rod and at the top it is 4-6 microns with 80% coverage (Figure 27). This trend is consistent with the eddy current liftoff data. In the third test (500 ppb O₂), the hydrogen peroxide increased substantially to 1500 ppb (peak) and the O₂⁻ increased to 15 ppb (peak), but the maximum nodular oxide thickness near the bottom of the fuel rod is only 6-8 microns with a coverage of 30-60% and at the top it is 4-8 microns with 50-90% coverage (Figure 28). The increase in corrosion between Tests 2 and 3 is most evident in the eddy current profiles that do show a slight increase in liftoff.

Table 17
Comparison of Hitachi's Radiolysis Model Calculations with Experimental Data for the Fuel Rod Irradiation Tests

Test	Location	Time Years	Depth mm	Dose rate		Fuel Material	Fuel Type	Fuel Rod ID	Fuel Rod Length mm	Fuel Rod Diameter mm	Major Chemistry						Reference
				Range kGy/h	Center kGy/h						1H	2H	12C	16O	18O	20O	
2	Low Oxygen	1	0-20	3.6-11	8.5-11	Measured	UO ₂	100	38	10.5	0	0	0	0	0	0	10
											0	0	0	0	0	0	
3	Intermediate Oxygen	2	0-8	1.5-4	8.5-11	Measured	UO ₂	100	38	10.5	0	0	0	0	0	0	10
											0	0	0	0	0	0	
4	High Oxygen	1-2	0-8	1.5-4	8.5-11	Measured	UO ₂	100	38	10.5	0	0	0	0	0	0	10
											0	0	0	0	0	0	
5	High Oxygen	3	0-20	3.6-11	8.5-11	Measured	UO ₂	100	38	10.5	0	0	0	0	0	0	10
											0	0	0	0	0	0	
6	High Oxygen with Cerium	3	0-20	3.6-11	8.5-11	Measured	UO ₂	100	38	10.5	0	0	0	0	0	0	10
											0	0	0	0	0	0	

Concentration of cerium is 0.1 wt% in the fuel rod. The concentration of cerium is 0.1 wt% in the fuel rod.

Cerium species	UO ₂	UO ₂	UO ₂	UO ₂	UO ₂	UO ₂	UO ₂	UO ₂	UO ₂	UO ₂	UO ₂	UO ₂	UO ₂	UO ₂	UO ₂	UO ₂	UO ₂
	UO ₂	UO ₂	UO ₂	UO ₂	UO ₂	UO ₂	UO ₂	UO ₂	UO ₂	UO ₂	UO ₂	UO ₂	UO ₂	UO ₂	UO ₂	UO ₂	UO ₂
	UO ₂	UO ₂	UO ₂	UO ₂	UO ₂	UO ₂	UO ₂	UO ₂	UO ₂	UO ₂	UO ₂	UO ₂	UO ₂	UO ₂	UO ₂	UO ₂	UO ₂
	UO ₂	UO ₂	UO ₂	UO ₂	UO ₂	UO ₂	UO ₂	UO ₂	UO ₂	UO ₂	UO ₂	UO ₂	UO ₂	UO ₂	UO ₂	UO ₂	UO ₂

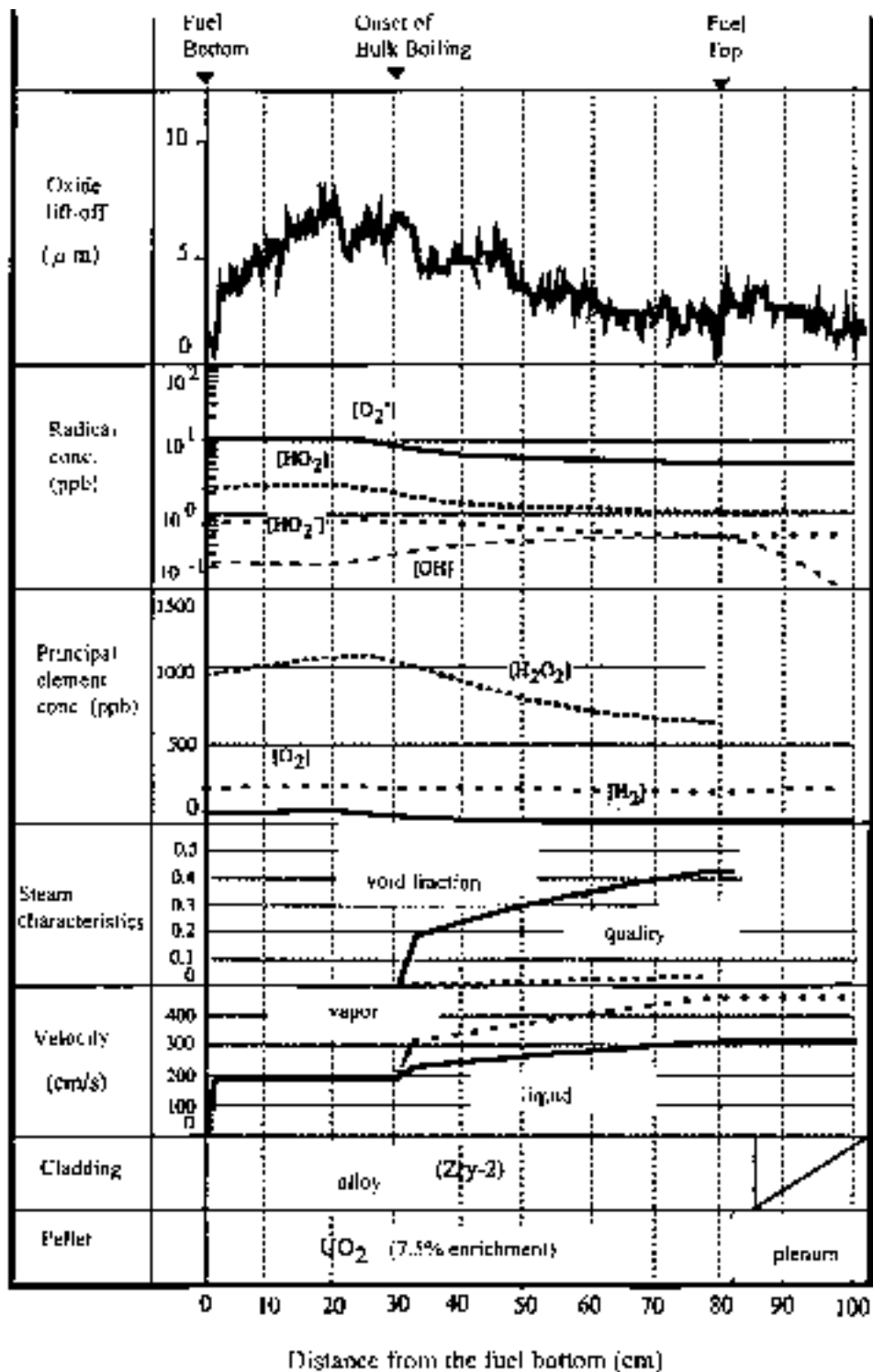


Figure 22 Hitachi's Water Chemistry Analysis of Fuel Rod Irradiation Test 1 (inlet dissolved oxygen conc: 250 ppb, inlet dissolved hydrogen conc: 50 ppb)

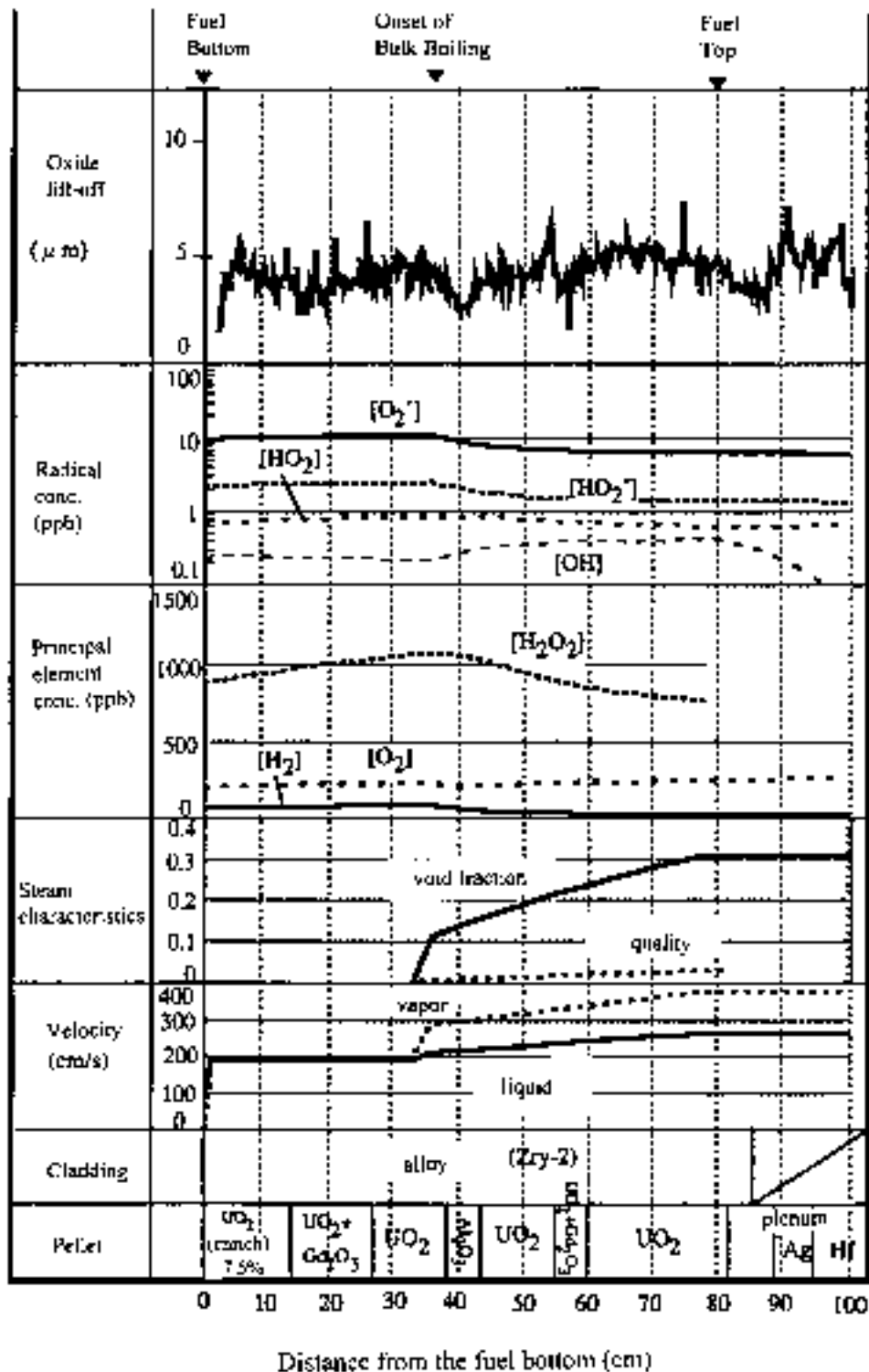


Figure 23 Hitachi's Water Chemistry Analysis of Fuel Rod Irradiation Test 2 (inlet dissolved oxygen conc: 350 ppb, inlet dissolved hydrogen conc: 30 ppb)

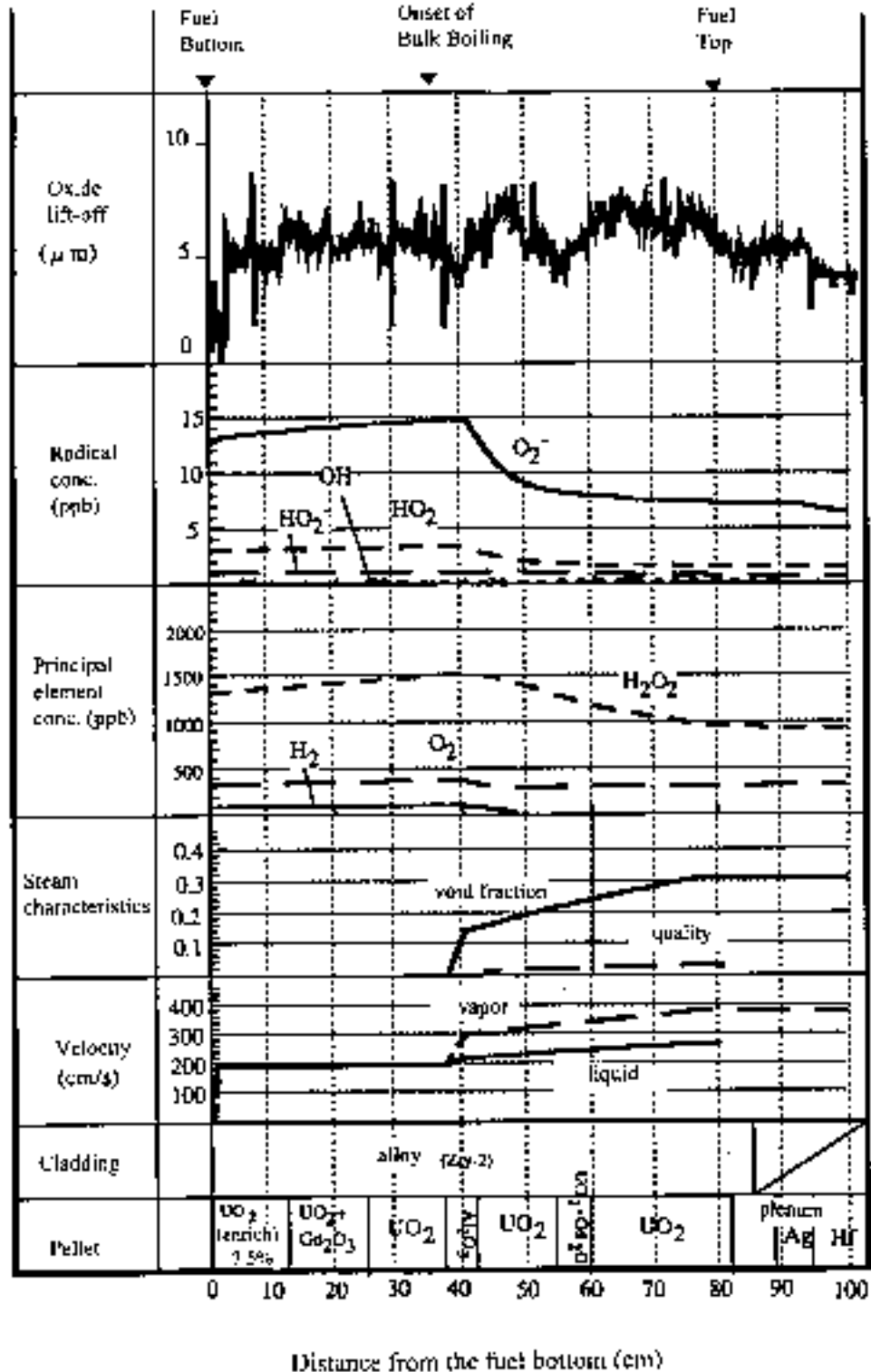


Figure 24 Hitachi's Water Chemistry Analysis of Fuel Rod Irradiation Test 3 (inlet dissolved oxygen conc: 500 ppb, inlet dissolved hydrogen conc: 30 ppb)

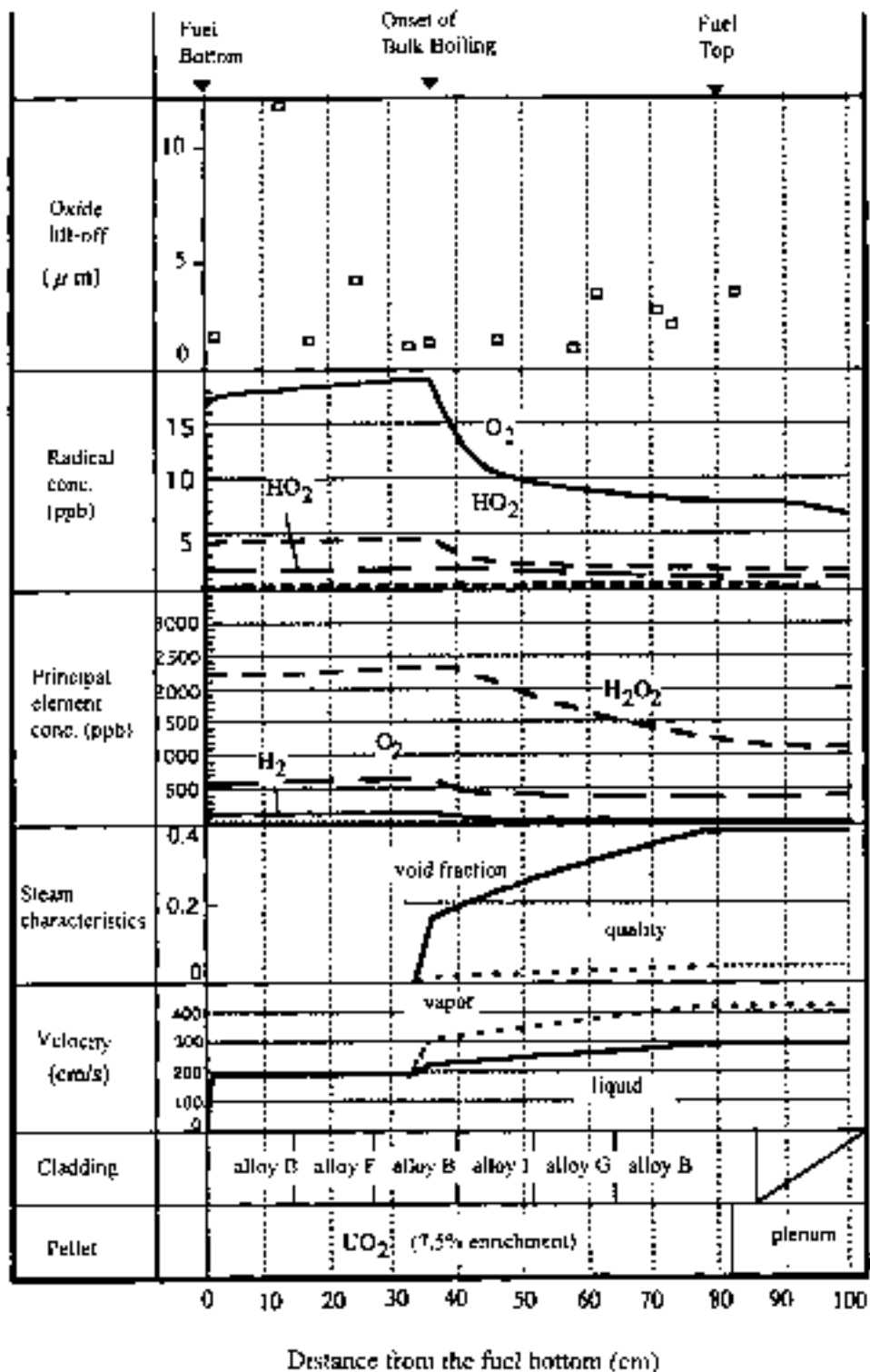


Figure 25 Hitachi's Water Chemistry Analysis of Fuel Rod Irradiation Test 4 (inlet dissolved oxygen conc: 1000 ppb, inlet dissolved hydrogen conc: 40 ppb)

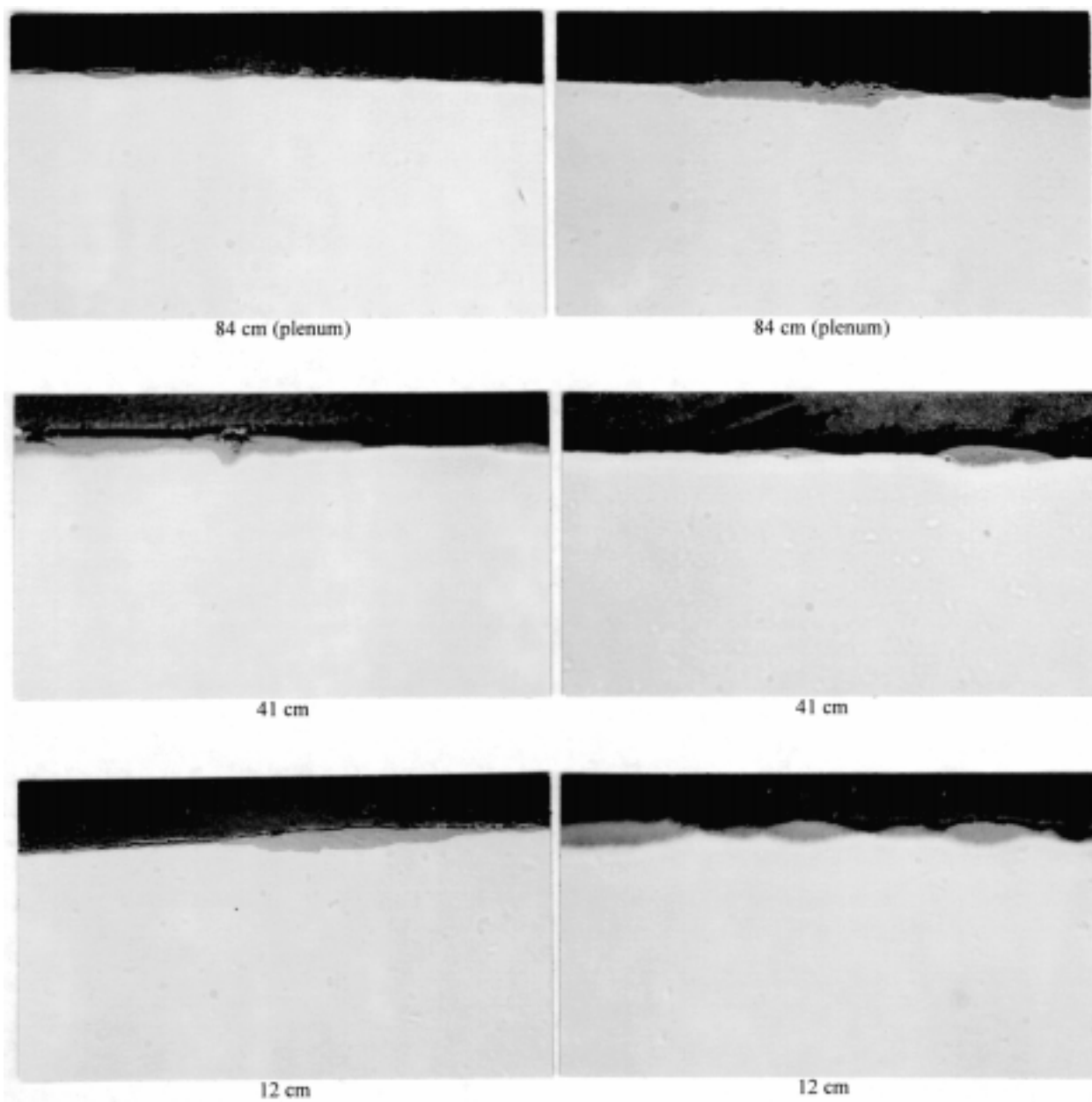


Figure 26 Outer Surface Oxide Thickness of Zircaloy-2 Alloy C Fuel Cladding in the First Fuel Rod Test with 250 ppb Dissolved Oxygen (500X)

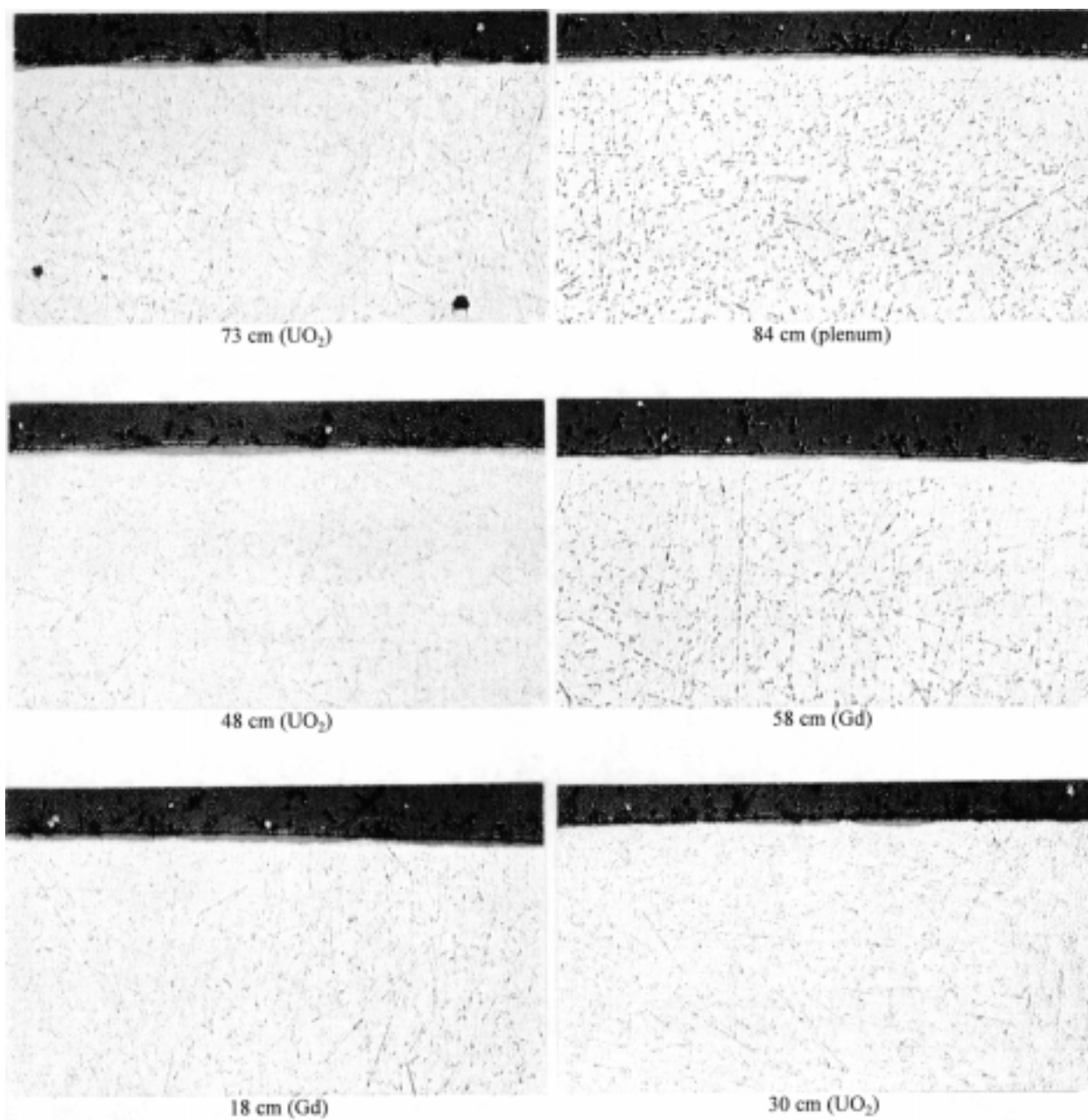


Figure 27 Outer Surface Oxide Thickness of Zircaloy-2 Alloy C Fuel Cladding in the Second Fuel Rod Test with 350 ppb Dissolved Oxygen (250X)

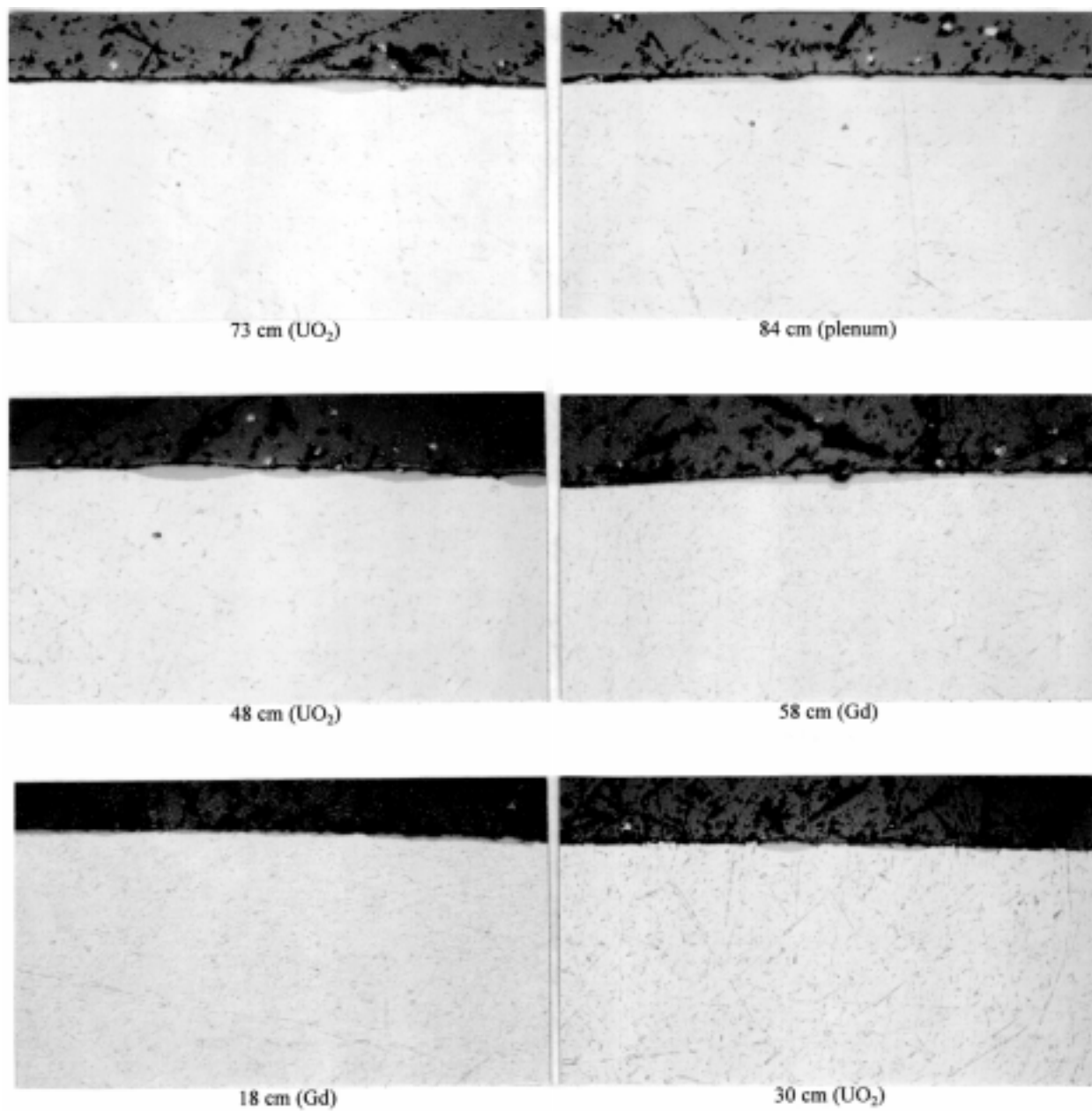


Figure 28 Outer Surface Oxide Thickness of Zircaloy-2 Alloy C Fuel Cladding in the Third Fuel Rod Test with 500 ppb Dissolved Oxygen (250X)

In Test 4, the oxygen concentration was increased to 1000 ppb but the Zircaloy-2 material was changed from Alloy C to Alloy B. A direct comparison of Zircaloy-2 corrosion in 1000 ppb O_2 cannot be made to the corrosion in Tests 1-3. However, a comparison of Alloys B and C can be made.

The peak hydrogen peroxide concentration in the fourth test was approximately 2300 ppb. Near the bottom of the rod, Alloy B did not develop nodular corrosion as did Alloy C in Tests 1-3, and the uniform oxide remained thin at 1-2 microns (Figure 29). Near the top of the fuel rod, where the peroxide concentration is 1000 ppb, which is comparable to the concentration near the top of the Test 3 rod, the maximum nodular oxide thickness is 3-7 microns with a coverage of only 10-30%. The eddy current liftoff decreased in Test 4 compared to Test 3. The potential for increased corrosion exists, as the oxygen content increases due to increased radiolysis. But the corrosion did not increase and this is attributed to the superior corrosion resistance of the tubeshell heat treated Alloy B Zircaloy-2.

It should be noted that in the radiolysis modeling for Tests 2 and 3, the gadolinia and alumina pellets were not accounted for. Incorporation of these pellet types into the model will not affect the trends that have been noted.

Hydrogen Water Chemistry Simulation. The environment of hydrogen water chemistry (HWC) was simulated in the fuel rod tests by using a time-averaged concentration 350 ppb hydrogen (measured at the outlet) and no oxygen injection. The corrosion of Zircaloy-2 Alloy B was reduced compared to the normal water chemistry (NWC) reference test of 1000 ppb O_2 . The difference between the HWC and NWC tests is manifested in the upper portion of the two fuel rods. In NWC, the lower portion of the fuel rod has a thin 1-2 micron uniform oxide and the upper portion of the fuel rod has 3-7 micron thick nodules with 10-30% coverage (Figure 29). In HWC, nodular corrosion was suppressed along the entire length of the rod, which has a 0.9-2 micron uniform oxide (Figure 30). The eddy current liftoff is also lower in HWC than it is in NWC (Figures 25 and 31).

The simulated HWC test was analyzed using Hitachi's radiolysis model code [11-12]. The calculated concentrations of oxygen, hydrogen, hydrogen peroxide and other species along the entire length of the fuel rod is shown in Figure 31. The radiolytic production of oxidizing species is very small in this case. The most significant radiolytically produced species is approximately 100 ppb of hydrogen peroxide. The hydrogen content was reduced from 400 ppb at the rod bottom to 50 ppb at the rod top but the peroxide profile remained relatively flat. The concentration of O_2^- is less than 1 ppb.

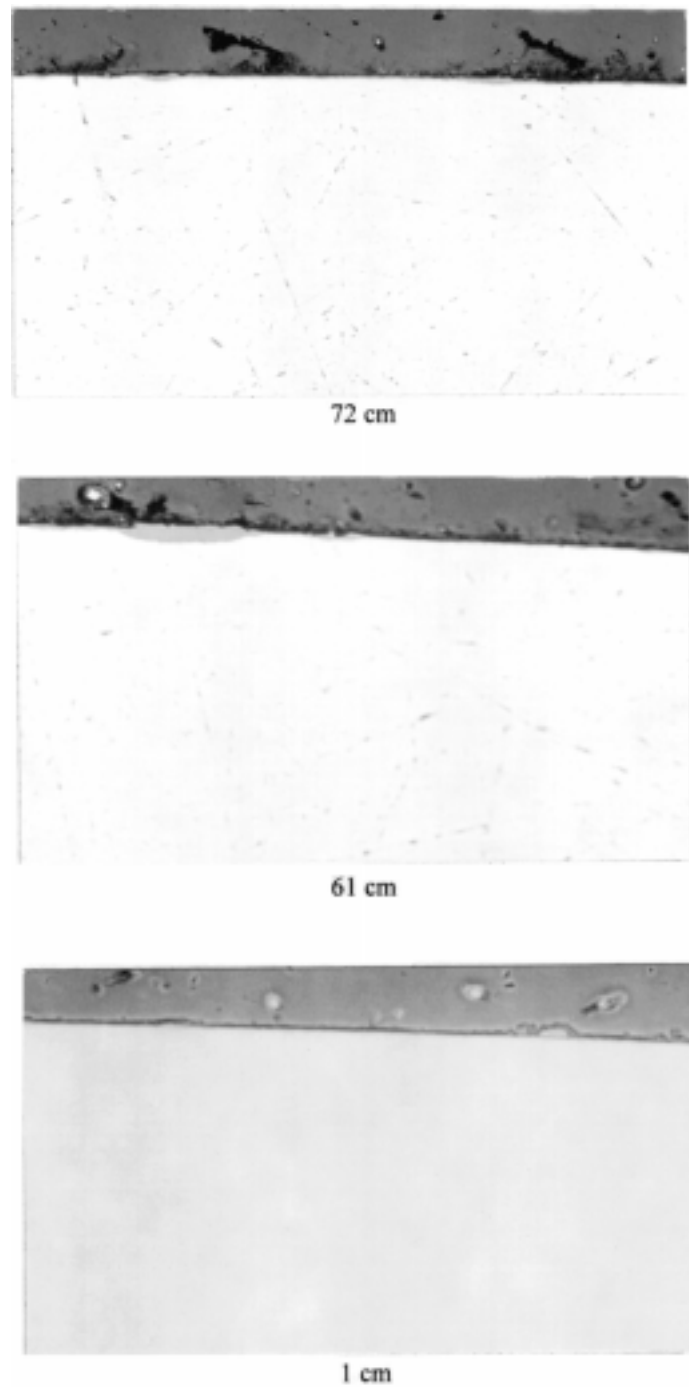


Figure 29 Outer Surface Oxide Thickness of Zircaloy-2 Alloy B Fuel Cladding in the Fourth Fuel Rod Test with 1000 ppb Dissolved Oxygen (250X)

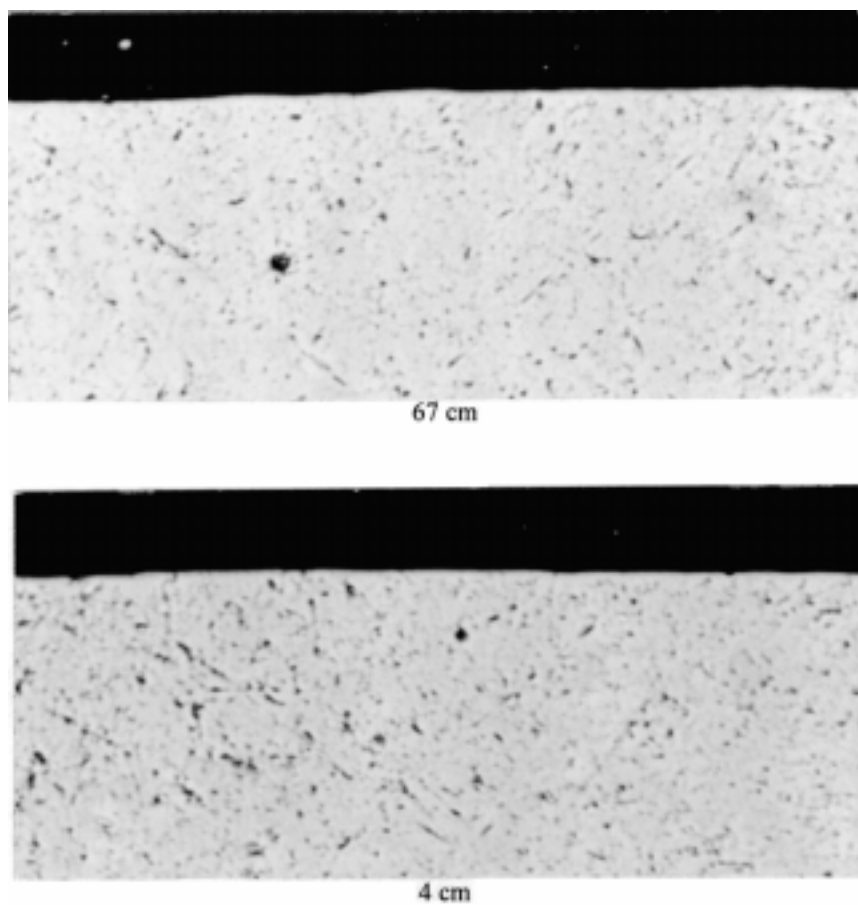


Figure 30 Outer Surface Oxide Thickness of Zircaloy-2 Alloy B Fuel Cladding in the Fifth Fuel Rod Test with 350 ppb Dissolved Hydrogen (hydrogen water chemistry simulation) (500X)

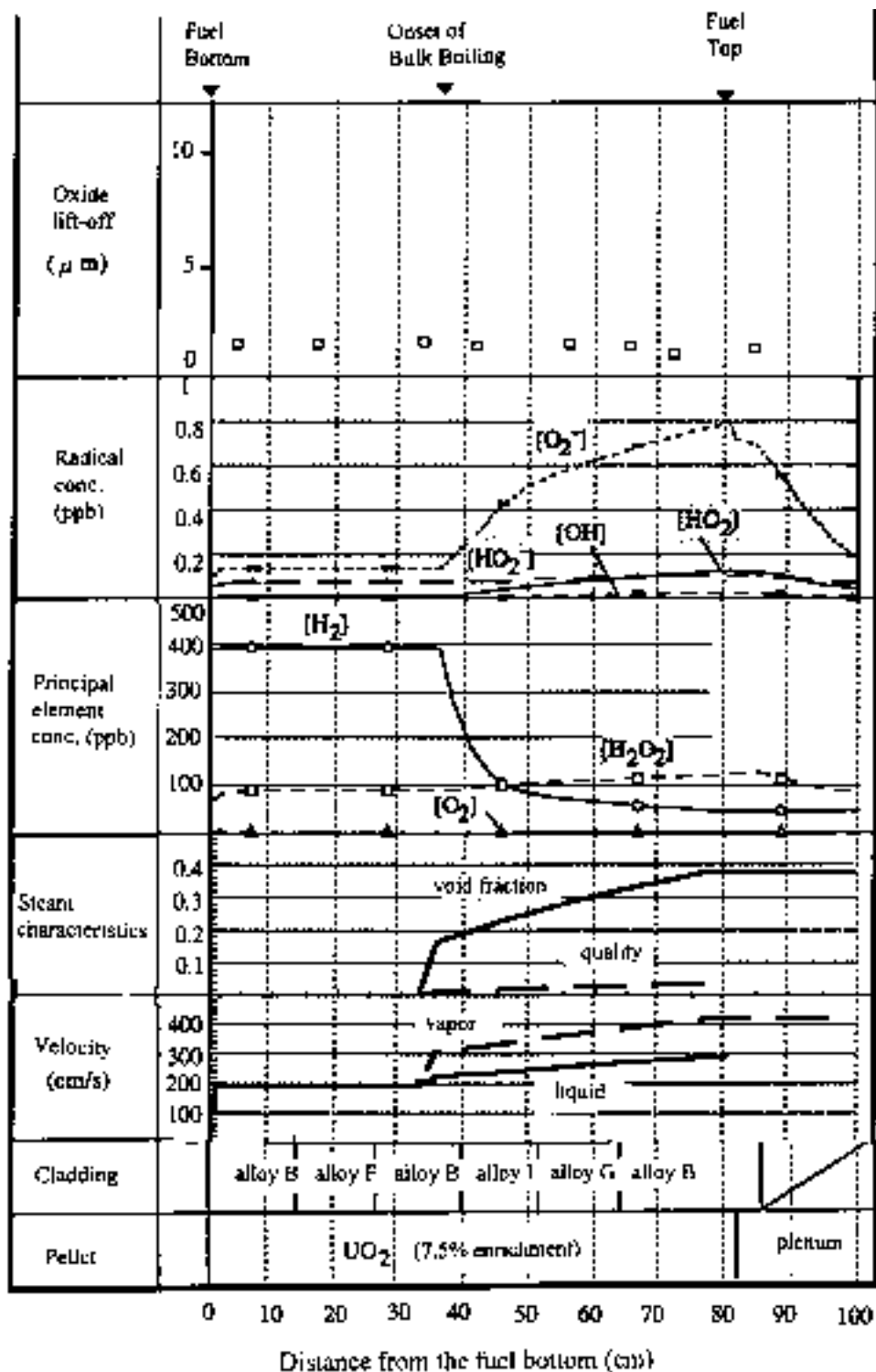


Figure 31 Hitachi's Water Chemistry Analysis of Fuel Rod Irradiation Test 5
(inlet dissolved oxygen conc: 0 ppb; inlet dissolved hydrogen
conc: 400 ppb)

The low production of radiolytic species occurs because the decomposition of water is suppressed and because the recombination reactions are promoted by an excess of hydrogen. The radiolytic production of oxygen is low because it is produced by a secondary reaction with water's decomposition products. An excess amount of dissolved hydrogen suppresses water radiolysis and promotes a reducing environment. As has been discussed with the mini-autoclave test results, the suppression of radiolysis also apparently suppresses Zircaloy-2 oxidation.

Hydrogen Water Chemistry + ZnO The environment of hydrogen water chemistry (HWC) + ZnO was simulated in the fuel rod tests using 400 ppb H_2 and approximately 25 ppb Zn^{2+} . The corrosion of Zircaloy-2 (Alloy B) was reduced compared to the NWC reference test of 1000 ppb O_2 . In NWC, the lower portion of the fuel rod has a thin 1-2 micron uniform oxide and the upper portion of the fuel rod has 3-7 micron thick nodules with 10-30% coverage. The corrosion was reduced in HWC + ZnO and the entire rod has an ~ 1-2 micron thick oxide (Figure 32). The oxide thickness in the HWC + ZnO environment is slightly greater (~1 micron) than the oxide in the HWC environment.

NaHCrO₄ + 1000 ppb O₂ The uniform corrosion of Zircaloy-2 (Alloy B) was accelerated in the NaHCrO₄ fuel rod test; nodular corrosion did not occur in this test. The average oxide thickness is 9.7 microns in the plenum and 13.8 to 15.7 microns at the other three axial locations (Figure 33). This fuel rod also developed a relatively thick (~30 microns) adherent crud layer.

This test was analyzed using Hitachi's radiolysis model code [11,12, 15] through the aforementioned *assumed* reactions shown in Figure 18 and discussed with the NaHCrO₄ mini-autoclave test results. The calculated concentrations of oxygen, hydrogen, hydrogen peroxide, O_2^- and other species along the axial length of the fuel rod are shown in Figure 34, whereas the chromium chemical species are shown in Figure 35. The most prevalent oxidizing chromium species are CrO_4^{3-} (~100 ppb) and CrO_4^{2-} (~80 ppb); the distributions of the chromium species are relatively flat. The hydrogen peroxide peaks at approximately 1700 ppb and the O_2^- concentration is less than 10 ppb.

The oxide thickness is essentially the same in the plenum (non-heat flux) and in the fueled region of the cladding. This fact implies that the presence of the thick crud deposit did not accelerate the uniform corrosion by causing the cladding surface temperature to rise.

A corrosion mechanism is proposed (eq. 3 and 4) in which the $HCrO_4^-$ ion oxidizes Zr and produces ZrO_2 , Cr_2O_3 and $Cr(OH)_3$. It should be noted that the crud deposit in this test was identified as Cr_2O_3 and/or $CrOOH$ and that Cr_2O_3 and $Cr(OH)_3$ can be combined to form $CrOOH$.



Figure 32 Outer Surface Oxide Thickness of Zircaloy-2 Alloy B Fuel Cladding in the Sixth Fuel Rod Test with 400 ppb Dissolved Hydrogen + ZnO (500X)

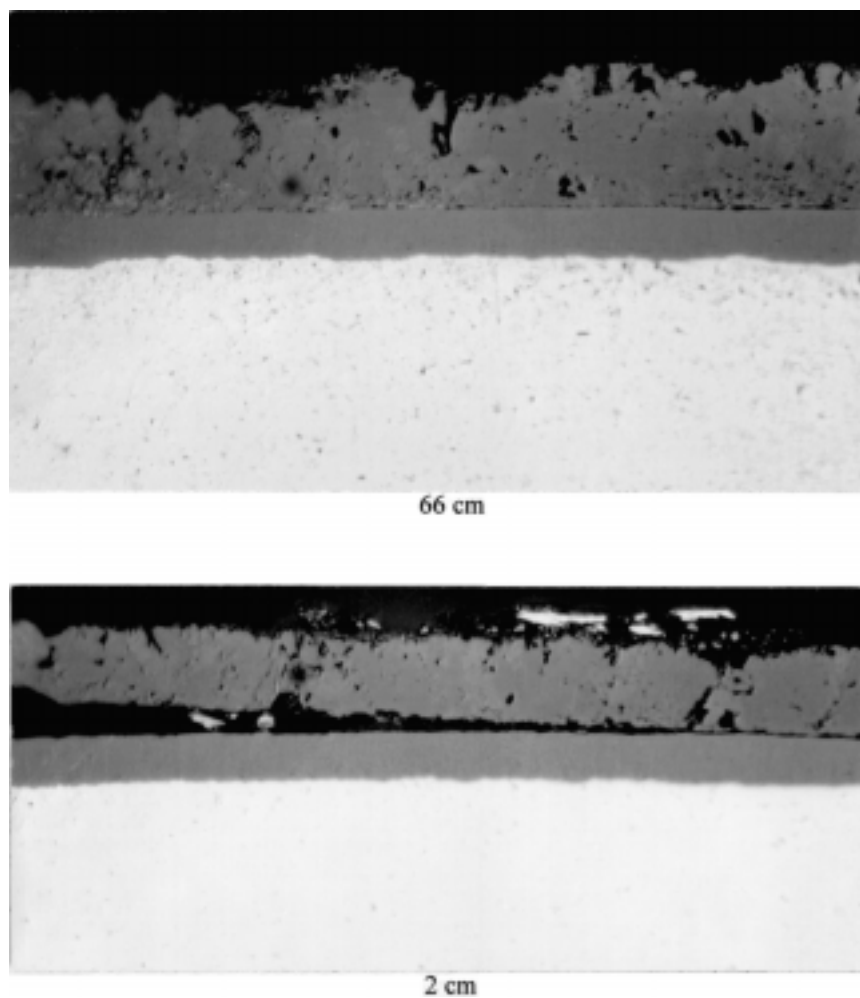


Figure 33 Outer Surface Oxide Thickness of Zircaloy-2 Alloy B Fuel Cladding in the Sixth Fuel Rod Test with NaHCrO_4 + 1000 ppb Dissolved Oxygen (500X)

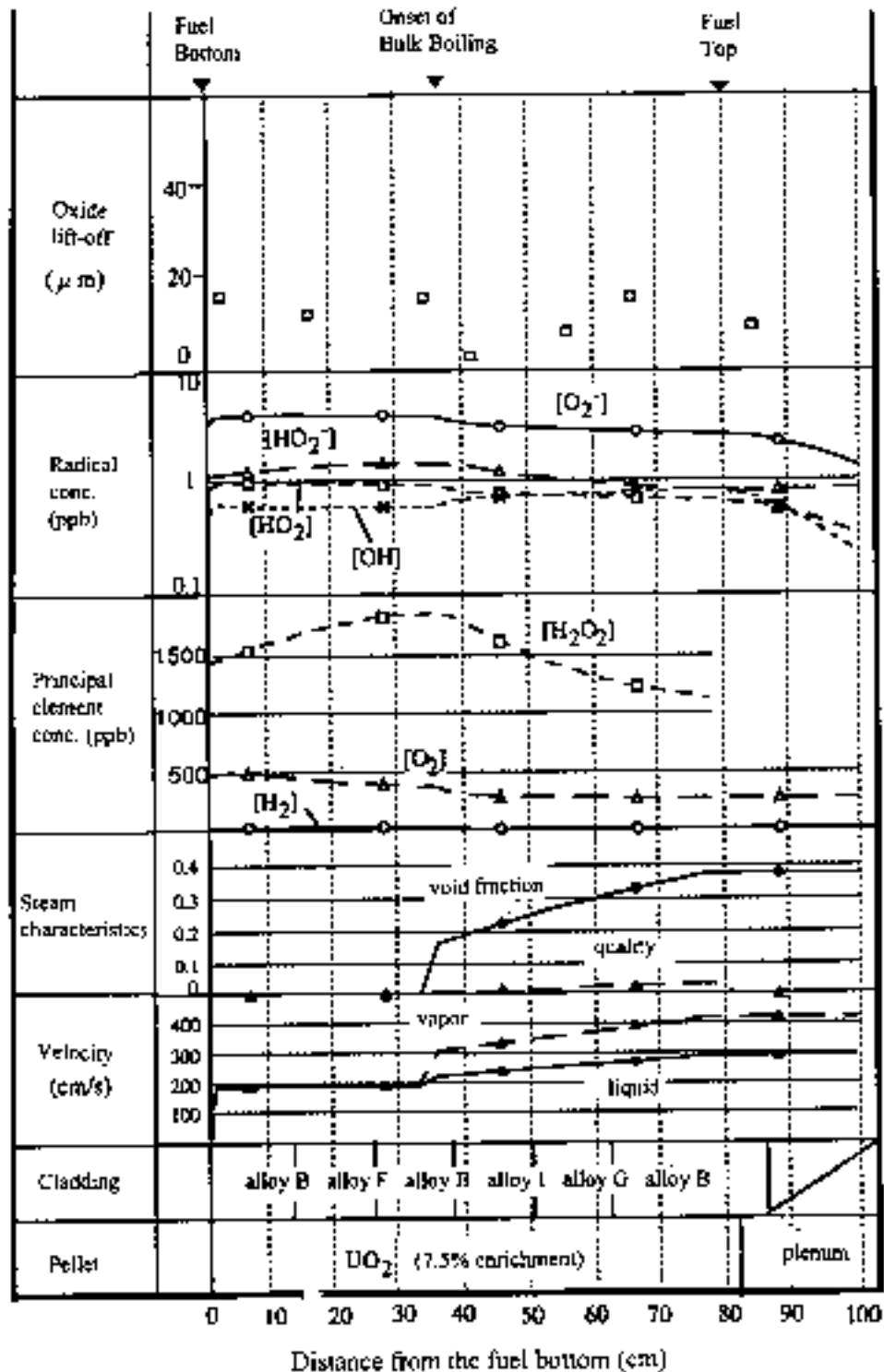


Figure 34 Water Chemistry Analysis of Fuel Rod Irradiation Test 6b
(inlet dissolved oxygen conc: 1000 ppb; inlet dissolved hydrogen
conc: 0 ppb)

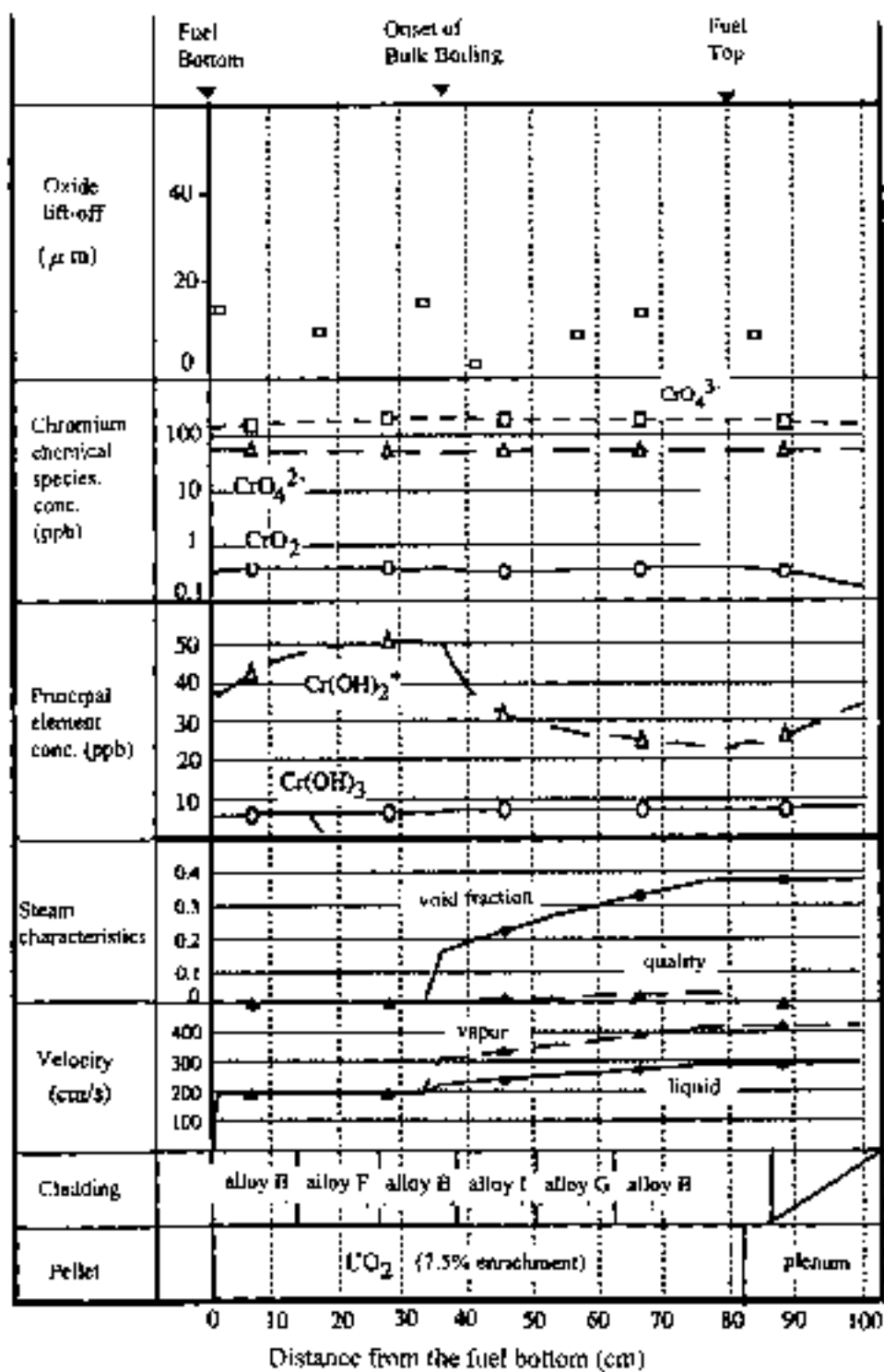
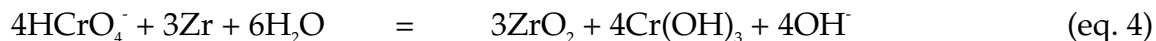


Figure 35 Water Chemistry Analysis of Fuel Rod Irradiation Test 6b
(chromium chemical species)



In $\text{NaHCrO}_4 + 1000 \text{ ppb O}_2$, the calculated peak hydrogen peroxide concentration is about 1700 ppb, which is lower than the 2400 peak peroxide concentration in the 1000 ppb NWC reference test. Similarly, the concentration of O_2^- is lower in NaHCrO_4 than in the reference test. This comparison demonstrates that the accelerated corrosion of Zircaloy-2 in NaHCrO_4 is *not* due to an increase in oxidizing species associated with high concentrations of oxygen and/or the radiolytic decomposition products of water. Rather, the accelerated corrosion is most likely caused by the HCrO_4^- ion.

Far more chromium is added continuously in this test than would ever occur during the normal operation of a BWR. Although it has been shown that NaHCrO_4 accelerates the uniform corrosion of Zircaloy-2, the applicability of this result to BWRs operating with <10 ppb Cr in the reactor water is debatable. Certainly the effect would be much less in an environment containing trace amounts of chromium species.

Heat Flux and Poison Effects

The fuel rods in Tests 2 and 3 included one 12 cm zone and one 5 cm zone of enriched $\text{UO}_2 + 4\% \text{ Gd}_2\text{O}_3$, one 5 cm zone of non-fueled Al_2O_3 , one 8 cm sleeve of Hf in the plenum, and one 8 cm sleeve of Ag in the plenum. This complex design was used to study the effect of heat flux and thermal neutron poisons on the corrosion of Zircaloy-2.

The corrosion of Zircaloy-2 in the Gd regions is similar to the UO_2 regions (Figures 27-28). There is significant nodular corrosion along the whole length of the Test 2 and 3 fuel rods, including the segments containing the lowered heat flux pellets and sleeves; the Gd does not significantly affect the formation of nodular corrosion. In Test 3, the lower Gd segment has 3-4 micron (maximum) nodular oxide with 50% coverage, whereas the UO_2 segments just above and below have 6-8 micron (maximum) nodular oxide with 30-60% coverage. The upper Gd segment has 7 micron (maximum) nodular oxide with 50% coverage, whereas the UO_2 segments just above and below have 6-10.6 micron (maximum) nodular oxide with 70-80% coverage. One could argue that the corrosion in the Gd regions is slightly lower than in the UO_2 regions, but there is little practical difference between, for example, 3 micron nodules with 50% coverage and 6 micron nodules with 30% coverage.

The corrosion of Zircaloy-2 in the alumina regions is similar to the UO_2 regions. The absence of heat flux did not suppress nodular corrosion. In Test 3, the alumina segment has 5 micron (maximum) nodular oxide with 70% coverage, whereas the UO_2 segments just above and below have 5-8 micron (maximum) nodular oxide with 60-80% coverage. Again, the absence of heat flux had very little practical effect on the nodular corrosion of Zircaloy-2.

The corrosion of Zircaloy-2 in the Hf and Ag plenum regions is similar to the non-sleeved plenum segment of the plenum. The presence of the Hf and Ag sleeves did not significantly affect nodular corrosion and, in fact, there is a considerable amount of corrosion in the non-sleeved segment of the plenum. In Test 3, the Hf and Ag segments have 4 micron (maximum) nodular oxide with 80-90% coverages, whereas the non-sleeved plenum segment has 5.5 micron (maximum) nodular oxide with 80% coverage.

Effect of Water Chemistry Environment on Hydrogen Pickup of Zircaloy-2

Hydrogen is produced during the corrosion process, which for most processes is described by eq. 5. A fraction of the corrosion generated hydrogen, X , is absorbed into the metal. The total amount of hydrogen absorbed into the oxidizing metal is an important parameter and will be discussed below.



It should be pointed out again that all of the mini-autoclave specimen hydrogen contents and many of the fuel cladding specimen hydrogen contents were estimated from optical photomicrographs. A specimen estimated to have 25 ppm hydrogen could easily have 50 ppm hydrogen if analyzed by a more accurate method such as inert gas fusion. This level of uncertainty in the hydrogen content data must be taken into consideration.

Mini-Autoclave Tests

The discussion on hydrogen pickup of Zircaloy-2 in the mini-autoclave tests will focus on Alloy B. Alloy B was selected for the evaluation of hydrogen pickup because it was included in all of the mini-autoclave tests, and it did not have anomalous hydrogen absorption associated with Zr liner oxidation, as did Alloys A and C in Tests 1 and 2.

Figure 36 shows the relationship between the hydrogen content of Alloy B (Zircaloy-2) and each mini-autoclave environment. Mini-autoclave Test 1-C with 810 ppb dissolved oxygen is the reference to which the other tests can be compared. The hydrogen content of Alloy B in the reference test is estimated to be 15 ppm. The test environments that have at least 25 ppm higher hydrogen content than the reference test could *possibly* have increased hydrogen absorption.

It is seen in Figure 36 that the $\text{Zn}(\text{NO}_3)_2$, NaHCrO_4 , and N_2 environments have higher apparent hydrogen absorption. This is understandable because they experienced accelerated corrosion. The EHC oil, Na_2SiO_3 , HWC/NWC, HWC, ZnSO_4 /HWC, SiO_2 , and ZnSO_4 environments also have higher hydrogen absorption but the corrosion for these environments is actually comparable to or less than the reference. This apparently higher hydrogen pickup associated with the HWC environments may be due to the

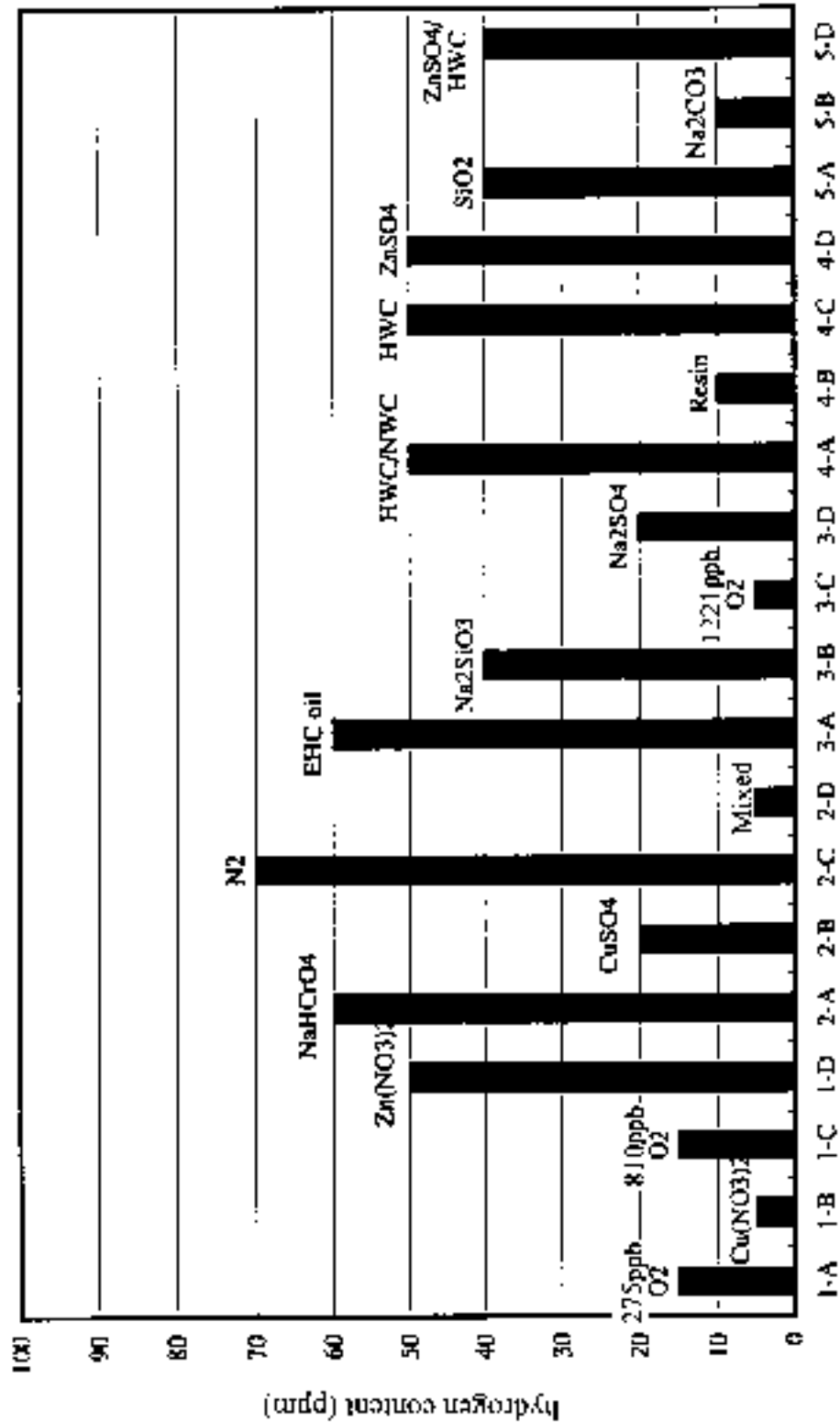


Figure 36 Hydrogen Content of Zircaloy-2 Alloy B in the Mini-Autoclave Tests

uncertainty associated with estimating hydrogen levels using metallographic standards. Increased hydrogen pickup of Zircaloy-2 in HWC was not observed by Cheng, who examined Zircaloy-2 BWR fuel cladding after it was exposed to two 18-month cycles of HWC [17]. However, it must be pointed out that, although Dresden was operating under “HWC” conditions, the fuel was exposed to a water chemistry environment that was different than that in the simulated HWC tests used at Halden.

Fuel Rod Tests

The discussion of hydrogen pickup in the fuel rod tests will focus on Zircaloy-2 Alloy B in Tests 4, 5, 6a, and 6b using the data summarized in Table 12. In the fuel rod tests, the hydrogen contents were determined by both metallographic estimates and inert gas fusion. The 1000 ppb O_2 normal water chemistry test (Test 4) is the reference to which the other tests (HWC, HWC + ZnO , and $NaHCrO_4$ + 1000 ppb O_2) can be compared. The average hydrogen content of Alloy B in Test 4 is approximately 13 ppm.

Hydrogen Water Chemistry Simulation

The hydrogen water chemistry environment was simulated by using 350 ppb hydrogen (measured at the outlet). The average hydrogen content of Zircaloy-2 Alloy B in the simulated HWC fuel rod test is 12 ppm, compared to 13 ppm for the NWC reference test. HWC did not increase the hydrogen content of Zircaloy-2 in the HWC fuel rod test.

Hydrogen Water Chemistry + ZnO

The hydrogen water chemistry + ZnO environment was simulated by using 400 ppb hydrogen plus ~25 ppb Zn^{2+} . The average hydrogen content of Zircaloy-2 Alloy B in the simulated HWC + ZnO fuel rod test is 21 ppm, compared to 13 ppm for the NWC reference test. This difference in hydrogen content is too small to be considered an indication of increased hydrogen absorption in HWC + ZnO when compared to the NWC test hydrogen contents which were estimated metallographically.

$NaHCrO_4$ + 1000 ppb O_2

The average hydrogen content of Zircaloy-2 Alloy B in the $NaHCrO_4$ + 1000 ppb O_2 fuel rod test is 17 ppm, compared to 13 ppm for the NWC reference test. The interesting point to note about this test is that the hydrogen content of the fuel rod is extremely low for such a thick uniform oxide (> 9.7 microns). The hydrogen pickup fraction in the $NaHCrO_4$ test is considerably lower than the reference test because hydrogen is not produced directly in the proposed corrosion model (eq. 4 and 5).

Performance of Alternate Alloys in Mini-autoclave and Fuel Rod Tests

Both corrosion and hydriding in the mini-autoclave and fuel rod tests must be considered when evaluating the overall performance of the alternate alloys. The corrosion resistances of the alternate alloys in the mini-autoclave tests were ranked in the same manner as the Zircaloy-2 materials. An evaluation of the alternate alloy hydrogen pickups was done only for the 810 ppb NWC reference mini-autoclave test. Each alloy will be discussed in turn.

Alloy E

This alloy is a promising candidate for further study. Alloy E was only included in the mini-autoclave tests. Its corrosion resistance is equal to or better than the best Zircaloy-2 (Alloy A) in all of the mini-autoclave environments, as shown in the corrosion ranking in Table 18. In the 810 ppb NWC reference test, Alloy E and Zircaloy-2 Alloy A both have < 2 micron uniform oxide and do not develop nodules; in the aggressive environments of 1221 ppb O₂, Zn(NO₃)₂, and N₂, Alloy E has slightly better corrosion resistance than Zircaloy-2 Alloy A.

The hydrogen pickup of Alloy E in the 810 ppb NWC reference test is compared in Figure 37 to Zircaloy-2 Alloy B. Both Zircaloy-2 Alloy B and Alloy E have about 15 ppm hydrogen.

Alloy F

This alloy is a promising candidate for further study. It has corrosion resistance and hydrogen pickup characteristics that are equivalent to or slightly better than Zircaloy-2.

The corrosion resistance of Alloy F is equal to or better than the best Zircaloy-2 (Alloy A) in all of the mini-autoclave environments, as shown in the corrosion ranking in Table 18. In the 810 ppb NWC reference test, Alloy F and Zircaloy-2 Alloy A both have <2 micron uniform oxide and do not develop nodules. In the aggressive environments of 1221 ppb O₂, Zn(NO₃)₂, and N₂, Alloy F has slightly better nodular corrosion resistance than Zircaloy-2 Alloy A.

The corrosion resistance of Alloy F is comparable to Zircaloy-2 Alloy B in the 1000 ppb O₂, 400 ppb H₂, and 400 ppb H₂ + ZnO fuel rod test environments, as shown in Figure 38; Alloy F and Alloy B both have <2.1 micron uniform oxide (at comparable axial locations) and do not develop nodules in these environments. In NaHCrO₄ + 1000 ppb O₂, Alloy F has a somewhat lower uniform oxide thickness than does Zircaloy-2 Alloy B.

The hydrogen pickup of Alloy F in the 810 ppb NWC mini-autoclave reference test is compared in Figure 37 to Zircaloy-2 Alloy B. Both Alloy F and Zircaloy-2 Alloy B have about 15 ppm hydrogen.

The hydrogen content of Alloy F in the 1000 ppb O₂, 400 ppb H₂, 400 ppb H₂ + ZnO, and NaHCrO₄ + 1000 ppb O₂ fuel rod test environments is shown in Figure 39. The hydrogen content of Alloy F and Zircaloy-2 Alloy B is between 10 and 25 ppm in these fuel rod tests. There is no discernible difference in the hydrogen pickup between Alloy F and Zircaloy-2 in these tests.

Table 18
Comparison of Corrosion Resistance of Alternate Zr Alloys and Zircaloy-2
(Alloy A) in Mini-Autoclave Irradiation Tests

	High	← Corrosion Resistance →	Low	
	Rank			
Test Water Chemistry	1	2	3	4
5C: RWCE	A,E,F,G,I		H	
4C: HWC simulation (501 ppb H ₂)	A,E,F,G,H,I	J	J	
5D: 1 ppm Zn[ZnSO ₄] + 385 ppb H ₂	A,E,F,G,H,I	J		
1B: 300 ppb Cu[Cu(NO ₃) ₂] (271 ppb O ₂)	A,E,F,G,H,I,J			
1A: 275 ppb O ₂	A,E,F,G,H,I,J			
5A: 200 ppm SiO ₂ (703 ppb O ₂)	A,E,F,G,H	I		
4D: 1 ppm Zn [ZnSO ₄] (747 ppb O ₂)	A,E,F,G,H,I	J	J	
3A: EHC oil (759 ppb O ₂)	A,E,F,G,H,I,J			
2B: 300 ppb Cu[CuSO ₄] (780 ppb O ₂)	A,E,F,G,H,I	J		
3D: 500 ppm Na ₂ SO ₄ (796 ppb O ₂)	A,E,F,G,H,I,J			
4A: HWC/NWC alternate (483 ppb H ₂ /742 ppb O ₂)	A,E,F,G,H,I		J	
4B: Resin (729 ppb O ₂)	A,E,F,G,H,I		J	
2D: CILC (Cu,Zn,Na) (796 ppb O ₂)	A,E,F,G,I,J	H		
5B: 162 ppm Na[Na ₂ CO ₃] (723 ppb O ₂)	A,E,F,G,I	H		
3B: 200 ppm Na ₂ SiO ₃ (813 ppb O ₂)	A,E,F,G,H,I,J			
1C: 810 ppb O ₂	A,E,F,G,I,J		H	
3C: 1221 ppb O ₂	A,E,F,G,H,I,J			
1D: 100 ppb Zn[Zn(NO ₃) ₂] (287 ppb O ₂)	E,F,G,H,I,J	A		
2C: 300 ppb N ₂ (765 ppb O ₂)	E,F,G,H,I,J	A		
2A: 300 ppb Cr[NaHCrO ₄] (821 ppb O ₂)		G,H,I	A,E,F	J

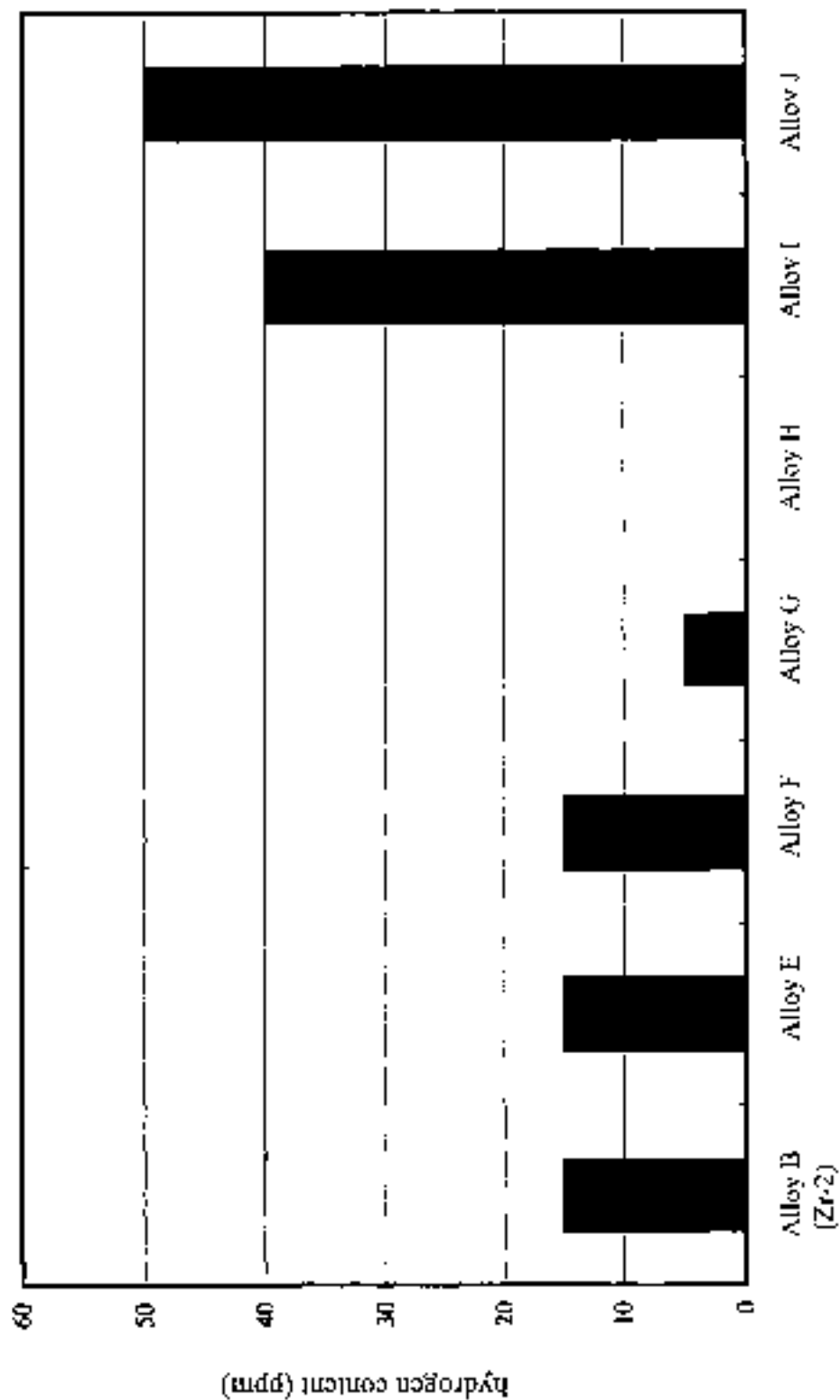


Figure 37 Hydrogen Content of Zircaloy-2 and the Alternate Alloys in the Mini-Autoclave 810 ppb O₂ Normal Water Chemistry Condition

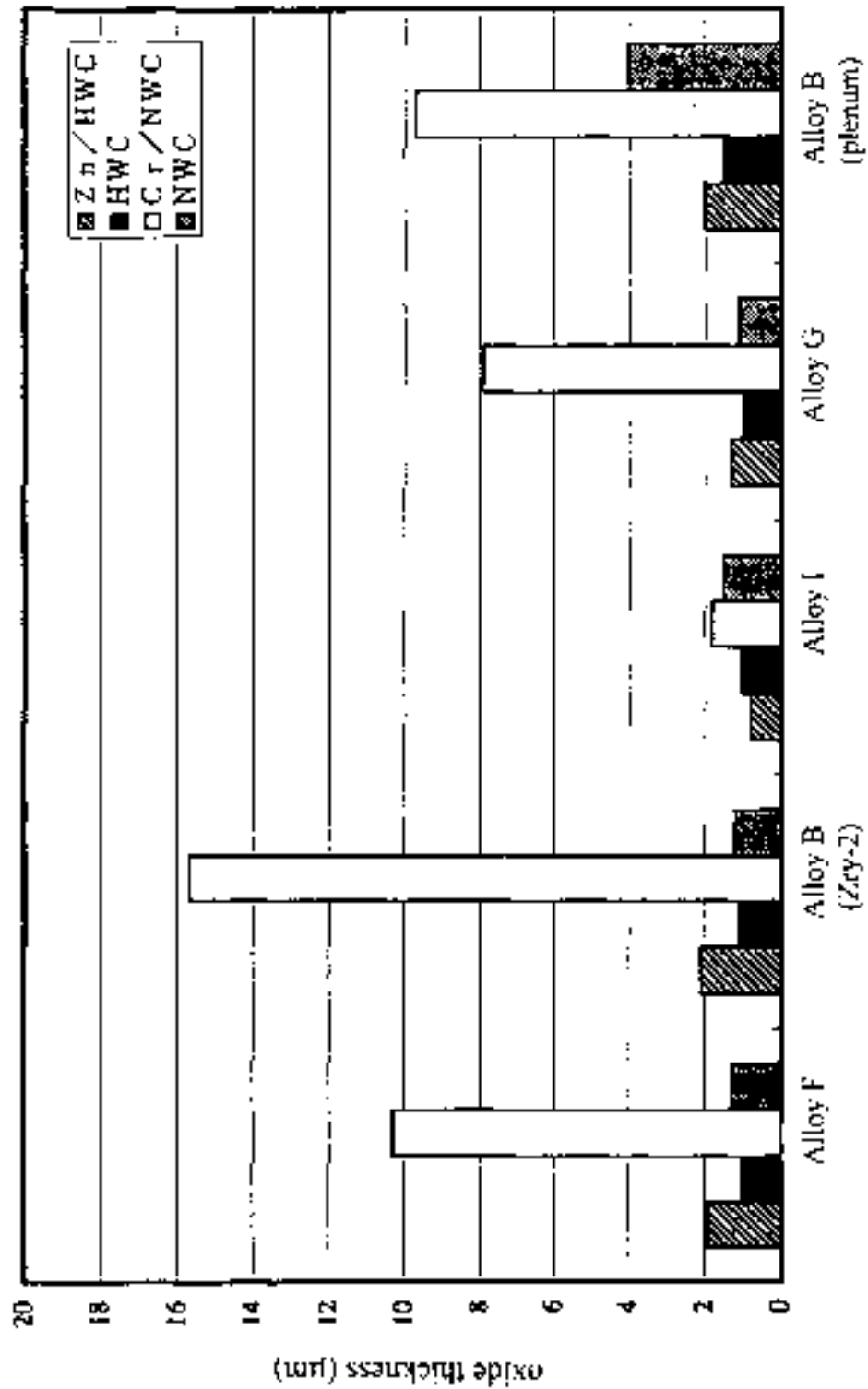


Figure 38 Comparison of the Oxide Thickness of Zircaloy-2 Alloy B and the Alternative Alloys in the Fuel Rod Irradiation Tests

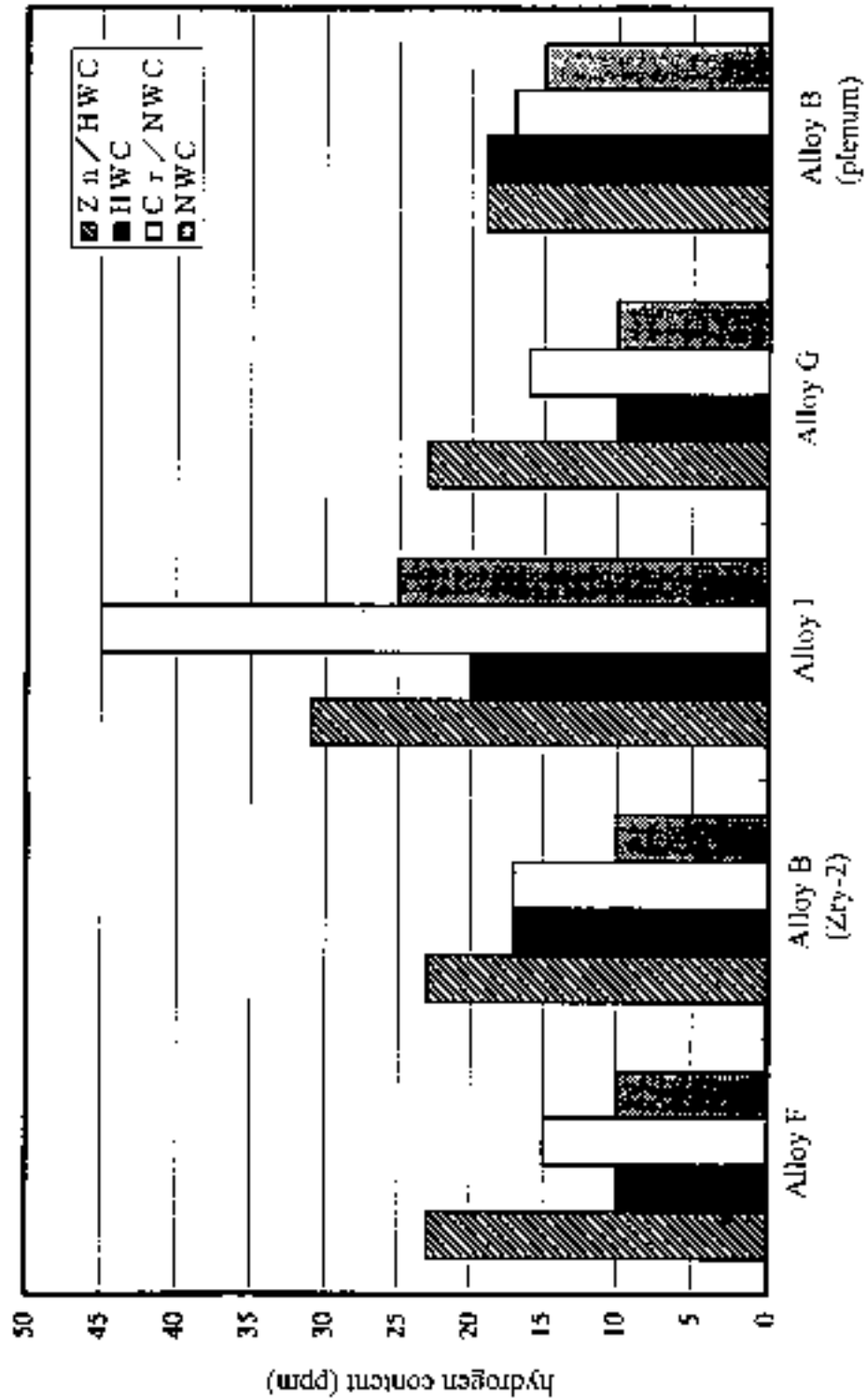


Figure 39 Comparison of the Hydrogen Content of Zircaloy-2 Alloy B and the Alternative Alloys in the Fuel Rod Irradiation Tests

Alloy G

This alloy is a promising candidate for further study. It has corrosion resistance and hydrogen pickup characteristics that are equivalent to or slightly better than Zircaloy-2.

The corrosion resistance of Alloy G is equal to or better than the best Zircaloy-2 (Alloy A) in all of the mini-autoclave environments, as shown in the corrosion ranking in Table 18. In the 810 ppb NWC reference test, Alloy G and Zircaloy-2 Alloy A both have <2 micron uniform oxide and do not develop nodules. In the aggressive environments of 1221 ppb O₂, Zn(NO₃)₂, and N₂, Alloy G has slightly better nodular corrosion resistance than Zircaloy-2 Alloy A.

The corrosion resistance of Alloy G is comparable to Zircaloy-2 Alloy B in the 1000 ppb O₂, 400 ppb H₂, and 400 ppb H₂ + ZnO fuel rod test environments, as shown in Figure 38; Alloy G and Alloy B both have <2.1 micron uniform oxide (at comparable axial locations) and do not develop nodules in these environments. In NaHCrO₄ + 1000 ppb O₂, Alloy G has a somewhat lower uniform oxide thickness than does Zircaloy-2 Alloy B.

The hydrogen pickup of Alloy G in the 810 ppb NWC mini-autoclave reference test is compared in Figure 37 to Zircaloy-2 Alloy B. Alloy G has 5 ppm hydrogen, whereas Zircaloy-2 Alloy B has 15 ppm hydrogen. This difference is not considered to be significant.

The hydrogen content of Alloy G in the 1000 ppb O₂, 400 ppb H₂, 400 ppb H₂ + ZnO, and NaHCrO₄ + 1000 ppb O₂ fuel rod test environments is shown in Figure 39. The hydrogen content of Alloy G and Zircaloy-2 Alloy B is between 10 and 25 ppm in these fuel rod tests. There is no discernible difference in the hydrogen pickup between Alloy G and Zircaloy-2 in these fuel rod tests.

Alloy H

This alloy is a promising candidate for further study from a low hydrogen pickup perspective. Alloy H was only included in the mini-autoclave tests. It has corrosion resistance that is comparable to the best Zircaloy-2 (Alloy A) in most, but not all, of the mini-autoclave environments, as shown in the corrosion ranking in Table 18. In particular, Alloy H developed 12 micron nodules with 50% coverage in the 810 ppb reference mini-autoclave test, whereas Zircaloy-2 Alloy A did not develop nodules. It is peculiar that in the environments that accelerated the nodular corrosion of Zircaloy-2 [e.g., Zn(NO₃)₂], Alloy H did not develop nodules. In some of the other mini-autoclave environments, Alloy H developed slightly thicker uniform oxide than did Zircaloy-2.

The hydrogen pickup of Alloy H in the 810 ppb NWC reference test is compared in Figure 37 to Zircaloy-2 Alloy B. It is quite remarkable that Alloy H absorbed 0 ppm

hydrogen compared to 15 ppm for the Zircaloy-2. This low hydrogen pickup behavior was also observed in many of the other mini-autoclave tests. If the hydrogen content is the main concern for a given application and some corrosion can be tolerated, Alloy H should certainly be considered for further testing and development.

Alloy I

This alloy is not a promising candidate for further study primarily because it has exceptionally high hydrogen pickup; however, it does seem to have exceptionally high uniform corrosion resistance.

The corrosion resistance of Alloy I is comparable to or better than the best Zircaloy-2 (Alloy A) in all of the mini-autoclave environments except SiO_2 , as shown in the corrosion ranking in Table 18. In the 810 ppb NWC reference test, Alloy I and Zircaloy-2 Alloy A both have <2 micron uniform oxide and do not develop nodules. In the aggressive environments of 1221 ppb O_2 , $\text{Zn}(\text{NO}_3)_2$, and N_2 , Alloy I has slightly better nodular corrosion resistance than Zircaloy-2 Alloy A. In NaHCrO_4 , Alloy I has ~2.5 micron uniform oxide, whereas Zircaloy-2 Alloy A has ~3 micron uniform oxide.

The corrosion resistance of Alloy I is comparable to Zircaloy-2 Alloy B in the 1000 ppb O_2 , 400 ppb H_2 , and 400 ppb $\text{H}_2 + \text{ZnO}$ fuel rod test environments, as shown in Figure 38; Alloy I and Alloy B both have <2.1 micron uniform oxide (at comparable axial locations) and do not develop nodules in these environments. But in $\text{NaHCrO}_4 + 1000$ ppb O_2 , Alloy I has a remarkably lower uniform oxide thickness than does Zircaloy-2 Alloy B (~2 vs. ~10-16 microns). Alloy I seems to have superior uniform corrosion resistance compared with Zircaloy-2. However, the applicability of the low uniform corrosion results in NaHCrO_4 to high burnup exposure in NWC or HWC conditions in a commercial BWR is not known.

The hydrogen pickup of Alloy I in the 810 ppb NWC mini-autoclave reference test is compared in Figure 37 to Zircaloy-2 Alloy B. Alloy I has 40 ppm hydrogen, whereas Zircaloy-2 Alloy B has 15 ppm hydrogen. This difference could be significant and indicates that Alloy I may tend to absorb more hydrogen than does Zircaloy-2.

The hydrogen content of Alloy I in the 1000 ppb O_2 , 400 ppb H_2 , 400 ppb $\text{H}_2 + \text{ZnO}$, and $\text{NaHCrO}_4 + 1000$ ppb O_2 fuel rod test environments is shown in Figure 39. The hydrogen content of Alloy G and Zircaloy-2 Alloy B is between 10 and 45 ppm in these fuel rod tests. The hydrogen content of Alloy I is always higher than Alloy B. The most notable difference in hydrogen content occurs for the $\text{NaHCrO}_4 + 1000$ ppb O_2 test. In this test, Zircaloy-2 Alloy B has about 17 ppm hydrogen but Alloy I has 45 ppm hydrogen. This difference in hydrogen content is especially significant because the oxide thickness of Alloy I is ~5-8 times less than Alloy B.

Alloy J

Alloy J does not offer any particular advantage over Zircaloy-2 and, in fact, may have inferior corrosion resistance and hydrogen pickup.

Alloy J was only included in the first four mini-autoclave tests. It has corrosion resistance that is comparable to the best Zircaloy-2 (Alloy A) in some of the mini-autoclave environments as shown in the corrosion ranking in Table 18. In the 810 ppb NWC reference test, Alloy J and Zircaloy-2 Alloy A both have <2 micron uniform oxide and no nodules. But in the hydrogen water chemistry simulation, the alternating HWC/NWC test, in the resin test, and in the ZnSO_4 test, Alloy J developed 3 micron nodules with 10-20% coverage; Zircaloy-2 Alloy A did not develop nodules in these tests.

The hydrogen pickup of Alloy J in the 810 ppb NWC reference test is compared in Figure 37 to Zircaloy-2 Alloy B. It is noteworthy that Alloy J has a higher hydrogen content (50 ppm) than Zircaloy-2 Alloy B (15 ppm) or any of the other alternate alloys.

Crud Deposition Behavior

The fuel rod crud deposits are influenced by the water chemistry environment. The fuel rod crud deposits were evaluated by visual examinations, SEM/EPMA analyses, and x-ray diffraction. The crud deposition characteristics of Test 4 (NWC), Test 5 (HWC), Test 6(a) (HWC + ZnO), and 6(b) (NaHCrO_4 + 1000 ppb O_2) will be discussed in turn.

Normal Water Chemistry (NWC)

The cladding surface before and after crud removal (by brushing) is shown in Figure 40. The crud deposition is characterized as light. The few crud deposits that were observed by SEM/EPMA are nickel and iron rich.

Hydrogen Water Chemistry (HWC)

The cladding surface before and after crud removal (by brushing) is shown in Figure 40. The crud deposition is heavy compared to the NWC test; there is a delineation between fueled and un-fueled regions, i.e., essentially no crud is deposited in the un-fueled regions. The crud is loose and easily removed by brushing. X-ray diffraction identified the crud as ferrimagnetic nickel ferrite (NiFe_2O_4).

Corrosion products are released from the stainless steel and Inconel components of the test loop when the water chemistry is switched from oxidizing NWC conditions to reducing HWC conditions. Based on laboratory data, the release occurs because the oxide film on stainless steel changes its structure [18]. This phenomenon has been observed in several BWRs switching from NWC to HWC [18].

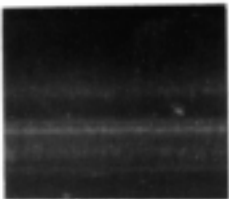
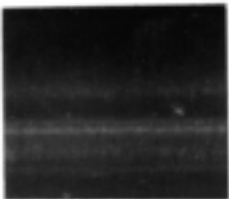
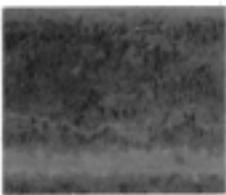
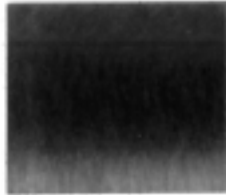

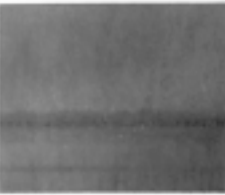
Test Number	Fuel rod appearance		Characteristics	Composition
	before brushing	after brushing		
Test 4 Normal Water Chemistry			No deposition	—
Test 5 H ₂ injection			Copious Non-adherent	NiFe ₂ O ₄
Test 6(a) H ₂ +Zn injection			Outer layer similar to Test 5 Inner thin, tenacious layer	NiO NiFe ₂ O ₄ ZnFe ₂ O ₄ (?)

Figure 40 Crud Deposition Characteristics in the Fuel Rod Irradiation Tests

Hydrogen Water Chemistry + ZnO (HWC + ZnO)

The cladding surface before and after crud removal (by brushing) is shown in Figure 40. The crud deposition is similar to the HWC test. The majority of the crud is loose and easily removed by brushing. However, a tenacious layer of crud 1-2 microns thick remains after brushing. The HWC + ZnO crud is primarily iron and nickel rich but it does contain zinc; the structure of the crud was identified by x-ray diffraction as NiO and ferrimagnetic nickel ferrite (NiFe_2O_4). The crud is comprised of several percent zinc which is probably in the form of a mixed nickel-zinc ferrite ($\text{ZnFe}_2\text{O}_4 + \text{NiFe}_2\text{O}_4$).

Figure 41 shows the fuel rod axial liftoff profile by eddy current testing for the zinc injection test. The liftoff drastically decreased by brushing, but as the liftoff is still 5 to 10 μm after brushing, it overestimates the true oxide thickness by at least a factor of 5. The discrepancy between the eddy current and the metallographic measurements of the oxide thickness is attributed to the adherent ferrimagnetic crud.

NaHCrO_4 + 1000 ppb O_2

The NaHCrO_4 test promoted the deposition of a black, tenacious crud deposit, as seen in Figure 33. The crud thickness is approximately 30 μm and was observed to spall occasionally. The fuel rod eddy current liftoff profile before and after brushing is shown in Figure 42. The liftoff after brushing is 40 to 50 μm , which is almost the same as the sum of the oxide and crud thicknesses. Since this crud is also observed in the plenum region, the mechanism of crud deposition is probably not the same as the evaporation-condensation process that occurred under HWC conditions.

The crud was identified by x-ray diffraction to be Cr_2O_3 and/or $\text{CrO}(\text{OH})$; $\text{CrO}(\text{OH})$ is a combination of Cr_2O_3 and $\text{Cr}(\text{OH})_3$. Cr_2O_3 is paramagnetic, which explains why the eddy current liftoff measurements were not significantly influenced by the thick and tenacious crud as occurred for the tenacious crud in the HWC + ZnO fuel rod test.

Corrosion of Mini-Autoclave Containers

The mini-autoclave tests were conducted by placing corrosion coupons inside four mini-autoclaves. Each mini-autoclave is fabricated from tubeshell heat treated Zircaloy-2 (Alloy B). The design of the corrosion loop is such that the outer mini-autoclave surfaces are in contact with $\sim 280^\circ\text{C}$ water, while the inside surfaces are in contact with the specific environment being tested in that mini-autoclave. In mini-autoclave Tests 1-4 there was a significant difference between the mini-autoclave container inner and outer surface oxide thicknesses, as shown in Figure 43 [i.e., 19-28 microns (outer surface) and 1-8 microns (inner surface)].

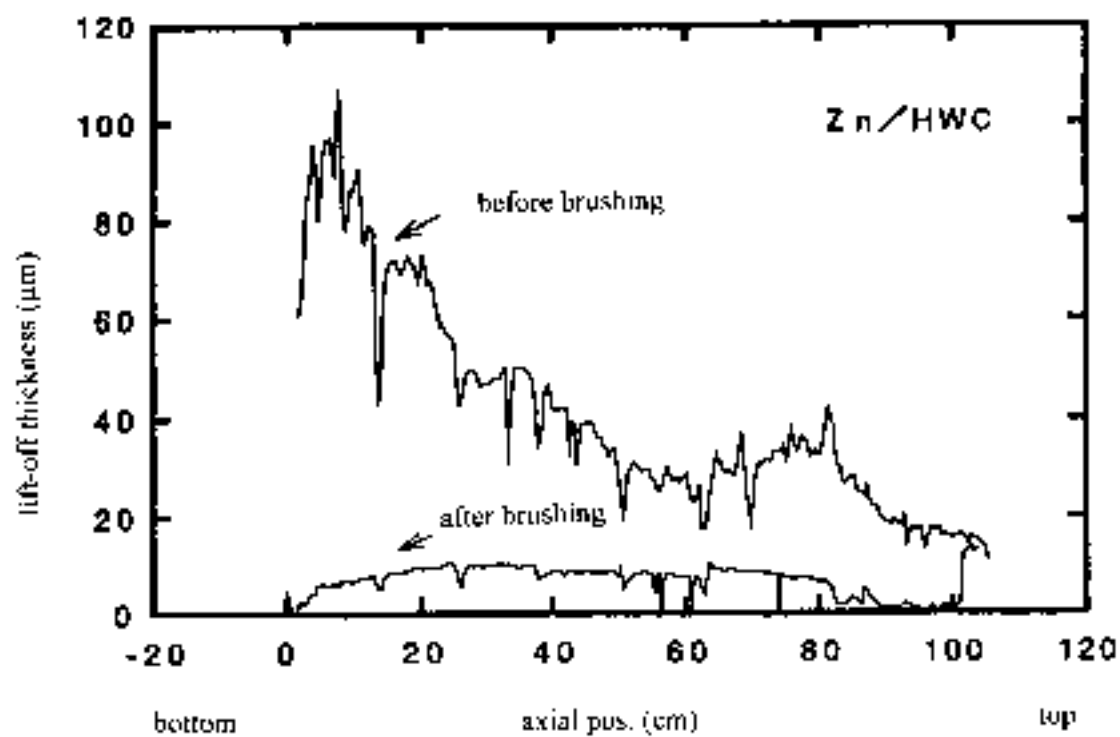


Figure 41 Axial Oxide Thickness Profile (Eddy Current) of the Fuel Rod in the Hydrogen Water Chemistry + Zinc Injection Fuel Rod Irradiation Test

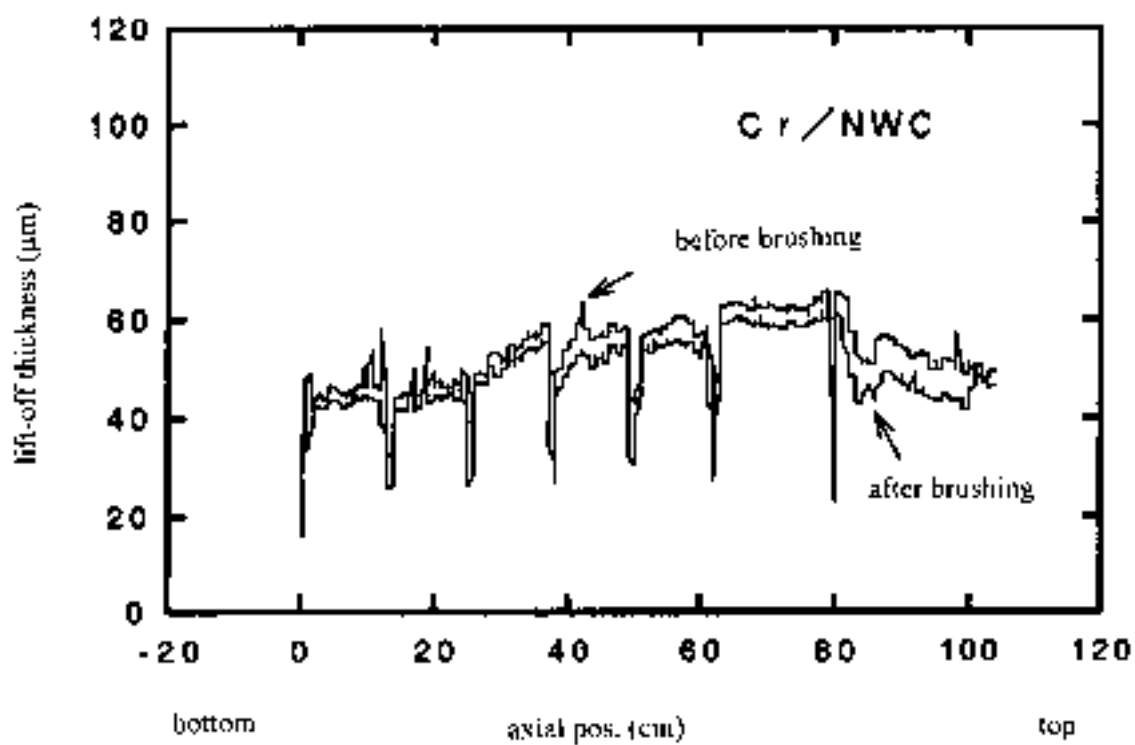


Figure 42 Axial Oxide Thickness Profile (Eddy Current) of the Fuel Rod in $\text{NaHCrO}_4 + 1000 \text{ ppb O}_2$ Fuel Rod Irradiation Test

Two hypotheses were proposed to explain the difference in outer surface vs. inner surface corrosion:

- *Galvanic* - In Tests 1-4, the mini-autoclave loop flow channel and mini-autoclave inlet and outlet tubing were Inconel 600 and stainless steel, respectively. It was hypothesized that the Zircaloy-2 mini-autoclave containers were galvanically coupled to the tubing and/or flow channel and that this coupling caused the accelerated corrosion.
- *Shadow* - In Tests 1-4, the mini-autoclave loop flow channel was Inconel 600. It was hypothesized that there was a shadow corrosion effect (an effect of β emission [19]).

In Test 5, the flow channel and tubing were replaced with Zircaloy-4. The mini-autoclave container outer surface oxide was much lower in Test 5 at 1-2 microns. Apparently, the hardware *was* the cause of the accelerated outer surface corrosion. But because both proposed mechanisms are based on the presence of the hardware, the change did nothing to elucidate the cause of the accelerated corrosion.

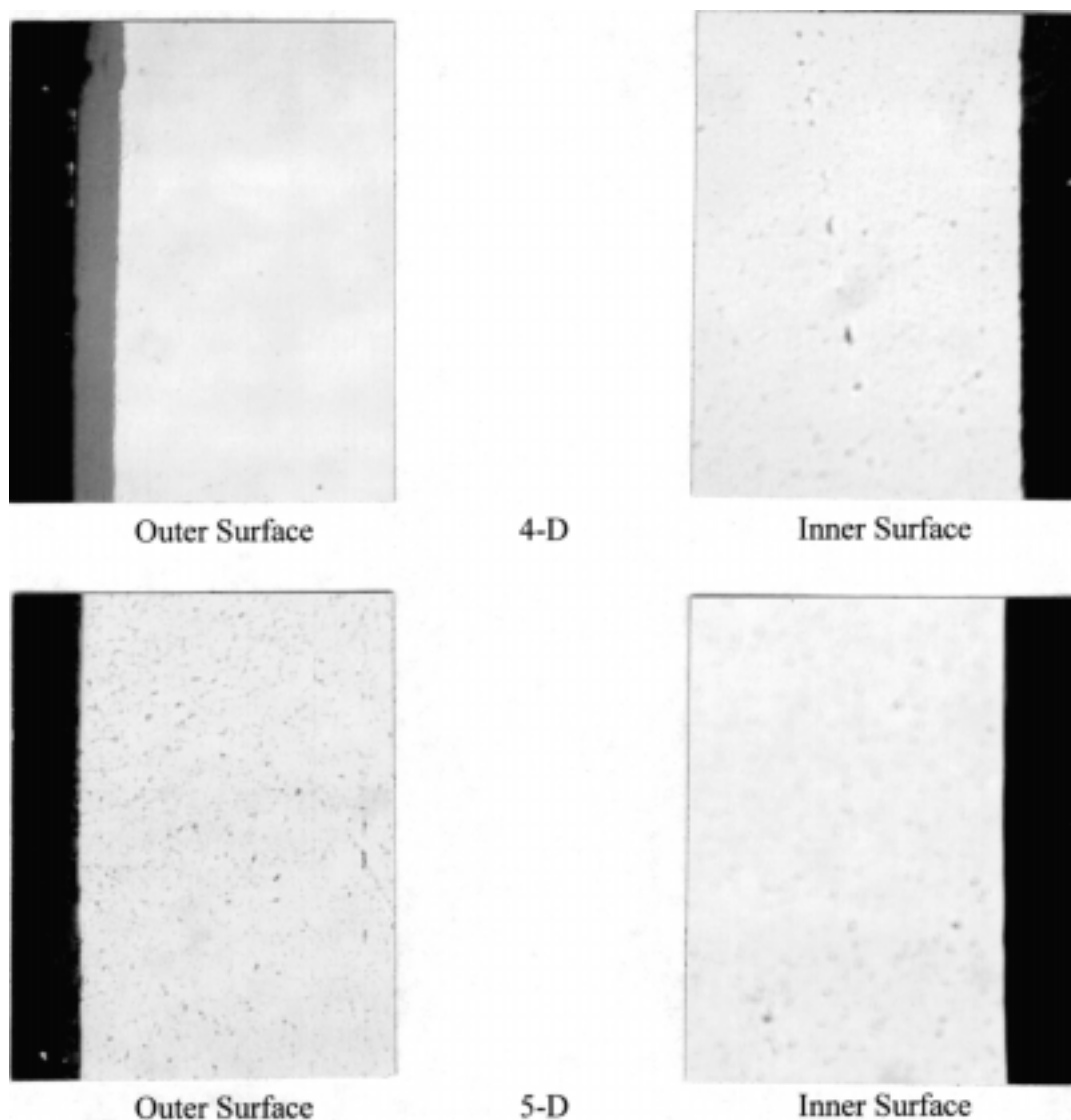


Figure 43 Comparison of the Mini-Autoclave Container Inner and Outer Surface Oxide Thickness for Mini-Autoclave Tests 4-D and 5-D [The Test 4-D mini-autoclave container is typical of those in Tests 1, 2, and 3]

4

CONCLUSIONS

The extensive testing of Zircaloy-2 and alternate Zr-alloys in the Halden BWR corrosion loop has led to the following conclusions about the effect of water chemistry impurities on corrosion:

1. The Halden BWR corrosion loop simulates the corrosion environment that fuel cladding and fuel components are subjected to in commercial BWRs. Significant nodular and uniform oxide growth occurred in the 100-140 day duration of the fuel rod and mini-autoclave tests.
2. Oxygen accelerates the nodular corrosion of Zircaloy-2 but its effect can be reduced by the presence of other impurities.
3. The production of hydrogen peroxide is proportional to the dissolved oxygen content in the core water; other radiolytic species also increase as the oxygen content is increased but to a lesser extent. Hydrogen peroxide and O_2^- are the most likely species to accelerate corrosion.
4. Radiolysis calculations show that hydrogen water chemistry promotes a reducing environment by suppressing the formation of radiolytic species that are thought to accelerate nodular corrosion of Zircaloy-2. Hydrogen water chemistry therefore suppresses nodular corrosion of Zircaloy-2 by maintaining a reducing environment.
5. Corrosion is reduced in a combined hydrogen water chemistry and ZnO environment, but the amount of corrosion is approximately 1 micron greater than in hydrogen water chemistry alone.
6. The nodular corrosion of Zircaloy-2 is accelerated in zinc nitrate.
7. The nodular corrosion of Zircaloy-2 is accelerated in nitrogen.
8. NaHCrO_4 accelerates the uniform corrosion of Zircaloy-2. The acceleration is attributed to the HCrO_4^- ion.
9. $\text{Cu}(\text{NO}_3)_2$, CuSO_4 , ZnSO_4 , Na_2SO_4 , Na_2SiO_3 , SiO_2 , Resin, and EHC oil either suppress or do not accelerate the corrosion of Zircaloy-2.

Conclusions

10. The sulfate ion seems to suppress the formation of radiolytic species and thus reduces the nodular corrosion of Zircaloy-2.
11. Copper retards the recombination of O₂ and H₂.
12. The deleterious effects of oxidizing water chemistry conditions are reduced for Zircaloy-2 that has high nodular corrosion resistance.
13. Compared to the highest corrosion-resistant Zircaloy-2 material used in this study, three of the six zirconium-based alternate alloys have slightly better nodular corrosion resistance and equivalent hydrogen pickup. One alternate alloy has low hydrogen pickup but inferior corrosion resistance; one alternate alloy has exceptionally high hydrogen pickup; and one alternate alloy has inferior corrosion resistance and high hydrogen pickup.
14. Hydrogen water chemistry promotes the deposition of crud onto the fuel rod in the Halden BWR corrosion loop.
15. Eddy current liftoff techniques can significantly overestimate the oxide thickness of Zircaloy-2 fuel cladding when exposed to an environment, such as a combination of hydrogen water chemistry and ZnO, which promotes the presence of a tenacious, magnetic crud layer.

5

REFERENCES

1. Cheng, B., "BWR Water Chemistry and Zircaloy Corrosion Tests (RP3247)," GE report NEDC-31916-1P, February 1991.
2. Cheng, B., "BWR Water Chemistry and Zircaloy Corrosion Tests (RP3247)," GE report NEDC-31916-2P, August 1991.
3. Cheng, B., Shimada, S., "BWR Water Chemistry and Zircaloy Corrosion Tests (RP3247)," GE report NEDC-31916-3P, April 1992.
4. Levin, H., "BWR Water Chemistry and Zircaloy Corrosion Tests (RP3247)," GE report NEDC-31916-4P, April 1993.
5. Levin, H., Lin, C.C., Zimmerman, D.L., Hoshi, E.V., "BWR Water Chemistry and Zircaloy Corrosion Tests (RP3247)," GE report NEDC-31916-5P, April 1993.
6. Chen, J.S.F., Levin, H., Lin, C.C., Zimmerman, D.L., Hoshi, E.V., "BWR Water Chemistry and Zircaloy Corrosion Tests (RP3247)," GE report NEDC-31916-6P, October 1993.
7. Chen, J.S.F., Levin, H., Lin, C.C., "BWR Water Chemistry and Zircaloy Corrosion Tests (RP3247)," GE report NEDC-31916-7P, April 1994.
8. Chen, J.S.F., Levin, H., Lin, C.C., Zimmerman, D.L., "BWR Water Chemistry and Zircaloy Corrosion Tests (RP3247)," GE report NEDC-31916-8P, October 1994.
9. Lutz, D.R., Lewis, J.E., Warner, R.W., Lin, C.C., "BWR Water Chemistry and Zircaloy Corrosion Tests (RP3247)," GE report NEDC-31916-9P, December 1995.
10. Lutz, D.R., "BWR Water Chemistry and Zircaloy Corrosion Tests (RP3247)," GE report NEDC-31916-10P, September 1996.
11. Ibe, E., Uchida, S., Journal of Nuclear Materials, 130, 45, 1985.
12. Ibe, E., et al., Journal of Nuclear Science Technology, 24, 220-226, 1987.

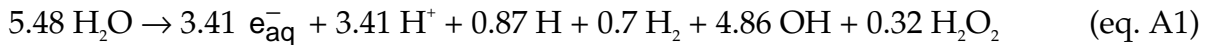
References

13. Ichikawa, N., et al., Proc. Water Chemistry of Nuclear Reactor Systems 6, Vol. 2, 127, 1992.
14. Ruiz, C.P., et al., Proc. Water Chemistry of Nuclear Reactor Systems 6, Vol. 2, 141, 1992.
15. Ibe, E., Watanabe, Y., Takahashi, M., Water Chemistry of Nuclear Reactor Systems 6, BNES, London, Paper 35, 1992.
16. Lin, C.C., Smith, F.R., "Decomposition of Hydrogen Peroxide at Elevated Temperatures," EPRI NP-6733, March 1990.
17. Cheng, B., "Hydrogen Water Chemistry Fuel Surveillance at Dresden-2," EPRI NP-6956-D, August 1990.
18. Lin, C.C., "Hydrogen Water Chemistry Effects on BWR Radiation Buildup," EPRI TR-104605, December 1994.
19. Chen, J.S.F., Adamson, R.B., "Observations of Shadow Phenomena on Zirconium Alloys," Proceedings of the 1994 International Topical Meeting on Light Water Reactor Fuel Performance, West Palm Beach Florida, pp. 309-313, April 17-21, 1994.

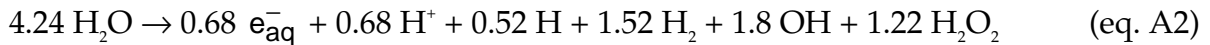
Appendix A

FUNDAMENTALS OF WATER RADIOLYSIS

Water decomposes in the gamma and fast neutron radiation fields typical of the core region of a boiling water reactor. This process is known as radiolysis and produces stable and radical species such as H_2 , O_2 , H_2O_2 , O_2^- , HO_2 , HO_2^- , OH , e_{aq}^- , H^+ and OH^- . Most of these species are unstable in nature so that direct measurement of their concentrations in the radiation field is practically impossible. Although the detailed mechanism of water radiolysis is complex, a simple scheme has been well established to explain experimentally observed effects. The overall simplified general expressions for the decomposition reactions are shown in eqs. 1 and 2:



and



where the numerical coefficients in the equations are called “G” values of the product species, or the yields of the species produced or destroyed per 100 eV of radiation energy absorbed in water.

Computer codes have been developed, and used in the current study, to simulate the radiolytic process by Hitachi [11-12], Toshiba [13], and GE [14]. A brief discussion of the fundamentals of water radiolysis and the development of eqs. 1 and 2 is presented below to provide a basis for understanding these models.

The primary radiolytic process is to produce H and OH radicals:



Many of these radicals react with each other in regions of high local concentration to form molecular products, H_2 and H_2O_2 or reform water according to the reactions:



The molecular products H_2 and H_2O_2 may be destroyed and water is reformed by the following chain reaction:



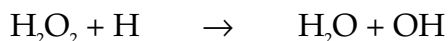
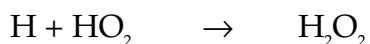
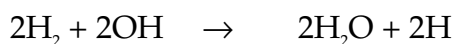
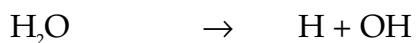
The production of molecular O_2 is brought about by the following reactions:



H_2O_2 is also catalytically decomposed to O_2 . Although the true mechanism may be very complex, the overall H_2O_2 decomposition is written as:



For the recombination of H_2 and O_2 , a balanced set of reactions can be written as:



Similar to a chemical reaction, water decomposition and $H_2 + O_2$ recombination can reach an equilibrium very quickly in the liquid phase, and the equilibrium concentrations of H_2 and O_2 depend on the dose rate in the system.



In the presence of excess H_2 in water, the water decomposition and production of O_2 can be suppressed through a chain reaction which rapidly reduces the concentration of OH and H_2O_2 in the reactions.



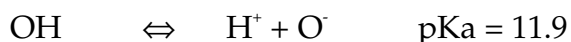
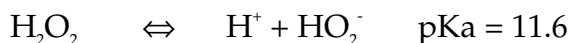
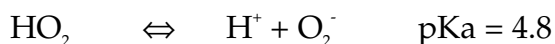
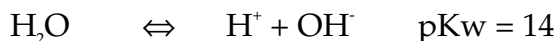
These two species are normally the precursors of O_2 in the reactions, as shown in eqs. 9-11. The overall reaction can be written as:



The excess H_2 provides the excess H radical to remove OH and H_2O_2 from a chain reaction to stop radiolysis, and there is no net consumption of H_2 in the process. In the presence of excess O_2 in water, the water decomposition production of H_2 can also be suppressed in a similar fashion, but probably with a different rate and efficiency. In a system where O_2 is present initially with excess H_2 in water, the radiation effect is to remove the O_2 in water with a small consumption of H_2 :



It is of interest to point out that only neutral species are used in the illustration of free radical reactions (eqs. 3-18). In fact, many free radicals may exist in acid/base equilibrium similar to water dissociation such as the following:



The dissociation constants vary with temperature, and the concentrations of charged species also depend on the pH in water.

It is also important to note that when water is decomposed to free radicals, the oxidizing and reducing species are equally divided; some of them are very strong oxidizing species, (e.g., OH, HO₂) and some of them are very strong reducing species (e.g., e_{aq}⁻ and H). The lifetimes of these free radicals are generally very short, less than 1 ms, and their equilibrium concentrations in water are several orders of magnitude lower than the stable decomposition products, H₂, O₂ and H₂O₂. The stable decomposition products are also stoichiometrically divided; H₂O₂ and O₂ are oxidizing species and H₂ is a reducing species. Although they are equally divided, the oxidizing process seems to proceed faster in most cases.

Water Radiolysis Model Calculations

The tests outlined in Tables A1 and A2 were analyzed using Toshiba's, Hitachi's, and GE's radiolysis model codes. The main results of the mini-autoclave analyses are summarized in Tables A3 and A4.

The radiation water chemistry test (5-C) was used to validate the radiolytic models. A brief description of the first two radiation water chemistry mini-tests is given below, as these results were not discussed in the body of this report.

[Case 1] DO:0ppb, DH:0ppb

This case was executed as radiation water chemistry experiment A-1. The measurements taken during the test showed that both the dissolved oxygen (DO) and dissolved hydrogen (DH) at the test equipment outlet were 0 ppb. The Toshiba and Hitachi analyses accounted for oxygen consumption from the stainless steel corrosion, etc. Their calculated results agreed very well with the measured DO and DH values. On the other hand, the GE analysis did not consider oxygen consumption and the calculated results did not agree as closely with the measured outlet DO and DH values. This implies that it is important to consider oxygen consumption in the test loop. Figure A1 shows the chemical distributions along the mini-autoclave test loop. In the vicinity of the mini-autoclave where the radiation dose is significant, hydrogen peroxide, oxygen and hydrogen are generated due to the radiolytic decomposition of water. Hydrogen peroxide is the most prevalent species with a concentration of ~250-450 ppb. The radiolytic species recombine outside the high flux test zone and thus they are not detected. In addition to oxygen, hydrogen and hydrogen peroxide, species like O_2^- , HO_2^- , OH etc. are observed in the mini-autoclave but their concentrations are less than 2 ppb.

[Case 2] DO:305ppb,DH:0ppb

This case was executed as radiation water chemistry experiment B-1. The outlet DO and DH measurements taken during the test were 16 ppb and 0 ppb, respectively. The calculated outlet DO concentration is ~100-200 ppb. This discrepancy is attributed to the oxygen consumption rate used in the calculation. Since there is an adequate consistency between the measured DO and DH and the calculated values in other cases, the oxygen consumption rate adopted in this analysis is not of importance. Figure A2 shows the chemical distributions along the loop. In the vicinity of the mini-autoclave where the radiation dose is significant, hydrogen peroxide (~800-1400 ppb), oxygen (~230-270 ppb) and hydrogen (65-104 ppb) are generated due to the radiolytic decomposition of water. The concentration of other species such as O_2^- are less than about 15 ppb.

Table A1
Analysis Cases for the Mini-Autoclave Irradiation Tests

Case	Inlet Dissolved Oxygen Conc.	Inlet Dissolved Hydrogen Conc.	Code	Remarks
1	0	0	H/T/GE	RWCE A-1
2	305	0	H/T	RWCE B-1
3	810	0	H/T/GE	MAC 1-C
4	1221	0	H/T/GE	MAC 3-C
5	275	26	H/T/GE	MAC 1-A
6	0	501	H/T/GE	MAC 4-C
7*	765	0	Toshiba	MAC 2-C
8**	850	0	Hitachi	MAC 2-A

* N₂(300 ppb) injection

** CrO₄²⁻(291 ppb) injection

Table A2
Analysis Cases for the Fuel Rod Irradiation Tests

Case	Inlet Dissolved Oxygen Conc.	Inlet Dissolved Hydrogen Conc.	Remarks
1	250	50	Test 1 (UO ₂)
2	350	30	Test 2 (UO ₂ , (U,Gd)O ₂)
3	500	30	Test 3 (UO ₂ , (U,Gd)O ₂)
4	1000	40	Test 4 (UO ₂ , Zebra cladding)
5	0	400	Test 5 (UO ₂ , Zebra cladding)
6*	1000	0	Test 6b (UO ₂ , Zebra cladding)

* 300 ppb Cr injection

Table A3
Comparison of GE's, Hitachi's, and Toshiba's Radiolysis Model Calculations for the Mini-Autoclave Irradiation Tests

Test #	Experimental						Calculation				MAC Chemistry								Concentration in ppm		
	Inlet			Outlet			Inlet		Outlet		O ₂	H ₂	H ₂ O ₂	O ₂ *	HO ₂ *	H ₂ O ₂	HO ₂	OH			
	O ₂	H ₂		O ₂	H ₂		O ₂	H ₂		O ₂										H ₂	
	GE*	Hit*	Tos*	GE*	Hit*	Tos*	GE*	Hit*	Tos*	GE*										Hit*	Tos*
RWCE Al	0	0	0	0	0	0	136.0	16.0	22.0	30.0	445.0	-	-	-	-	-	-	-			
	H**	0	0	0	0	0	0.2	1.5	7.4	20.3	320.0	1.1	0.2	6.4	0.4	1.2	1.2				
	T**	0	0	0	0	0	0.0	0.3	5.8	16.0	238.0	1.7	1.9	6.3	0.3	1.5	1.5				
RWCE BI	GE*	0	0	0	0	0	175.7	77.0	271.0	104.0	1430.0	12.3	2.0	3.2	0.2	0.2	0.2	0.2			
	Hit*	0	0	0	0	0	127.1	9.7	270.2	65.1	782.0	15.3	5.9	2.5	0.3	0.3	0.3	0.3			
	T**	0	0	0	0	0	1109.0	37.0	447.0	91.0	2265.0	-	-	-	-	-	-	-			
3-C	GE*	0	0	0	0	0	399.0	28.0	364.0	137.0	7095.0	16.2	1.5	3.9	0.2	0.2	0.2	0.2			
	Hit*	0	0	0	0	0	371.0	130.9	521.0	83.1	1790.0	19.9	9.3	3.7	0.3	0.3	0.3	0.3			
	T**	0	0	0	0	0	396.0	18.2	687.0	106.0	2715.0	-	-	-	-	-	-	-			
3-C	GE*	1221	0	719	0	0	1472.0	41.0	448.0	153.0	2385.0	18.0	1.8	4.4	0.1	0.1	0.1	0.1			
	Hit*	0	0	0	0	0	509.0	31.0	747.6	101.0	1701.0	22.5	12.1	4.0	0.2	0.2	0.2	0.2			
	T**	0	0	0	0	0	660.0	24.7	747.6	101.0	1701.0	22.5	12.1	4.0	0.2	0.2	0.2	0.2			
1-A	GE*	275	26	7	29	26	231.0	20.0	42.0	34.0	619.0	-	-	-	-	-	-	-			
	Hit*	0	0	0	0	0	9.0	15.0	4.5	20.0	248.0	0.9	0.2	0.2	1.3	0.7	0.7	0.7			
	T**	0	0	0	0	0	11.0	0.1	4.5	20.0	248.0	0.9	0.2	0.2	1.3	0.7	0.7	0.7			
4-C	GE*	0	0	0	0	0	0.2	524.0	0.0	527.0	52.0	-	-	-	-	-	-	-			
	Hit*	0	0	0	0	0	0.1	524.0	0.0	527.0	52.0	-	-	-	-	-	-	-			
	T**	0	0	0	0	0	0.0	422.0	0.0	427.0	42.4	0.0	0.3	0.0	0.0	0.0	0.0	0.0			

*No Oxygen Consumption on Metal Surface

**Oxygen Consumption on Metal Surface considered

Table A4

Test #	Experimental						Model Calculation						Model Calculation						Concentration in ppb
	Inlet			Outlet			Inlet			Outlet			MAC Chemistry						
	O2	H2	N2	O2	H2	N2	O2	H2	N2	O2	H2	N2	O2	H2	N2	O2	H2	N2	
2-C	765	0	300	348	0	N.A.	752	0	340	369	25	270.4	434.2	86.7	1230.5	18.2			
													HO2	HO2	OH	N2			
													6.67	4.21	0.257	263.51			
													NH3	NH4+	NO	NO2			
													0.285	2.56	0.02	13.3			
													NO3						
													118.2						

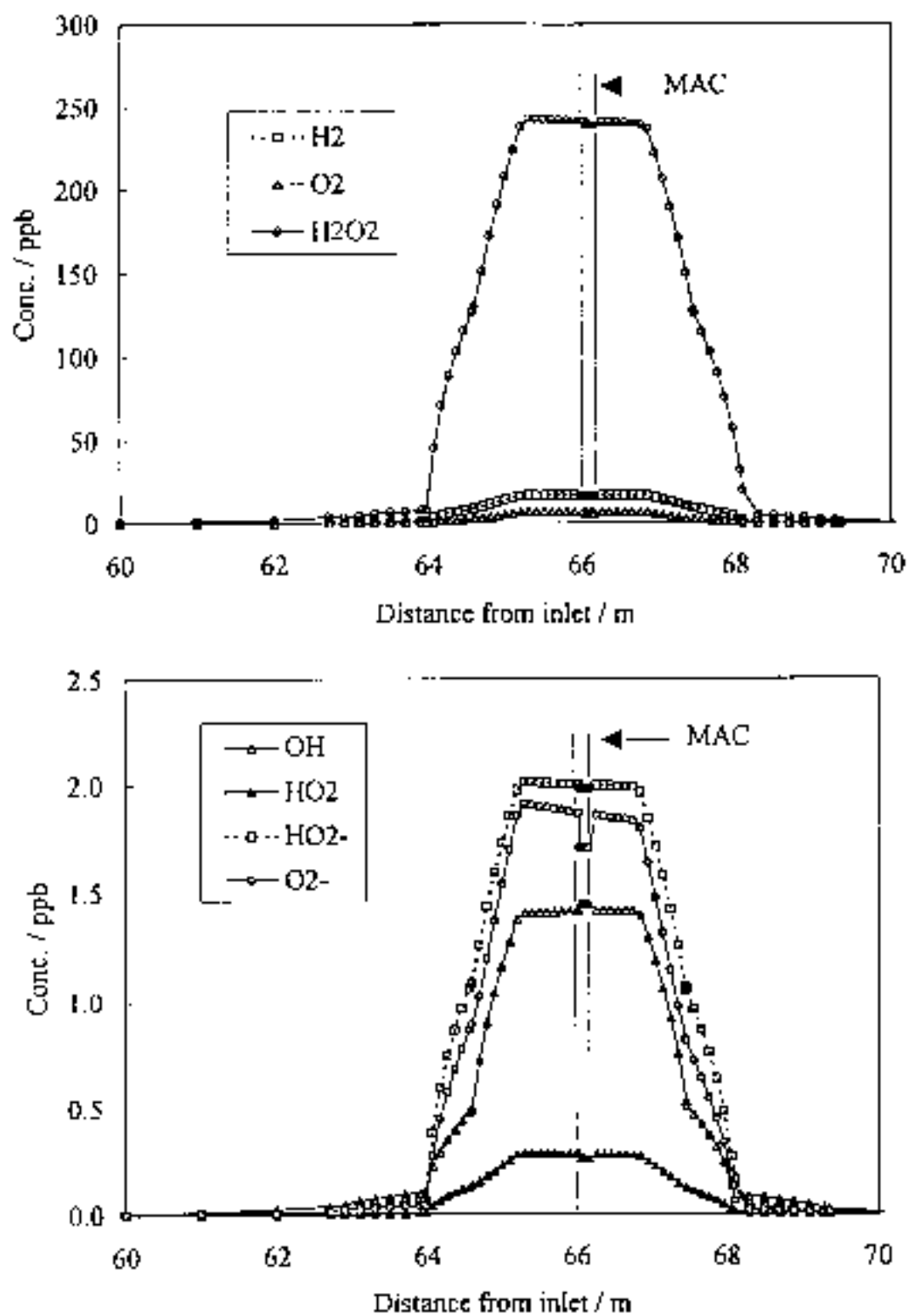
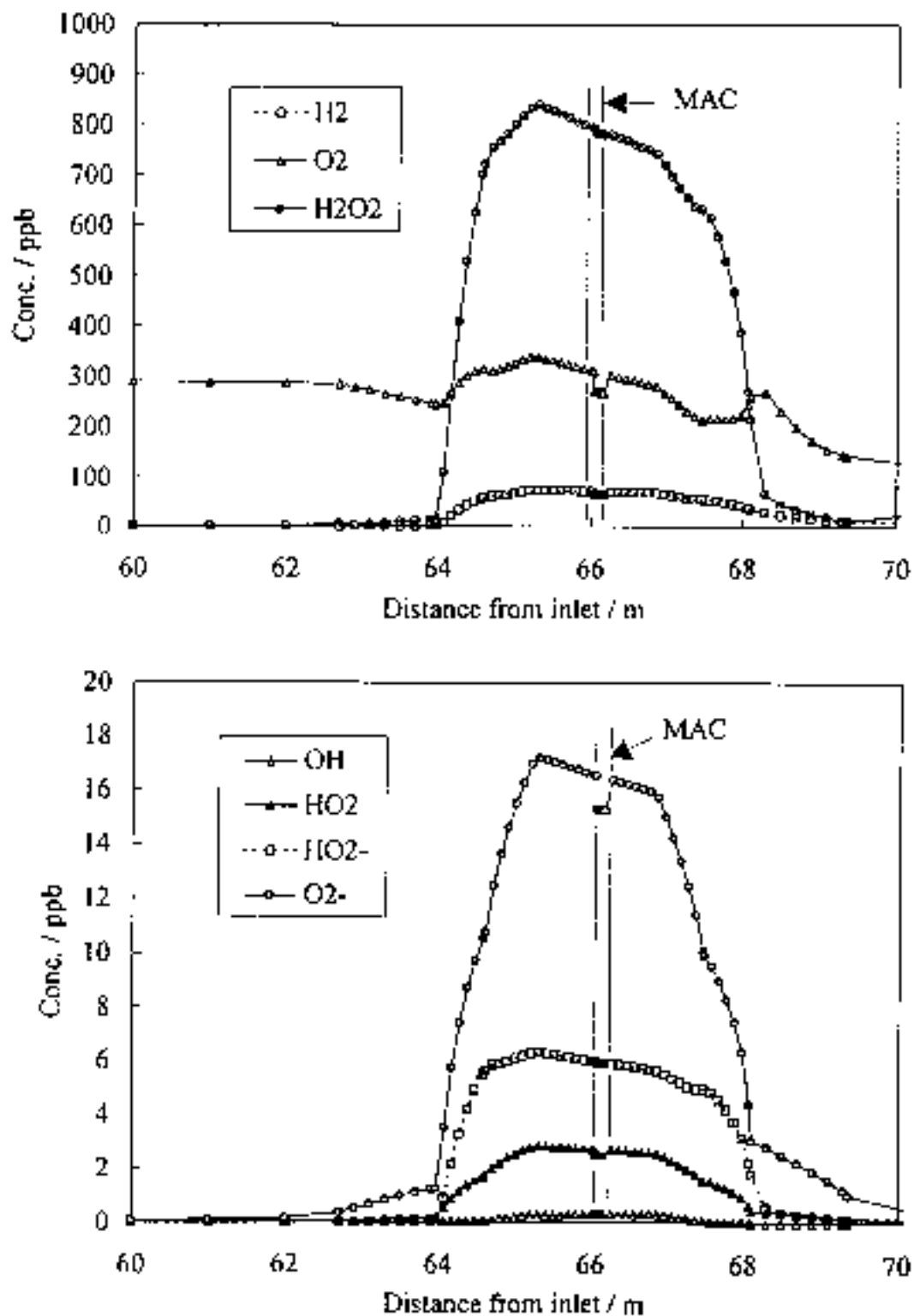


Figure A1 Mini-Autoclave Analysis Case 1 (RWCE A-1) ($O_2 = 0$ ppb, $H_2 = 0$ ppb)

Figure A2 Mini-Autoclave Analysis Case 1 (RWCE B-1) ($\text{O}_2 = 305$ ppb)



WARNING: This Document contains information classified under U.S. Export Control regulations as restricted from export outside the United States. You are under an obligation to ensure that you have a legal right to obtain access to this information and to ensure that you obtain an export license prior to any re-export of this information. Special restrictions apply to access by anyone that is not a United States citizen or a Permanent United States resident. For further information regarding your obligations, please see the information contained below in the section titled "Export Control Restrictions."

Export Control Restrictions

Access to and use of EPRI Intellectual Property is granted with the specific understanding and requirement that responsibility for ensuring full compliance with all applicable U.S. and foreign export laws and regulations is being undertaken by you and your company. This includes an obligation to ensure that any individual receiving access hereunder who is not a U.S. citizen or permanent U.S. resident is permitted access under applicable U.S. and foreign export laws and regulations. In the event you are uncertain whether you or your company may lawfully obtain access to this EPRI Intellectual Property, you acknowledge that it is your obligation to consult with your company's legal counsel to determine whether this access is lawful. Although EPRI may make available on a case by case basis an informal assessment of the applicable U.S. export classification for specific EPRI Intellectual Property, you and your company acknowledge that this assessment is solely for informational purposes and not for reliance purposes. You and your company acknowledge that it is still the obligation of you and your company to make your own assessment of the applicable U.S. export classification and ensure compliance accordingly. You and your company understand and acknowledge your obligations to make a prompt report to EPRI and the appropriate authorities regarding any access to or use of EPRI Intellectual Property hereunder that may be in violation of applicable U.S. or foreign export laws or regulations.

About EPRI

EPRI creates science and technology solutions for the global energy and energy services industry. U.S. electric utilities established the Electric Power Research Institute in 1973 as a nonprofit research consortium for the benefit of utility members, their customers, and society. Now known simply as EPRI, the company provides a wide range of innovative products and services to more than 1000 energy-related organizations in 40 countries. EPRI's multidisciplinary team of scientists and engineers draws on a worldwide network of technical and business expertise to help solve today's toughest energy and environmental problems.

EPRI. Electrify the World

SINGLE USER LICENSE AGREEMENT

THIS IS A LEGALLY BINDING AGREEMENT BETWEEN YOU AND THE ELECTRIC POWER RESEARCH INSTITUTE, INC. (EPRI). PLEASE READ IT CAREFULLY BEFORE REMOVING THE WRAPPING MATERIAL.

BY OPENING THIS SEALED PACKAGE YOU ARE AGREEING TO THE TERMS OF THIS AGREEMENT. IF YOU DO NOT AGREE TO THE TERMS OF THIS AGREEMENT, PROMPTLY RETURN THE UNOPENED PACKAGE TO EPRI AND THE PURCHASE PRICE WILL BE REFUNDED.

1. GRANT OF LICENSE

EPRI grants you the nonexclusive and nontransferable right during the term of this agreement to use this package only for your own benefit and the benefit of your organization. This means that the following may use this package: (I) your company (at any site owned or operated by your company); (II) its subsidiaries or other related entities; and (III) a consultant to your company or related entities, if the consultant has entered into a contract agreeing not to disclose the package outside of its organization or to use the package for its own benefit or the benefit of any party other than your company.

This shrink-wrap license agreement is subordinate to the terms of the Master Utility License Agreement between most U.S. EPRI member utilities and EPRI. Any EPRI member utility that does not have a Master Utility License Agreement may get one on request.

2. COPYRIGHT

This package, including the information contained in it, is either licensed to EPRI or owned by EPRI and is protected by United States and international copyright laws. You may not, without the prior written permission of EPRI, reproduce, translate or modify this package, in any form, in whole or in part, or prepare any derivative work based on this package.

3. RESTRICTIONS

You may not rent, lease, license, disclose or give this package to any person or organization, or use the information contained in this package, for the benefit of any third party or for any purpose other than as specified above unless such use is with the prior written permission of EPRI. You agree to take all reasonable steps to prevent unauthorized disclosure or use of this package. Except as specified above, this agreement does not grant you any right to patents, copyrights, trade secrets, trade names, trademarks or any other intellectual property, rights or licenses in respect of this package.

4. TERM AND TERMINATION

This license and this agreement are effective until terminated. You may terminate them at any time by destroying this package. EPRI has the right to terminate the license and this agreement immediately if you fail to comply with any term or condition of this agreement. Upon any termination you may destroy this package, but all obligations of nondisclosure will remain in effect.

5. DISCLAIMER OF WARRANTIES AND LIMITATION OF LIABILITIES

NEITHER EPRI, ANY MEMBER OF EPRI, ANY COSPONSOR, NOR ANY PERSON OR ORGANIZATION ACTING ON BEHALF OF ANY OF THEM:

- (A) MAKES ANY WARRANTY OR REPRESENTATION WHATSOEVER, EXPRESS OR IMPLIED, (I) WITH RESPECT TO THE USE OF ANY INFORMATION, APPARATUS, METHOD, PROCESS OR SIMILAR ITEM DISCLOSED IN THIS PACKAGE, INCLUDING MERCHANTABILITY AND FITNESS FOR A PARTICULAR PURPOSE, OR (II) THAT SUCH USE DOES NOT INFRINGE ON OR INTERFERE WITH PRIVATELY OWNED RIGHTS, INCLUDING ANY PARTY'S INTELLECTUAL PROPERTY, OR (III) THAT THIS PACKAGE IS SUITABLE TO ANY PARTICULAR USER'S CIRCUMSTANCE; OR
- (B) ASSUMES RESPONSIBILITY FOR ANY DAMAGES OR OTHER LIABILITY WHATSOEVER (INCLUDING ANY CONSEQUENTIAL DAMAGES, EVEN IF EPRI OR ANY EPRI REPRESENTATIVE HAS BEEN ADVISED OF THE POSSIBILITY OF SUCH DAMAGES) RESULTING FROM YOUR SELECTION OR USE OF THIS PACKAGE OR ANY INFORMATION, APPARATUS, METHOD, PROCESS OR SIMILAR ITEM DISCLOSED IN THIS PACKAGE.

6. EXPORT

The laws and regulations of the United States restrict the export and re-export of any portion of this package, and you agree not to export or re-export this package or any related technical data in any form without the appropriate United States and foreign government approvals.

7. CHOICE OF LAW

This agreement will be governed by the laws of the State of California as applied to transactions taking place entirely in California between California residents.

8. INTEGRATION

You have read and understand this agreement, and acknowledge that it is the final, complete and exclusive agreement between you and EPRI concerning its subject matter, superseding any prior related understanding or agreement. No waiver, variation or different terms of this agreement will be enforceable against EPRI unless EPRI gives its prior written consent, signed by an officer of EPRI.

Programs:

TR-106830

Nuclear Power

© 1997 Electric Power Research Institute (EPRI), Inc. All rights reserved. Electric Power Research Institute and EPRI are registered service marks of the Electric Power Research Institute, Inc. EPRI. ELECTRIFY THE WORLD is a service mark of the Electric Power Research Institute, Inc.

♻️ Printed on recycled paper in the United States of America